The Pennsylvania State University

The Graduate School

Department of Electrical Engineering

HIGH PERFORMANCE SMALL-MOLECULE ORGANIC THIN FILM TRANSISTORS

A Thesis in

Electrical Engineering

by

Chung-Chen Kuo

Submitted in Partial Fulfillment
of the Requirements
for the Degree of

Doctor of Philosophy

December 2005

The thesis of Chung-Chen Kuo was reviewed and approved* by the following:

Thomas N. Jackson
Robert E. Kirby Chair Professor of Electrical Engineering
Thesis Advisor
Chair of Committee

Christopher R. Wronski
Leonhard Professor of Microelectronic Devices and Materials
Professor Emeritus of Electrical Engineering

Jerzy Ruzyllo
Professor of Electrical Engineering and Materials Science and Engineering

Srinivas Tadigadapa
Associate Professor of Electrical Engineering

Qing Wang
Assistant Professor of Materials Science and Engineering

W. Kenneth Jenkins
Professor of Electrical Engineering
Head of the Department of Electrical Engineering

*Signatures are on file in the Graduate School

ABSTRACT

The roadmap of developing microelectronics has a new branch: organic electronics. Organic electronics, which utilizes the electrical properties of organic materials in the active or passive layers, is an emerging technology that has received much attention. In conjunction with today's demands for new materials and devices, many technologies have emerged for developing organic electronics and consolidating applications and markets. An organic thin-film transistor is the essential device in this paradigm in addition to organic photodiodes and organic light emitting diodes.

This thesis presents advances made in design and fabrication of organic thin-film transistors (OTFTs) using small-molecule organic semiconductors (pentacene, anthradithiophene, and their derivatives) as the active layer with record device performance. In this work OTFT test structures fabricated on oxidized silicon substrates were utilized to provide a convenient substrate, gate contact, and gate insulator for the processing and characterization of vapor-deposited organic materials and their transistors. By developing a gate dielectric treatment using silane coupling agents the performance and yield of pentacene OTFTs was improved and a field-effect mobility of larger than 2 cm^2/V-s was achieved. Such device performance is comparable to a-Si:H TFTs and have the potential for electronic applications.

In addition, the first direct photolithographic process for top contacts to pentacene OTFTs on oxidized silicon with an acceptable performance (a field-effect mobility of 0.3 cm^2/V-s, an on/off current ratio of 10^7, and a subthreshold slope of 1 V/decade) was developed. The multiple layer photoresist process demonstrated the feasibility of creating source and drain metallic electrodes on vapor-deposited pentacene thin films with a resolution less than 10 μm.

Subsequently, solution-processed OTFTs were then investigated and high performance transistors, with field-effect mobilities > 1 cm^2/V-s and an on/off current ratio of $10^{6.5}$, were developed with a processing-temperature of less than 90 ºC. This record performance was obtained with devices based on triethylsilylethynyl anthradithiophene (TES ADT) and triisopropylsilylethynyl pentacene (TIPS pentacene).

Chemically modified source and drain contacts and gate dielectric were used to achieve such device performance, a performance that is still limited by the contacts. The studies were extended to several solution deposition methods which included blade coating, bar coating, dip casting, and spin casting. In addition to the above two materials, the design and characterization of four synthesized organic semiconductors with substituted functional groups was carried out. In this work it was found that the stacking of molecules with a large and two-dimensional π-orbital overlap is crucial in determining its device performance and electron transport. The results of such molecular design approach offer great potential of obtaining suitable materials for large-area, low-cost electronic applications using low-temperature solution-processing technology.

It is shown in this work that desirable performance can be achieved from both vapor-deposited and solution-processed OTFTs.

TABLE OF CONTENTS

LIST OF FIGURES

LIST OF TABLES

ACKNOWLEDGEMENTS

I wish to express my sincerest appreciation to my thesis advisor Thomas N. Jackson for his continued support and my thesis committee members Christopher R. Wronski, Jerzy Ruzyllo, Srinivas Tadigadapa, and Qing Wang. I thank current and former colleagues in Jackson's Electronic Research Group, our technician, Lloyd, and former and current secretaries, Erin and Cheryl, and friends in Dept. of Electrical Engineering. Additionally, much of the work documented here would not be possible without contributions and assistance from co-workers, particularly John E. Anthony and Marcia M. Pane from University of Kentucky. I express my deepest appreciation to my parents and my family for their support and encouragement. Lastly, I wish to earnestly express much appreciation to the teacher of Penn State Y. X. Qigong Club for great care and many thanks to friends in the club.

Chapter 1

Introduction

1.1 New Trends of Microelectronics and Their Applications

Utilizing semiconductor electronics has sparked and driven tremendous new applications into human life and new scientific developments. These technologies emerged and set the foundation for the information revolution (the third wave after the agricultural revolution and the Industrial Revolution) in the last four decades. Using these new science and technology we created an innovative, functional microelectronic world. For example, the greatest demands are for high operating speed, large device density, and many functions in electronic applications. Microfabrication and later nanofabrication technology bring them into reality. Today, a high-performance personal computer with 55 million transistors running at 3 GHz on a 2 cm^2 silicon chip inside the CPU can fulfill most people's needs. Because it is as cheap as a television, it is available in some supermarkets that are open twenty four hours daily, seven days a week. This electronic innovation is terrific.

In contrast, the dimensions of an entire personal computer system have not changed much in comparison with those from twenty years ago. Why is that? While the microfabrication of millions of high performance and small crystalline silicon devices inside the processor in the computer is possible, their advantages are not useful and actually may be shortcomings because human interaction with the computer cannot be easily scaled down. The dimension, structure, or functionality of interfacing is mutually limited by the machines' functionality and the dimensions, precision, and ability of a human being. More often we wish them to be big, and the bigger the better. A typical example is the flat panel display for computers, cell phones, digital cameras, and televisions. Users can take advantages of its high image quality, space savings, small footprint, light weight, low power consumption, and absence of harmful radiation.

Because of the manufacturing cost, the unit price was never compelling to buyers until recently, when now they competed with CRT monitors. Today, users prefer a flat panel display to a CRT. In the computer display market the NPD Group reported that in May 2003, for the first time, active matrix liquid crystal displays (AMLCDs) outsold cathode-ray tube (CRT) monitors, and accounted for 52 % of units sold and 70 % of sale revenue [Smith and Dolan 2003]. This market has become one of the two largest portions of the microelectronic industry and becoming larger. Thus, the demand for large-area, large-volume electronic applications is strong and rising. The economic potential of such a demanding market is huge, and finding new ways to lower the manufacturing cost, rather than using the costly conventional semiconductor processing, remains an important strategy in the research and technological development.

Thin film transistors (TFTs) are the technology of choice for large-area, low-cost electronics, where they often act as the switches behind each pixel on a large backplane. TFT is a field-effect transistor with a thin semiconducting film as the active layer, unlike the fragile and expensive crystalline semiconductor of metal-oxide-semiconductor field-effect transistors (MOSFETs). The main stream technology is based on hydrogenated amorphous silicon (a-Si:H) TFT's using an amorphous silicon thin-film for electron transport. Device performance is much lower than that of silicon MOSFETs. The field-effect mobility of electrons in an a-Si:H TFT is 0.5 – 1.2 cm^2/V-s, just one hundredth or one thousandth of that in crystalline silicon. In comparison with 60 mV/decade in silicon devices, the subthreshold slope is 0.5 V/dec due to the large trap density near the mid-bandgap; the nature of such a material results in a low operating speed and a large operating voltage of 20 V. Although the TFT's device performance is very low, it is actually sufficient for many large-area, low-cost electronic applications because of TFT's advantages: TFTs can be inexpensively and easily fabricated over substrates a meter in size; the manufacturing does not require high temperature (> 600 ºC) processes; and offers more options for substrates such as glasses. Today most large area electronic applications employ TFT technology.

Currently hydrogenated amorphous silicon (a-Si:H) TFTs dominate the market, but there is interested in other innovative technologies to solve the processing criteria

such as delicate glass substrates, high temperature-endurance plastic films associated with the process temperatures above 200 ºC. Alternatives such as organic semiconductors and their TFTs may allow for the use of cheap and flexible polymeric substrates and inexpensive processes.

1.2 **Organic Thin Film Transistors**

Organic TFTs based on organic semiconductors have emerged in the last decade as an alternative technology. Organic thin film transistor (OTFT) performance has improved rapidly over the past several years, especially pentacene TFTs. OTFTs based on pentacene, α,α'-didecyloligothiophenes, et al. with field-effect mobility > 0.5 cm^2/V-s have been reported, which equals or exceeds that of a-Si:H TFTs [Lin, Gundlach 1997; Halik, Klauk 2003]. In addition, OTFTs offer the possibility for fabrication on large, cheap, polymeric substrates and processing from solutions. RFIDs and electronic paper are two applications where these merits are of great value.

RFIDs and smart inventory tags

The radio frequency identification tags (RFIDs) have drawn a lot of attention recently and their market potential is rising. Bar codes are currently the most widely used method in identification tags for tracking products and recognizing production and in-store inventories. The fabrication cost of bar codes is very low, usually less than a cent, but the capability of inline printing on paper or plastic adds flexible to manufacturers and stores. Corporations and manufacturers have long been concerned with security issues due to fraudulent products, difficulty in reading the tags, limited information, and the lack of wireless tracking and accessing. The idea of using radio frequency electromagnetic waves to read identification tags and taking advantage of wireless access to increase information capacity has been known for decades. Some implementations of RFID systems were built, but the costs of hardware and software, and the price per tag, were

too expensive to be useful for large volume applications. As technologies move forward, these obstacles for their development diminish and the interest in them grows. However, the strategic planning and decision made by enterprises to develop RFIDs were not dramatically changed until Wal-Mart's declaration to deploy this technology in 2002. Although the threshold cost of using RFIDs for the first year is as high as 9 million dollars, many retail companies and government organizations are planning to or are implementing RFIDs. IDC reports that the estimated RFID spending in the U.S. retail supply chains will grow more than tenfold over the next four years, from $91.5 million in 2003 to nearly $1.3 billion in 2008 [Bednarz 2004]. This indicates the presence of a very large market in the near future.

In addition to providing higher security and a capability to include more information in a tag accessible via wireless, RFIDs have the potential to save cost, to become embedded into automatic systems, and to check out automatically. On the other hand, RFID tags are currently more expensive, are unrecognizable by humans, with restricted fabrication flexibility. Solution-processed OTFTs should allow RFIDs to be manufactured in high volume on arbitrary substrates by printing or other low-cost fabrication techniques. Thus, OTFT technology can advance the advantages and acceptance of RFIDs.

Electronic paper

Many laboratory prototypes of electronic paper, in the form of a flexible plastic electronic display often as thin as a credit card, have been demonstrated since the idea of electronic ink was invented and realized in 1975 by Nick Sheridon at Xerox's Pola Alto Research Center. It has undergone earnest development in the 1990s. The main advantage of electronic paper is that it is made entirely with a process similar to ink-on-paper printing at a very low cost. Interest in this kind of paper—which could be used in electronic books, newspapers, magazines, billboards, and storefront advertisement—is great; the convenient Internet and wireless technologies available today allow for instantaneous updating via a local RF signal, wireless hotspots, or satellites. In April

2004 Sony and E Ink, a key developer and pioneer of electronic paper, jointly announced the availability of the first commercialized electronic paper— Sony EBR-1000 Librie eBook Reader ($380), an early milestone for a potentially huge business. Here is a quote from a reviewer, Kakyou: "Initial reports of the screen quality left me quite unprepared for the actual thing. The screen is unbelievable. Not quite paper, more like a dull plastic-like look. My first impression of the device was that it was not an actual working unit, but a plastic mock up made for stores. With high-contrast black text on a reflective background, the screen has a readability rivaling actual paper. The weight of the book is also quite a shock."[Kakyou 2004]. This technology may lead to ultra-thin, lightweight displays for next-generation consumer electronics.

The key element of electronic paper are the transistor for obtaining the required pixel resolution and addressing schemes for displaying information, where for most applications high switching speeds are not required. This allows for the use of transistors based on a variety of materials, particularly organic semiconductors which allows electronic applications on low-cost, rugged, flexible polymeric substrates. Thus, OTFT is an attractive technology for electronic paper.

Flat panel displays (FPDs)

Organic TFT technology offers several advantages for FPDs although flat panel displays using the a-Si:H TFTs and low-temperature polysilicon (LTPS) TFT backplanes are well-accepted. A few technical obstacles remain unsolved in the various silicon TFT technologies such as restricted rigid substrate types, passive backlight sources, and a relatively high manufacturing cost. There is a great interest in developing inexpensive, flexible displays, and it has focused on organic electronics technology using OTFTs and organic light emitting diodes (OLEDs). For instance, there has been a demonstration of the flexible OTFT / polydispersion liquid crystal(PDLC) display indicating the feasibility of low temperature (< 200 ºC) processes on flexible, transparent polymeric substrates for active matrix, passive backlight displays [Sheraw, Zhou 2002]. Active emissive displays using OLED pixels driven by OTFTs offer advantages in pixel design and process

compatibility [Chuman, Ohta 2004]. There is also great interest in solution-processed OTFTs, which would allow for ultra-low-cost circuits to be fabricated by printing as well as roll-to-roll technologies [Shaheen, Radspinner 2001] . An established OTFT technology could lead to a host of new applications for flat panel displays.

Recently, emerging OTFT research has focused on either demonstrations for real applications or on fundamental understanding and improvement of devices and materials. A sophisticated display demonstration of using an OTFT backplane requires many new or modified conventional processes. For example, at least five patterned layers (or five masks for gate electrodes, gate dielectric, source/drain electrodes, device isolation, and device passivation) are involved. Many new designs and processes as well as approaches to integration are as necessary for improving device performance and use of polymeric substrates. Additionally, the use of source/drain electrodes is often restricted to bottom contacts among several prototype structures because a direct lithographic process for fabricating top contacts on pentacene thin films and other organic semiconductors is not yet available. This leads to several limitations, such as higher contact resistances and mechanical fragility.

Techniques of improving device performance and stability are of great interest. This includes a gate dielectric treatment for larger carrier mobilities, methods of increasing the subthreshold slope or controlling the threshold voltages, and improving device stability. There is also great interest in understanding the nature of electronic transport and the molecular structure in these materials as well as their material science and physics. In addition, different classes of organic materials are being designed and synthesized to provide improvements in devices such as based on soluble pentacene and anthradithiophene derivatives.

Pentacene is a p-type small molecule organic semiconductor with five benzene rings fused in series, which is the most widely used active layer in OTFT development. Vapor-deposited pentacene OTFTs currently have the highest device performance in OTFTs: a typical field-effect mobility ~ 1 cm^2/V-s, a subthreshold slope ~ 1 V/decade, and a current on/off ratio of 10^7 when operated at 30 V. Several important issues have been addressed in this research, which have led to record high performance of these

OTFT's with studies being extended to their yield and incorporation in different circuits and applications.

There has been a great interest for a long time in solution-processed OTFTs because their technology offers the possibility of very low-cost fabrication techniques such as printing technique. Many studies have focused on TFTs based on large molecule organic semiconductors such as semiconducting polymers, but even the best device performance achieved using poly-3-hexylthiophene (P3HT) is inferior to that of pentacene TFTs and cannot be used in most applications as well as requiring process temperatures of about 200 ºC. In 1999 an interesting approach of improving pentacene was introduced based on molecular design and synthesis, similar to that carried out on large molecule organic semiconductors.

1.3 **Thesis Statement**

The potential applications and markets discussed above have attracted great interest in the development of an organic TFT technology. The early work on organic thin film transistors in the last decade has been expanded to cover a broad group of materials, a variety of prototypes, and a wide spectrum of fabrication techniques. The different active layer materials cover a range from polymers, such as regioregulated polythiophene and polyacetylene, to small molecule organic materials such as a-sexithiophene, metal-pthalocyanines, and several acenes (anthracene, pentacene, naphthacene, etc.). The majority of the previous studies have focused on the demonstration of desired performance in organic TFTs using simple test structures and circuits on oxidized silicon, glass substrates, polymeric substrates, and demonstration, and flat panel displays driven by organic TFTs. The Penn State work, which was a large part of this early work, also focused on a variety of fundamental material and device issues which included film morphology, molecular ordering in the active layers, gate dielectric surface treatments for improved device performance, and the performance of various device contacts.

In parallel, a series of feasibility studies and demonstrations were carried out: lithographically patterned pentacene OTFTs on flexible substrates, fast organic circuits, integrated complementary TFTs with n-type a-Si:H on flexible substrates, and a 16 × 16 pixel active matrix liquid crystal displays driven by pentacene organic TFTs. Along with these developments of, many techniques were developed, adapted, and extended into a set of fabrication techniques for organic semiconductors. Some of these key techniques include, but are not limited to, the purification of active materials, deposition methodologies, various gate dielectrics and their surface treatments to obtain high mobilities, selection and surface treatments of the source/drain metals, polymeric substrates and their processing, as well as lithographic isolation and passivation of active layers. Nevertheless, there are still many key problems that have to be addressed. These include issues related reproducibility and stability, poor carrier injection and large contact resistances, photolithographic processing, the lack of high- performance n-type semiconducting materials, and the control of threshold voltages. As a consequence, these key problems as well as opportunities have to be further explored and this thesis represents an important addition to and advancement of the work at Penn State.

In the first part the photolithographic fabrication of top contacts to pentacene OTFTs on oxidized silicon with an acceptable performance are demonstrated. A process for fabricating such pentacene OTFTs was developed where the device performance is comparable to that of pentacene OTFTs with bottom contacts. The lithographic resolution and preliminary process yields were estimated and the practicability was evaluated for photolithographically defined source and drain electrodes. By extending this process, new possibilities can be explored.

The second part of this thesis addresses the issue of new active layer materials, based on pentacene or anthradithiophene derivatives. As stated above, there are key problems that remain for pentacene OTFTs even though to date they have shown the best performance for any organic TFT materials. There is the possibility of finding a new material with improved electrical properties and stability as well as flexible processing. This portion of the thesis work focuses on solution-processed OTFTs based on functionalized pentacene. By substituting a bulky group on the molecular backbone or

modifying the backbone itself, these pentacene derivatives may have improved the π-orbital overlap for better electronic transport as well as being soluble in organic solvents. Among these materials, triethylsilylethynyl anthradithiophene (TES ADT) and triisopropylsilylethynyl pentacene (TIPS pentacene) are of great interest for the high-performance OTFTs fabricated with a solution process. A field effect mobility of 1.0 cm^2/V-s is demonstrated in TES ADT OTFTs, and also a mobility of > 0.8 cm^2/V-s in TIPS pentacene OTFTs. It was found that the method utilized in the solution process and the electrical contacts to these materials are important for obtaining reproducible devices with a uniform high performance. Thus, this has been addressed in this work, where the improvements that have been obtained indicate that there is potential for them in large-area, cheap electronic applications.

Chapter 2 reviews a brief history of organic thin film transistor technology, reviews the progress of organic thin film transistors, and summarizes the previous work on pentacene organic thin film transistors. It then covers the several techniques of the fabrication and characterization of OTFTs developed in this thesis work. This includes the modification of gate dielectrics with silane coupling agents deposited from solution and vapor as well as the thiol treatment for improved contacts.

The challenges encountered in processing fragile pentacene thin films are discussed in Chapter 3. The development of a fabrication process is then presented, for photolithographic fabrication of top contacts that yield high-performance pentacene OTFTs. A comparison of source and drain is presented which shows that top contacts to OTFTs are superior to bottom contacts.

Chapter 4 describes the design, fabrication, and performance of solution-processed OTFTs based on pentacene and anthradithiophene derivatives on oxidized silicon substrates. Advances in high performance OTFTs using solution deposition are demonstrated. It also addresses the issue of improving carrier transport by substituting functional groups in different molecules. It is found that the molecular stacking and overlap of π-orbitals are critical, where the two-dimensional slip stacking offers the highest probability of success.

In Chapter 5 future work is proposed. In the two Appendices, process parameters are listed and the software developed for controlling testing equipment is presented.

Chapter 2

High-Performance Pentacene Thin-Film Transistors

Many impressive advances in the field of organic electronics have proved capable of performing a wide variety of functions. The practical advantages primarily root from the following: (1) Large-area electronics in which the active devices are distributed and embedded over a large area. (2) Low-cost or large volume electronics. Cheap and disposable electronics are increasingly used as the replacement for bar codes and various forms of personal identification. (3) Flexible construction and electronics where ruggedness is necessary. (4) New advances in fabrication methods that may impact the manufacturing of organic electronics and conventional electronics. (5) Novel functionality. In the Center for Thin Film Devices at Penn State, one of the important areas is on the research and development of organic thin film transistors (OTFTs) that perform switching and amplifying functions, like those at a-Si:H TFTs, which are currently used in the pixel control of most active-matrix flat-panel displays.

2.1 **OTFT Technology**

In achieving this, finding an organic semiconductor that meets the criteria for OTFTs, particularly large field-effect mobilities, is a crucial step. A few milestones in the magnitude of field-effect mobility are listed in Tables **2-1** and **2-2** where also they illustrate the rapid development and progress in OTFT technology. Since Ebisawa demonstrated polymer TFTs using polyacetylene in 1983, extensive studies have been carried out with many reports of field-effect mobilities in semiconducting polymers less than 0.01 cm^2/V-s [Ebisawa, Kurokawa 1983]. The progress made has improved mobilities, where today they are about 0.12 cm^2/V-s with the synthesis of regioregular poly-3-hexylthiophene and the refined processing developed in the 1990s [Burroughes, Jones 1988; Greenham and Friend 1995; Salleo, Chabinyc 2002]. Such device

performance is applicable to low-end electronics such as electronic paper and identification tags, and there is much interest in continuing futher research.

Other interesting reports of OTFTs using small-molecule organic semiconductors like α-sexithiophene and pentacene have shown larger field-effect mobilities (> 0.1 $cm^2/V\text{-}s$) than that of semiconducting polymers in the first half decade of the 1990s. Pentacene emerged as the most promising candidate amongst potential materials. Applications based on pentacene OTFTs became very attractive when the field-effect mobility in these OTFTs passed 1.0 $cm^2/V\text{-}s$ in 1996 [Gundlach, Lin 1997; Lin, Gundlach 1997, 1997; Klauk, Gundlach 1999]. The reproducibility of devices was improved by the results presented in this chapter [Gundlach, Kuo 1999]. Pentacene OTFTs with even larger mobilities were also reported, where this level of device performance is comparable to that of a-Si:H TFTs [Hong, Kim 2005]. These advances show pentacene TFTs have the potential for high-end applications such as the backplanes of active matrix displays.

In addition, a few new classes of small-molecule organic semiconductors were designed and synthesized to provide more possible improvements. They often consist of one or two aromatic backbones (thiophenes or acenes) similar to those molecules that have been known to have large field-effect mobility. Examples include OTFTs based on soluble functionalized pentacene and anthradithiophene, where recently they have shown some interesting results. Nevertheless, fundamental understanding and improvement of OTFT active materials are still required for further advancement of OTFT technology.

Table 2-1: Reported mobility of organic semiconductors at room temperature (part 1). All references are listed in the bibliography.

Year	Authors	Active Material	Mobility	Journal
1983	F. Ebisawa, T. Kurokawa, S. Nara	polyacetylene(polymerization)	10^{-5}	J. Appl. Phys. v54, 3255,1983
1986	A. Tsumura, H. Koezuka, T. Ando	polythiophene (PT)	10^{-5}	Appl. Phys. Lett., v49, 1210,1986
1988	J. H. Burroughes, C.A. Jones, R.H. Friend	polyacetylene(precursor) (PA)	10^{-4}	Nature, v335,137,1988
1988	A. Assadi, C. Svensson, M. Willander, O. Inganas	poly(3-hexylthiophene)	10^{-4}	Appl. Phys. Lett., v53, 195, 1988
1989	G. Horowits, D. Fichou, X. Peng, Z. Xu, F. Garnier	aw-hexathiophene (a-6T) (sexithienyl)	10^{-3}	Solid State Comm., v72, 381,1989
1992	Z. Xie, M.S. Abdou, A. Lu, M.J. Deen, S. Holdcroft	poly(3-hexylthiophene)	0.045	Canadian J. Physics, v70(10-11), 1171, 1992
1992	G. Horowitz, X. Peng, D. Fichou, F. Garnier	aw-hexathiophene pentacene	0.02 $2x10^{-3}$	Synth. Met., v51, 419, 1992
1993	K. Hoshimono, S. Fujimori, S. Fujita, S. Fujita	Fullerene(n-type)	10^{-5}-10^{-2}	Jpn. J. Appl. Phys. P2, v32, L1070, 1993
1993	G. Horowitz, F. Deloffre, F. Garnier, R. Hajlaoui, M. Hmyene, A. Yasser	a-6T/plst	0.43	Synthetic Metals, v54, 435, 1993
1995	R.C. Haddon, A.S. Perel, R.C. Morris, T.T.M. Palstra, A.F. Hebard, R.M. Fleming	C60	0.3	Appl. Phys. Lett., v67, 121, 1995
1996	Y.Y. Lin, D.J. Gundlach, T.N. Jackson	pentacene	0.6	54th DRC 1996, 80
3/1997	D.J. Gundlach, Y.Y. Lin, T.N. Jackson, S.F. Nelson	pentacene/sil/tc	1.3	MRS Spring 1997
1997	Y.Y. Lin, D.J. Gundlach, S.F. Nelson, T.N. Jackson	pentacene/OTS/bc pentacene/OTS/tc	1.5/sil/bc 1.3/sil/tc	IEEE Electron Device Lett., v18, n12, 606, 1997
1997	H. Sirringhaus, N. Tessler, R. H. Friend	poly(3-hexylthiophene)	0.1	Science 280, 1741 (1998).
09/1998	J.H. Schon, C. Kloc, R.A. Laudise, B. Batlogg	a-4T(crystal) a-6T(crystal) pentacene(crystal)	0.06 0.52 1.4	Phys. Rev. B, 58, 12952, (1998)
02/1999	D.J. Gundlach, C.C. Kuo, S.F. Nelson, T.N. Jackson	pentacene/OTS	2.1/sil/tc	57th DRC 1999
10/1999	C. R. Kagan, D. B. Mitzi, C. D. Dimitrakopoulos	phenethylammonium SnI4	0.6/	Science Oct, 1999
2002	A. Afzali, C.D. Dimitrakopoulos, and Breen	pentacene precursor	0.9	J. Am. Chem. Soc., 124, p. 8812 (2002)

Table 2-2**: Reported mobility of organic semiconductors at room temperature (part 2).**

Year	Authors	Active Material	Mobility	Journal
03/2003	M. Halik, H. Klauk, U. Zschieschang, G. Schmid	α,α'-didecyloligothiophenes	0.5	J. Appl. Phys., 93, (2003).
06/2003	K. Shankar, C.D. Sheraw, E. Bullock, J.E. Anthony	TIPS pentacene	0.18	61st DRC 2003
06/2004	C.C. Kuo, M. Pane, etc.	TES anthradithiophene/solution	1.0	62nd DRC 2004, J. Am. Chem. Soc., 127, p.4986 (2005)
05/2005	M. Hong, B. S. Kim, Y. U. Lee, etc.	pentacene	7.0	SID International Symposium 2005

Charge Transfer Theory

The carrier transport of organic semiconductors is not well understood as a result of the wide variety of their electrical properties. A lack of a dominant transport mechanism associated with the weak and complicated intermolecular interaction, unlike transport in crystalline inorganic semiconductors, leads to several mechanisms being proposed to explain for the different conductivity regimes and take account of the different molecular structures (small molecules, polymers, and charge transfer complexes).

Band theory developed for inorganic semiconductors could be used in explaining the carrier transport in crystals of small molecules, such as anthracene, with drift mobilities on the order of 1 – 10 cm^2/V-s using time of flight measurements. The mechanism of coherent charge transfer is analogous to charge carrier transport in the extended states of the conduction and valence bands of single crystal inorganic semiconductors. Several distinctive characteristics of organic semiconductors are incorporated. A major one is the strong covalent bonds within molecules and weak bonds between molecules, which consist mostly of dipole-dipole attraction and London dispersion forces or van der Waals forces. This causes substantially less overlap of wavefunctions, particularly π-orbitals, that contributes to the narrower band widths (on the order of 0.1 kT) and consequently, a short mean free path (5-10 nm) and large effective mass. In addition, the movement of charge carriers in molecular solids involves many electrons rather than a single electron in inorganic semiconductors so the band model needs to introduce a many-electron approximation. Mobility in the band model is dominated by scattering of either phonons or impurities. Because the scattering is proportional to the scattering cross-section, which increases with temperature in the band theory, μ, mobility can be expressed as Eq. **2.1**

$$\mu \propto T^{-n} \qquad \textbf{(2.1)}$$

where T is the absolute temperature and the value of n is dependent on the dominant scattering mechanism. For pentacene, n is about 0.27 – 0.32 [Schon, Berg 2000; Thorsmølle, Averitt 2004; Ostroverkhova, Cooke 2005].

The hopping model approach to electrical conductivity describes a phonon-assisted charge transport over the potential barrier separating two adjacent molecular or ionic sites [Emin 1970, 1971; Silinsh, Klimkans 1995]. The mean free path of the carrier is reduced to a distance on the order of the molecular separation between nearest neighbor molecules. It emphasizes the molecular character of conduction states within a short range order rather than the collective character of conduction states in the band model. For a hopping process with a strongly localized carrier, mobility is proportional to the temperature, T, and activation energy, E, and expressed in Eq. **2.2**

$$\mu \propto \nu_P \exp\left(-E/kT\right)\exp\left(-2\alpha R\right) \qquad \textbf{(2.2)}$$

where ν_P is a lattice (phonon) frequency, E is the energy difference between the next hopping site and the originating one, k is Boltzmann's constant, and T is absolute temperature. The product, $\nu_P \exp(-E/kT)$, denotes the probability that the localized electron hops to the next site at an energy E above the initial one. This term reflects its thermally-activated nature where the mobility is positively correlated with the temperature. The quantity of the last term, $\exp(-2\alpha R)$, is the overlap of the wavefunctions between adjacent hopping sites, R is the separation between sites and α is determined by the decay rate of the wavefunction with distance. The actual transport mechanism depends on the electron exchange, electron-phonon interaction, and the type of interaction (intermolecular or intramolecular vibrations).

In addition to these two key models (band and hopping), several other mechanisms models are also considered in studying charge transport in organic semiconductors. One example is the tunneling mechanism which is a temperature-independent process, which describes the transition taking place between two matched energy levels by tunneling. However, a comprehensive theory of the electronic conduction of organic solids is lacking.

2.2 **Thin-Film Transistors**

In 1925 Julius Lilienfield described in a patent application the idea of "controlling the flow of an electric current in an electrically conducting solid of minute thickness" in solid-state devices, and O. Heil also made one independent patent application for a semiconductor using an electric field generated from a third electrode [Lilienfield 1930; Heil 1935; Lilienfield 1935] The device described is the insulated gate field effect transistor (IGFET), formed using a thin insulating material to physically separate the gate electrode from the semiconductor material. Shockley's attempts to modulate a current by either the field-effect of an insulated gate electrode (which was not successful because high surface states rendered the charges immobile) or the gate electrode separated by reversed-biased p-n junctions, [Shockley and Pearson 1948; Shockley 1952].

In 1961 Paul Weimer demonstrated an IGFET fabricated by evaporating all components of the transistor as thin films onto a glass substrate, with cadmium sulfide as the active layer material [Weimer 1961, 1962]. Figure **2-1a** shows the cross section of a thin film IGFET. Since this demonstration, thin film transistors (TFTs) have been successfully fabricated using a variety of active layer materials; cadmium sulfide, cadmium sellenide, chalcogenide glasses, and particularly hydrogenated amorphous silicon (a-Si:H) and polycrystalline silicon.

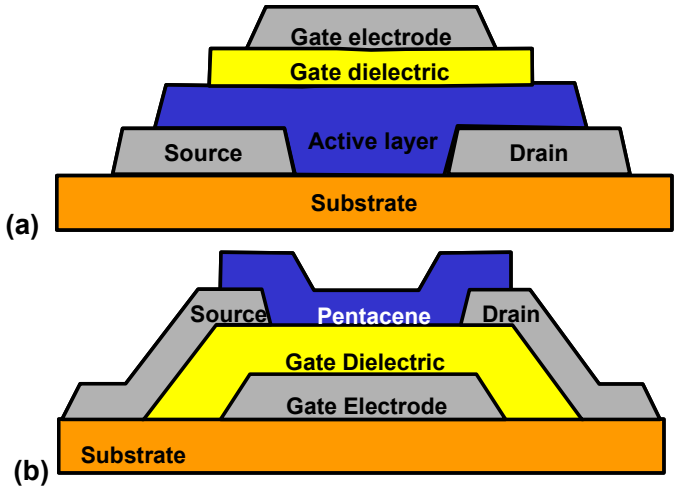

Figure 2-1**: Two typical OTFT structures with bottom source / drain electrodes and either (a) top gate electrode or (b) bottom gate electrode.**

As shown in Figure **2-2a**, a TFT has drain current characteristics like those of a conventional IGFET when it is biased by the gate electrode. For small voltages applied between the drain and the source, the drain current I_D varies linearly with drain-to-source voltage V_{DS} as in Figure **2-2b**. The channel region acts like a resistor. Such a characteristic can be expressed by Eq. **2.3**.

$$I_D = g_d \, V_{DS} \tag{2.3}$$

The channel conductance by Eq. **2.4** .

$$g_d = \frac{W}{L} \mu \left| Q \right| \tag{2.4}$$

where μ is the carrier mobility in unit of $cm^2/V\text{-}s$, |Q| is the sheet density of the charges accumulated at the surface or the inversion layer due to the gate field effect, and W and L are carrier channel width and length, respectively.

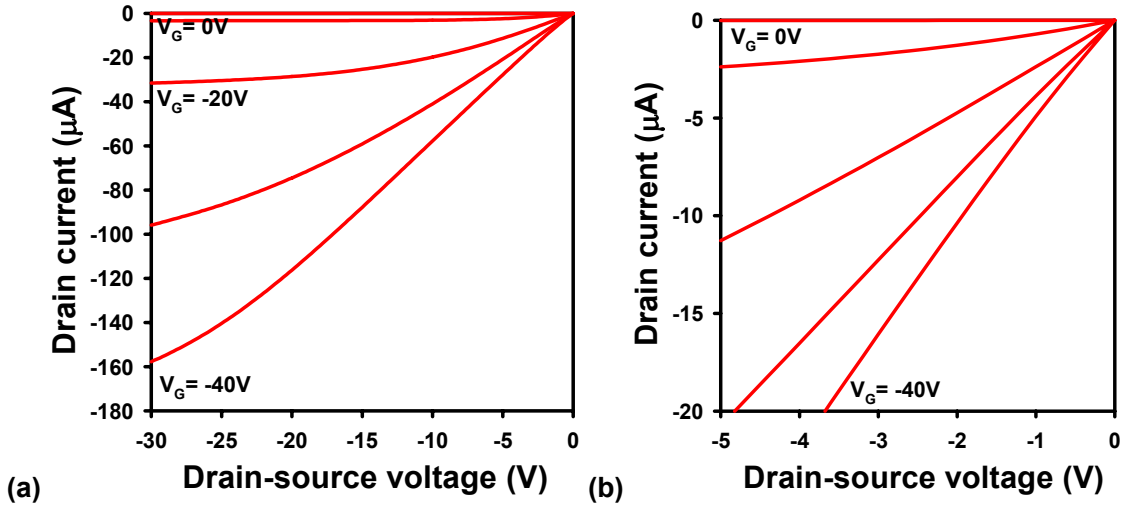

Figure 2-2**: (a) Output characteristics (I_D-V_{DS}) of a p-type TFT. (b) A blow-up of the linear region for small V_{DS}.**

The charge accumulated at the surface or the inversion layer charge is a function of the gate-to-source voltage V_{GS}. The magnitude of the drain current, I_D, up to the point where it saturates can be calculated by incremental integration, and the current-voltage

relationship is well documented elsewhere [Borkan and Weimer 1963]. It is shown that for a TFT biased in the linear region of operation, $V_{DS} < V_{GS}-V_T$, I_D varies as in Eq. **2.5.**

$$I_D = \frac{W\mu\varepsilon_O\,\varepsilon}{2Lt}\left[2(V_{GS}-V_T)V_{DS} - {V_{DS}}^2\right] \qquad (\mathbf{2.5})$$

where V_T is the threshold voltage, ε_o is the permittivity of free space, ε is the relative permittivity of the gate insulator, t is the thickness of the gate insulator, and all other terms remain as previously defined.

We can extract transconductance, g_m, and field-effect mobility, μ, in the linear region using the differentiation of Eq. **2.5**, and get Eqs. **2.6** and **2.7** .

$$g_m = \left(\frac{\partial I_D}{\partial V_{GS}}\right)_{V_{DS}=small,const.} = \frac{W\mu\,\varepsilon_o\,\varepsilon}{Lt}(V_{DS}) \qquad (\mathbf{2.6})$$

$$\mu = \frac{g_m\,L\,t}{W\,\varepsilon_o\,\varepsilon}\left(\frac{1}{V_{DS}}\right)_{V_{DS}=small,const.} \qquad (\mathbf{2.7})$$

Since at the knee (onset of drain current saturation) $V_{DS} = (V_{GS} - V_T)$ and the current remains substantially constant beyond the knee, the saturated drain current is given by Eq. **2.8.**

$$I_D = \frac{W\mu\,\varepsilon_o\,\varepsilon}{2Lt}\,(V_{GS}-V_T)^2 \qquad (\mathbf{2.8})$$

According to Eq. **2.8** we can express the field-effect mobility of carriers in the saturation region as Eq. **2.9**. Figure **2-3** shows the transfer characteristics ($\sqrt{I_D}$-V_{GS} and I_D-V_{GS}) of a TFT. This is a common way of extracting saturation mobility from the slope of the square root of drain current, $\partial\sqrt{I_D}\big/\partial V_{GS}$, as a function of V_{GS}.

$$\mu = \frac{2Lt}{W\,\varepsilon_o\,\varepsilon}\left(\frac{\partial\sqrt{I_D}}{\partial V_{GS}}\right)^2 \qquad (\mathbf{2.9})$$

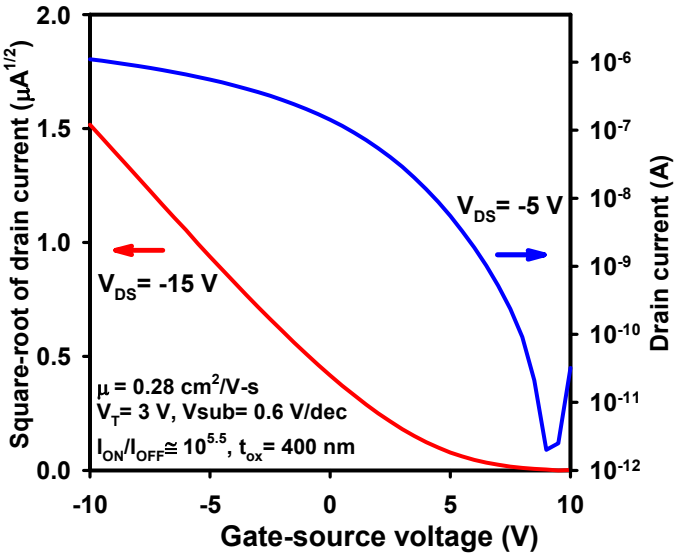

Figure 2-3**: The transfer characteristics ($\sqrt{I_D}$-V_{GS} and I_D-V_{GS}) of a TFT.**

The transconductance, g_m, in the saturated region is obtained by differentiating Eq. **2.8** and expressed by Eq. **2.10** .

$$g_m = \frac{\partial I_{Dsat}}{\partial V_G} = \frac{CW\mu}{L}(V_G - V_T) = \sqrt{\frac{2CW\mu}{L}}\sqrt{I_{Dsat}} \qquad \textbf{(2.10)}$$

Contact Resistance

In addition to the channel resistance of a TFT modulated to act as a switch, the contact resistance, also called peripheral resistance, often has equally significant effect on device performance. This is particularly true in organic thin-film transistors where contact resistances are very large. For low-level injection from an "ohmic" contact into a semiconductor or insulator, the current changes linearly with voltage across the contact and follows Ohm's law. This however may not be valid when the density of injected charge surpasses the intrinsic carrier concentration at a large bias voltage in OTFTs. Nevertheless, we still write it as Eq. **2.11** for low-level injection.

$$J = q\, n_o\, \mu \left(\frac{V}{L} \right) \qquad (\mathbf{2.11})$$

where J is the current density, q is electron charge, n_o is the intrinsic carrier density, μ is the carrier mobility, V is the applied voltage, and L is the separation between contacts.

These contact resistances can be included into Eq. **2.5** for the linear region where $V_{DS} < V_G - V_T$. Equation **2.12** gives the new relationship for I_D as a function of V_{DS} in the linear region of operation with the effect of series source and drain resistance R_{SD}:

$$I_D = \frac{W}{L} \frac{\varepsilon\, \varepsilon_o}{t} \mu\, (V_{GS} - V_T - 0.5 V_{DS}) \left(V_{DS} - I_D R_{SD} \right) \qquad (\mathbf{2.12})$$

where all terms remain as previously defined.

Defining the measured resistance R_m as V_{DS}/I_D for small V_{DS} gives the following relationship in Eq. **2.13** .

$$R_m = R_{ch} + R_{SD} \approx \frac{L}{W\, C_{ox}\, \mu (V_{GS} - V_T)} + R_{SD} \qquad (\mathbf{2.13})$$

where R_{ch} is the channel resistance and all terms remain as previously defined [Schroder 1998].

The normalized contact resistance R_C as a function of V_{GT} can be used to evaluate the performance of the contact to the organic active layer, where R_C is defined by Eq. **2.14** . Typical R_C characteristics of pentacene TFTs using bottom contacts have been published in several journal articles [Gundlach, Jia 2001; Klauk, Schmid 2003; Necliudov, Shur 2003].

$$R_C = \frac{R_{SD}}{2} W \qquad (\mathbf{2.14})$$

In OTFTs this contact resistance is often very large and comparable to the magnitude of the channel resistance. As a result, the device performance is often limited by its contact resistance.

In general, the electrical characteristics of an OTFT can be understood by a typical TFT model of inorganic semiconductors. Although the mechanisms of carrier transport are very different between inorganic and organic semiconductors, both types of TFTs have the same current-voltage relationships in the linear and saturation regions. In addition, OTFT circuits can be analyzed by the conventional circuit theory and simulated by the same software.

2.3 **Pentacene OTFTs**

Pentacene OTFTs are representative of the OTFT technology. Large effort on fabricating organic thin-film transistors using small-molecule organic semiconductors has been reported by Garnier, Jackson, and their collaborators [Lin, Gundlach 1997; Garnier 1998]. OTFTs using pentacene as the active material have been of great interest because of their superior device performance compared to other organic semiconductors, particularly their large field-effect mobility typically > 1 cm^2/V-s [Gundlach, Lin 1997; Lin, Gundlach 1997]. Such high performance is attributed to the electronic transport of pentacene films due to their high molecular ordering. Many studies point out that the morphology of vapor-deposited pentacene films on various substrates is dependent on deposition conditions and substrate conditions. Examples are the deposition rate, surface roughness, substrate temperature, surface preparation, surface chemistry, and surface energy. Here we report a few key steps in fabricating high performance pentacene OTFTs.

Pentacene, one of the conjugated polyacenes, is a p-type small molecule organic semiconductor consisting of five fused aromatic rings as illustrated in Figure **2-4**. It was reported three decades ago that pentacene powders at room temperature show high electrical conductivity, as high as 0.1 ohm-cm under high pressure even though it is insulating under ambient pressure [Rang, Haraldsson 2001]. Increased attention to pentacene OTFTs started in mid-1990s when its outstanding device performance was reported [Lin, Gundlach 1996; Gundlach, Lin 1997]. The large potential for pentacene

TFTs for electronics was then demonstrated with a variety of logic circuits and flat panel displays.

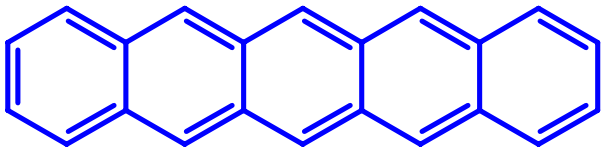

Figure 2-4**: Pentacene molecule.**

The purification of commercially available pentacene (from TCI) in powder form is necessary, and it is also difficult to obtain readily and cheaply. Impurities from the synthesis procedures or material degradation often coexist in the pentacene powders because pentacene is not soluble in most organic solvents; consequently, it is not possible to purify using multiple recrystallization processes from solution. This is responsible for its high material price and impracticality of using solution processing. The 6 and 13 positions of a pentacene molecule are more reactive. When pentacene is exposed to both ultraviolet light and oxygen, photostimulated electrons can transfer to oxygen and promote the formation of a linked dimer or an oxidized pentacene such as shown in Figure **2-5** [Maliakal, Raghavachari 2004]. These impurities result in molecular defects and trapping states in molecular crystals or thin films, which degrade the electronic transport. Thus, vacuum temperature-gradient sublimation at 300 ºC was used to purify pentacene twice.

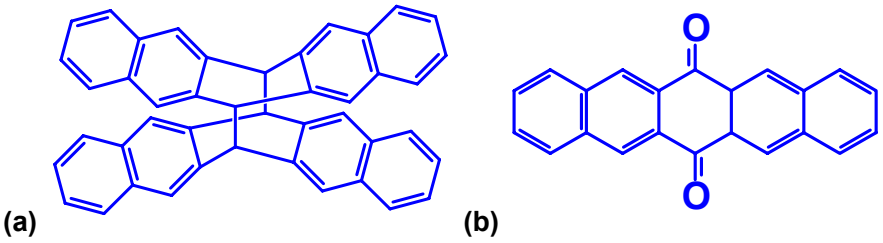

Figure 2-5**: Impurities often found in pentacene: (a) pentacene dimer and (b) quinone.**

Pentacene Deposition

Deposition of small molecule organic semiconductors in vapor phase is the most common technique to deposit the active layer of an OTFT. Devices with field-effect mobilities > 0.1 cm^2/V-s, which are suitable for applications can be achieved, with pentacene thin films deposited by thermal evaporation, molecular beam epitaxy, pulsed laser deposition, and organic vapor jet printing (OVJP). However, thermal evaporation is often preferred for its low-cost, convenience, and primarily the highest device performance.

Pentacene films are thermally deposited at a deposition rate between 0.1 to 1 Å/s, measured with a crystal monitor (density ~ 1.3 g/cm^3) onto substrates held at a temperature between 30 °C and 110 °C. Figure **2-6** is a diagram showing a thermal evaporator equipped with multiple filament buses dedicated for depositing organic materials. The deposition is carried out at a base pressure of about 5×10^{-7} torr and to avoid cross contamination one evaporator is loaded exclusively with pentacene for fabricating high performance transistors.

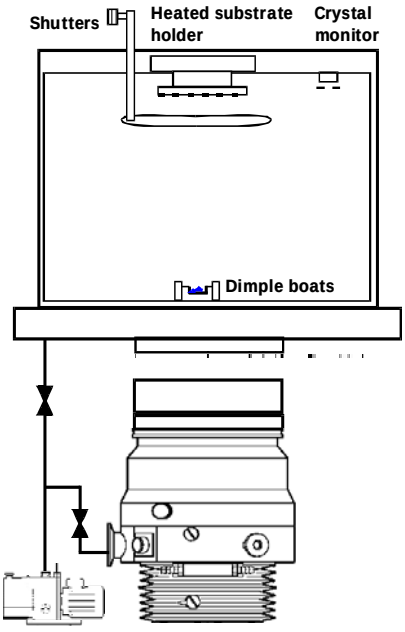

Figure 2-6**: Thermal evaporator for depositing organic semiconductors.**

Deposition rate has a strong influence on the morphology of pentacene films. Studies have reported on films and their OTFT performance using deposition rates that range from less than 0.1 Å/s to larger than 3 Å/s (also called flash deposition). It is possible to obtain pentacene OTFTs with moderate field-effect mobilities (> 0.5 cm^2/V-s) using a deposition rate from 0.1 to 1.0 Å/s. X-ray diffraction (XRD) analysis and atomic force micrographs indicate that pentacene films consist of more ordered crystalline grains when a lower deposition rate and an elevated substrate temperatures between 25 ºC and 90 ºC are used. In addition, we found from AFM measurements that more explicit molecular terraces in molecular crystals of vapor deposited-pentacene are obtained when a slower deposition rates (< 0.5 Å/s) are used as shown in Figure **2-7**. The OTFT performance is greatly improved in terms of the field-effect mobility > 1 cm^2/V-s, where at a low deposition rate ~ 0.4 Å/s high-performance pentacene devices are obtained.

The two AFM micrographs in Figure **2-7** show the influence of the deposition rate on the film morphology. These two pentacene films with an average thickness of 30 nm were deposited on a thermally oxidized silicon substrate held at 90 ºC at rates of 1.0 Å/s and 0.5 Å/s, respectively. In Figure **2-7a**, the film consists of smaller dendritic grains and doesn't have any noticeable coordination across grains. These grains are terraced, but the terraces are more closely packed compared to the film deposited with a lower deposition rate as shown in Figure **2-7b**. Because the latter film has large terraced grains, it may have a larger long-range ordering inside each molecular crystal, thus, improving the electronic transport. [Hiremath, Varney 2004]

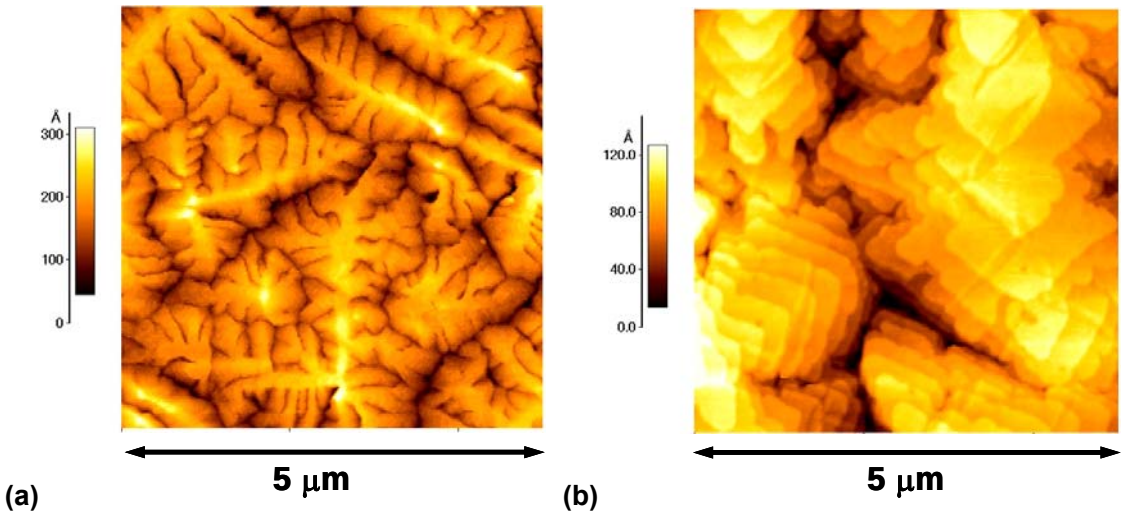

Figure 2-7**: Two 5 μm × 5 μm atomic force microscopy images of 50 nm thick pentacene films deposited on thermally oxidized silicon substrates held at 90 ºC, using deposition rates of (a) 0.5 Å/s and (b) 2-3 Å/s. The morphology and terraces of these dendritic grains are different.**

In addition, the correlated orientation of facets across grains suggests a structural association between grains where the two lines in Figure **2-8** indicate that the orientation of facets between adjacent grains are almost parallel to each other. One can infer from this that coordination may be induced from the first few bottom layers in which case, it indicates that a long-range ordering across molecular crystals exists and can assist carrier transport. This also suggests that the meaning of so-called grain boundary in this type of pentacene films should be revised.

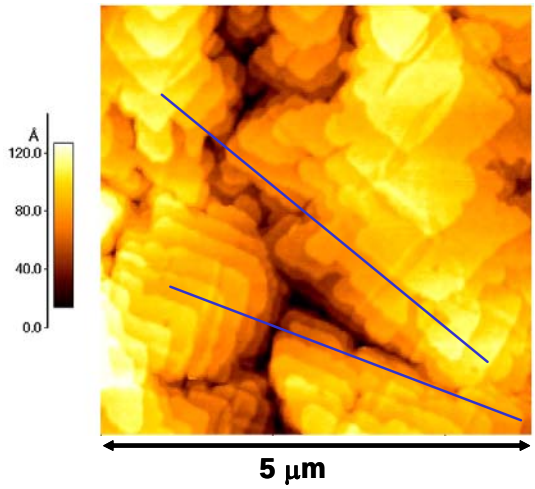

Figure 2-8**: A 5 µm × 5 µm atomic force microscopy image of 50 nm thick pentacene films deposited on thermally oxidized silicon substrates held at 90 ºC, using deposition rates of 0.5 Å/s.**

However, using ultra-low deposition rates (< 0.1 Å/s) does not lead to higher OTFT performance, but often the opposite. A few studies of pentacene film growth using a very slow deposition rate reported that not only do the films grow into well-ordered molecular crystals, but also that its growth follows an acknowledged nucleation model in the first four molecular layers. This would suggest that there is a similarity in crystal growth in the thermal evaporation of organic and inorganic materials [Ruiz, Nickel 2003; Ruiz, Nickel 2003]. Although molecular ordering was detected in these films, their device performance is not improved. So the relationship between film morphology and its electrical properties is still not understood. Consequently, there is great continuous interest in studying growth and understanding of pentacene films [Horowitz 1998; Haas, Haase 2004; Meyer, Heringdorf 2004].

Pentacene Molecular Crystals

Molecular ordering in thin-films of small organic semiconductors is critical to the performance of OTFTs. Many small molecule organic semiconductors of interest have a

strong tendency to form ordered molecular crystals using vapor deposition, where pentacene is a good example.

Pentacene usually forms three-dimensional large dendritic grains micron in size for vapor-deposited thin films on smooth silicon oxide surfaces. At a deposition rate of about 0.5 Å/s, an arriving pentacene molecule has a relatively high surface mobility on smooth dielectrics because the interactive force between the adatom and the dielectric surface is weak. Such high surface mobility allows adatoms to diffuse to a preferred site and grow into dendritic grains of a herring bone structure. Figure **2-9** is a 2.5 μm × 2.5 μm micrograph of pentacene molecular crystals obtained by atomic force microscopy (AFM). The molecular terraces in the grain have step-heights of approximately 1.5 nm. Because this height corresponds to the length of a pentacene molecule, thus it suggests that the long axis of pentacene molecules is almost perpendicular to the substrate surface.

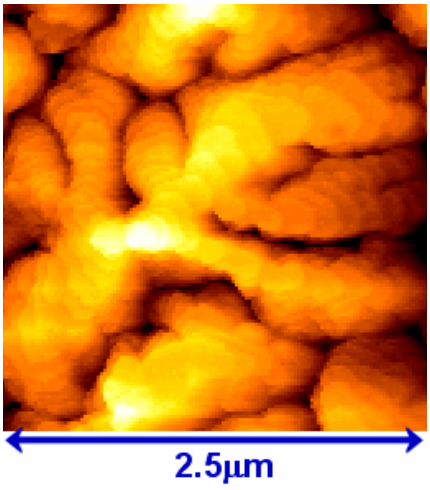

Figure 2-9**: A 2.5 μm × 2.5 μm AFM micrograph of a 50 nm pentacene thin film with dendritic molecular crystals on SiO_2.**

X-ray diffraction is a simple method to evaluate molecular ordering present in pentacene films deposited on thermally-oxidized silicon wafers or other types of surfaces deposited at different substrate temperatures and deposition rates. Figure **2-10** shows the θ-2θ X-ray diffraction scan (Cu Kα radiation with the diffraction vector aligned perpendicular to the substrate surface) for a pentacene film with an average thickness of

500 Å, deposited at a rate of 0.5 Å/s onto a chemically modified oxidized silicon substrate held at 60 ºC. The plane spacing of this pentacene film, as calculated from 001' peak, is about 15.5 Å in agreement with the result from the AFM micrographs.

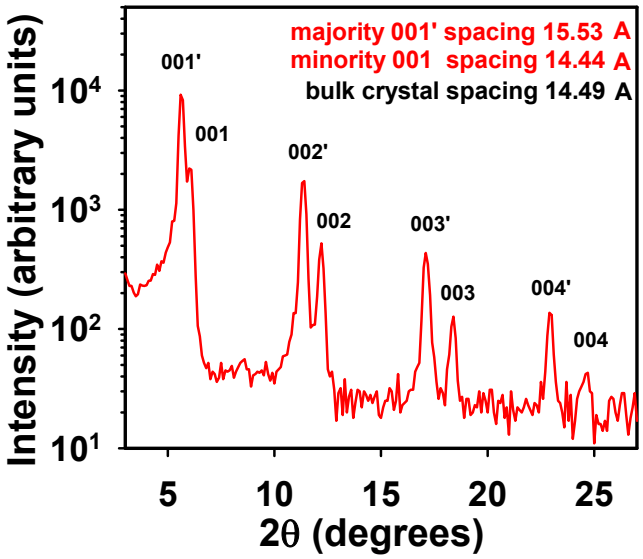

Figure 2-10**: θ-2θ x-ray diffraction scan of a 50 nm thick pentacene film deposited on thermally oxidized silicon with OTS treatment, held at 60 ºC.**

The organic molecular crystal of pentacene has a low symmetry crystal structure – triclinic due to the large asymmetry of the molecule. The crystal structure and lattice parameters of pentacene are listed in Table **2-3**. The single crystal pentacene has a 001 plane spacing of 14.49 Å that corresponds to the plane spacing of the minority 001 peak, which is associated with the bulk phase portion of the film in Figure **2-10**.

Table 2-3**: Crystal structure parameters for pentacene [Campbell, Robertson 1992].**

crystal parameter	pentacene
crystal structure	triclinic
a (Å)	7.90
b (Å)	6.06
c (Å)	16.01
α (degree)	101.9
β (degree)	112.6
γ (degree)	85.8
unit cell volume, V($Å^3$)	692
molecules/unit cell, z	2
space group	P1
density, d (g/cm^3)	1.30
molecular weight, M	278.36

Typical pentacene OTFTs can be obtained when those key conditions are met in addition to a clean, smooth gate dielectric and appropriate electrodes. Devices on silicon dioxide with top or bottom electrodes often have field-effect mobilities of 0.5 ± 0.1 cm^2/Vs. Figure **2-11** shows the electrical characteristics of a pentacene OTFT obtained by thermal evaporation onto silicon dioxide and patterned source and drain electrodes. The device has a field-effect mobility of 0.45 $cm^2/V\text{-}s$, a subthreshold slope of 3 V/decade, a threshold voltage of 11 V, and the on/off current ratio is about $10^{6.5}$.

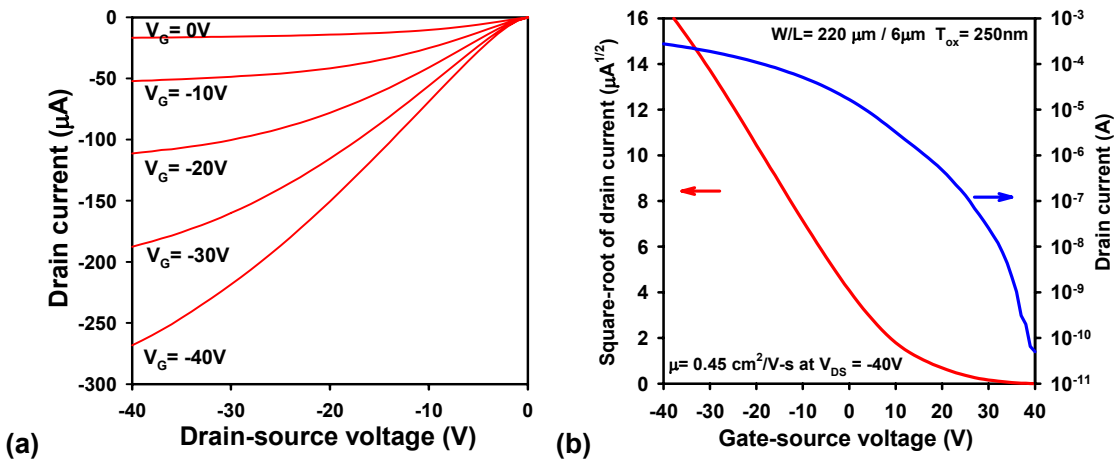

Figure 2-11**: Electrical characteristics of a pentacene OTFT with a field-effect mobility of 0.45 cm^2/V-s on thermally grown silicon dioxide: (a) output characteristics (I_D-V_{DS}) and (b) transfer characteristics ($\sqrt{I_D}$-V_{GS} and I_D-V_{GS}). (W / L = 220 μm / 6 μm, t_{ox} = 250 nm, pentacene thickness= 50 nm, T_{sub}= 60 °C).**

Pentacene OTFTs with this level of performance would have been utilized in real applications. However, these pentacene OTFTs have several stability problems. For example, the threshold voltage can shift tens of volt toward a more positive voltage upon the exposure to moisture or oxygen. In addition, the subthreshold slopes become less steep and the operating voltages dramatically increase. Because the film's adhesion to the bare silicon dioxide is not strong, some delamination also occurs. Thus, to achieve improvement an investigation of the interface between the gate dielectric and the pentacene films was carried out.

2.4 **High Performance Pentacene OTFTs**

The growth and morphology of pentacene films are greatly related to the properties of the surface on which pentacene molecular crystals nucleate and grow. It was found that the chemical modifications of gate dielectric or source/drain electrodes can improve the carrier transport and injection and thus yielding higher performance.

2.4.1 **Chemically Modified Gate Dielectrics**

Surface Modification using Silane Coupling Agents

The silane coupling agent, a surface-processing technique, can produce a uniform layer of well-organized organic molecules. Because it is necessary to have a smooth gate dielectric with little or none of aggregated silane clusters, an approximately silane monolayer is preferred. The term self-assembled monolayer (SAM) refers to a monolayer formation from the reaction of molecules and the surface in a solution such as a silane solution. In describing the processing techniques, the term Langmuir-Blodgett films (LB films) is commonly used to denote a molecular monolayer or multilayer transferred from the water-air interface (or liquid-gas interface) onto a solid substrate. This silane agent often has two major ends, which and allows separated reactions and interactions with each targeting surface. Once coated with a silane layer the surface properties are modified and these are associated with the outer silane layer.

After this surface treatment, the surface chemistry becomes associated with the surface group and the nature of the organic molecules. Because the surface energy is modified, contact angle measurements are an easy and quick method to estimate the surface energy. It has been widely reported that such surface energy difference cause many variations in the molecular structure in a pentacene thin film, and can lead to a large improvement of transistor performance when using a suitable processing technique and a given organic silane. Here we briefly introduce the basic working principles and their effects on the surface.

Silanes are hybrids of silica and of organic materials, expressed as $X_mSi(RY)_n$ as illustrated in Figure **2-12**, where organofunctional groups (R) and hydrolyzable groups are linked by stable silicon-carbon bonds. These organofunctional groups (R), including surface groups (Y), are selected to react with or to be compatible with the adjacent layer. Meanwhile, those hydrolyzable groups (X) proceed to alcoholysis, acylation, or hydrolysis reactions with mineral surfaces and bonding silane molecules to these mineral surfaces. Here we mainly rely on the hydrolysis reaction, which can occur on hydrated

silicon dioxide, aluminium oxide, or silicon nitride surfaces as well as organic surfaces with -OH reactants.

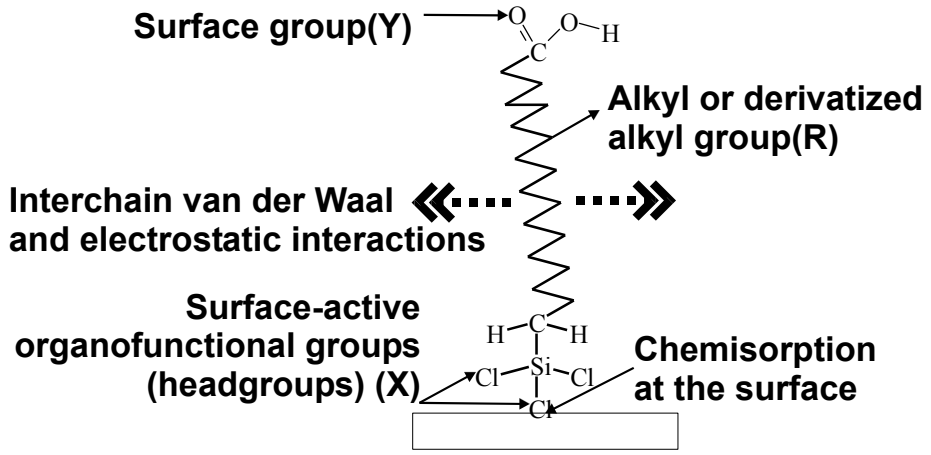

Figure 2-12**: A schematic view of a silane molecule.**

The hydrolysis reaction means that a hydrolyzable group (X) hydrolyzes with a water molecule and forms a silanol with the oxide surface. This silanol is linked by the strong Si-O-M bonds that can not be easily broken by organic solvents, heat, or water. For example, on the silicon dioxide surface with physically and chemically absorbed water, an n-octadecyltrichlorosilane (OTS), $CH_3(CH_2)_{17}SiCl_3$, will hydrolyze into $CH_3(CH_2)_{17}Si(OH)_3$, which subsequently reacts with other three Si-OH groups nearby. This results in three silanols, Si-O-Si, at the head of $CH_3(CH_2)_{17}Si(OSi)_3$. These three silanols can bond the OTS molecule to either another OTS or the silicon dioxide. Under properly controlled conditions, silane molecules will ultimately condense to siloxanes (Si-O-Si). Figure **2-13** illustrates the reaction diagram and the corresponding chemical equations. Therefore, the hydrolyzable group controls how a silane molecule bonds to the substrate surface and the microstructure of the self-assembled layer.

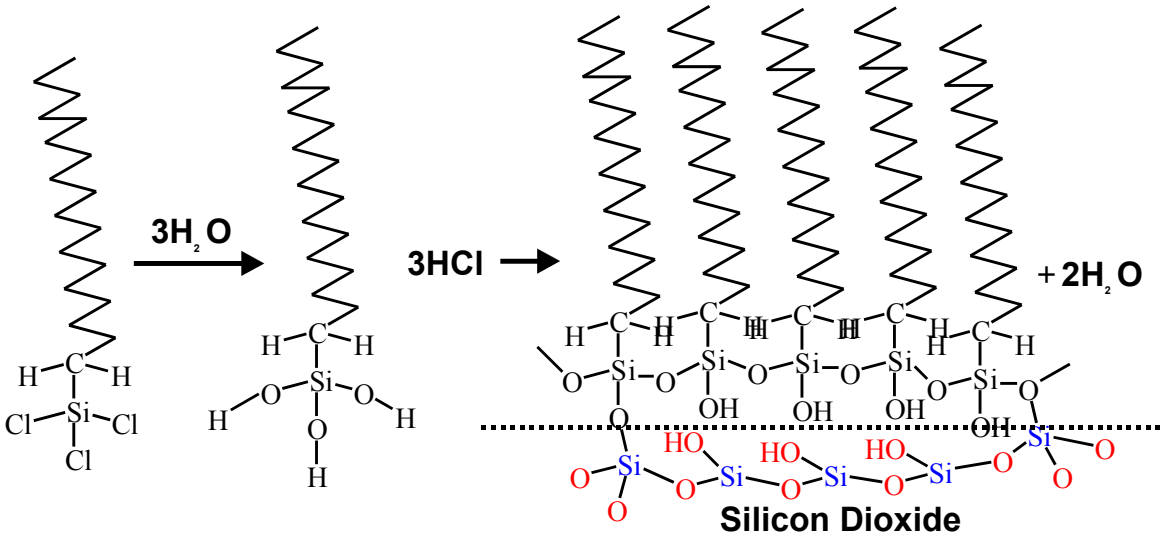

$$CH_3(CH_2)_{17}SiCl_3 + 3\ H_2O \rightarrow CH_3(CH_2)_{17}Si(OH)_3 + 3\ HCl$$

$$CH_3(CH_2)_{17}Si(OH)_3 + 3\ SiOH_{(solid)} \rightarrow CH_3(CH_2)_{17}Si(OSi)_{3(solid)} + 3\ H_2O$$

Figure 2-13: **The reaction diagram and chemical equations of OTS molecules on silicon dioxide.**

The surface group's (Y) and the organic layer's properties dominate the final surface properties, where the self-assembly molecules diffuse to and bind to the surface. The alkyl group, R, begins to interact when the molecule density increases and the intermolecular interaction becomes very strong. Such kinetics can have an affect on the final micro structure of the layer [Ulman 1991; Carraro, Yauw 1998]. Ultimately, the surface group, Y, can determine the surface condition, although only the organofunctional group participates in the chemisorption process. For instance, surfaces can sustain a high temperature after being treated with haloalkylsilane consisting of halogen elements in the organofunctional group. Unsaturated silanes, with carbon-carbon double bonds, act primarily as coupling agents and chemical intermediates, which can connect to another organic functional group. Alkoxysilanes can form a condensed monopolar layer with very low surface energy. Because OTS is widely studied and is often used in our device fabrication, more detailed information is presented here.

OTS in the organic solution readily forms a dense, ordered self-assembly monolayer on silicon dioxide with a strong Si-O-Si network between the OTS molecules.

In an almost anhydrous organic solution, such as a mixture of hexadecane and chloroform at 3 : 1 ratio, the chlorine side groups turn into –OH groups and HCl when reacting with H_2O on the oxide substrates [Angst and Simmons 1991; McGovern, Kallury 1994]. The high reactivity of the OH groups results in an extended network through interchain crosslinking. For well-ordered OTS layers, the substrate r.m.s. surface roughness can be reduced or preserved due to partial tethering of the OTS molecules to the silicon dioxide surface. Approximately one to two fifths OTS molecules directly bond to the silicon dioxide surface with the remaining OTS molecules bonded through interchain crosslinking [LeGrange and Markham 1993].

In addition to achieving the smooth surface of the gate dielectric, the surface energy is dramatically reduced by the CH_3 surface group and partially by the long alkyl chain. Contact angle measurements indicate a clean hydrophilic silicon dioxide surface ($\theta_{H2O} \approx< 5°$) can be made very hydrophobic by surface modification using OTS ($\theta_{H2O} > 95°$). Such a measurement, first proposed by Thomas Young in 1805 [Young 1805], is a reliable and easy method to measure the surface wettability and surface energy. By putting a constant volume of water on a solid surface, a drop is formed under the mechanical equilibrium of the three surface tensions seen in Figure **2-14** : γ_{LV} at the interface of the liquid and vapor phases, γ_{SL} at the interface of the solid and the liquid and γ_{SV} at the interface of the solid and vapor. The contact angle (θ) measured from the side view of this drop on the solid surface is defined as the angle between the radial line and the tangential line at the edge of the water drop (P). Therefore, the equilibrium condition can be described by Eq. **2.15**.

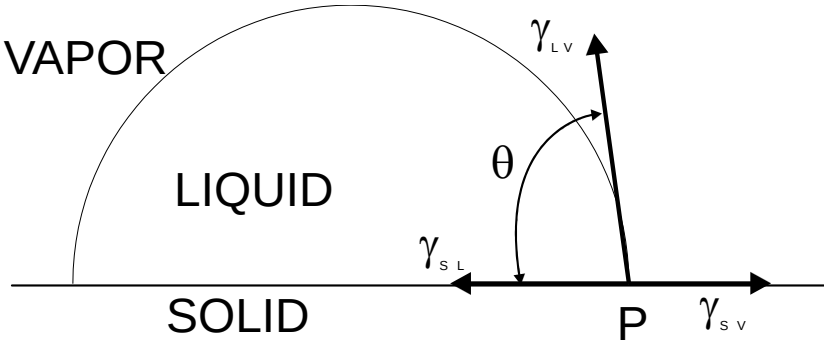

Figure 2-14**: A sessile drop's schematic in contact angle measurement. The vector γ_{LV} is parallel to the drop's tangent.**

$$\gamma_{SV} - \gamma_{SL} = \gamma_{LV} \cos\theta \qquad (\mathbf{2.15})$$

Table **2-4** is a list of surface energies and contact angles for common surfaces [Lide 2004]. From this table, it is possible to verify the change in the surface energy due to the silane treatment.

Table 2-4: The surface free energies (surface tension) of materials and their contact angles by water at 20 °C.

Solid surface or solvents	Surface energy Dynes/cm	Contact angle (H_2O)
silicon dioxide	> 100	< 5
OTS on SiO_2	22	> 95
Teflon FEP	< 18.5	> 108
hexane	24	-
H_2O	71.8	-
pentacene film	NA	~ 45
SiO_2 in storage	NA	30 - 45

Silane Treatment Methods

Surface preparation, surface chemistry, surface energy, and surface roughness all have a strong influence on pentacene film formation, but these factors are not

independent. For example, surface chemistry is often associated with the surface energy. Larger nucleation density and smaller grains in pentacene films are often found on a substrate with high surface energy or large surface roughness. On atomically smooth substrates with a low surface energy, pentacene tends to nucleate films with large, extended, and possibly coordinated grains. Thus, a reliable technique of yielding large dendritic grains with ordered molecular crystals that results in high device performance is crucial. We use silane coupling agents to chemically modify the surface chemistry and surface energy of gate dielectric without any tradeoff due to surface roughness.

Silane coupling agents (SCAs) have been widely used for surface modification [Ulman 1991, 1998; Gelest 2000]. The kinetic chemistry is based on the dehydrating reaction between hydroxyl groups on both reactants in solution. For example, a trichlorosilane molecule has three highly reactive chlorine side groups and results in three hydroxyl groups upon the contact with moisture. Many gate dielectrics have or can be induced to have hydroxyl groups on the surface such as silicon oxide or polymers, and they readily react with hydroxyl groups on silane molecules. With controlled experiments it was possible to radically change the surface chemistry and surface energy of smooth silicon dioxide without increasing the surface roughness. The quality of the silicon dioxide/pentacene interface modified by silane coupling agents (SCAs) was then investigated. Treatments using alkoxylsilanes with various lengths of hydrocarbon chains, such as octadecyltrichlorosilane (OTS), were found to improve the field-effect mobility, reduce the subthreshold slope, and yield devices with reproducibly smaller threshold voltages. We extensively studied this OTS treatment, using it as representing the typical effect of SCAs.

A reproducible OTS solution treatment requires a suitable substrate preparation, humidity control, a proper reaction time, and purified OTS. A controlled surface preparation includes the removal of particles and organic contaminants and the restoration of dense -OH groups. To achieve this oxygen plasma or UV ozone treatments were utilized. Due to three high reactive chlorine head groups, the moisture was controlled to be about 5 ppms by carrying out the experiments in a glovebox and the use of anhydrous solvents. We selected a mixture of hexadecane and carbon tetrachloride at

3:1 ratio, and about three hours of immersion in an OTS solution of 2 volume % (~ 10^{-3} molar). An immediate rinse by a dry solvent was carried out in the glovebox to remove excess OTS solution from the sample, which was then repeated several times.

With the three reactive hydroxyl head groups, converted from the trichlorine group, OTS reacts with the –OH groups on the surface and results in an extended monolayer network through interchain crosslinking. This often called self-assembled monolayer (SAM). In this SAM dependent on the processing conditions OTS molecules are tilted between 5 º and 30 º from the normal [LeGrange and Markham 1993; Brzoska, Azouz 1994; Bierbaum, Kinzler 1995]. It has a thickness of about 2.5 nm, a hydrophobic CH_3 terminated surface, and a r.m.s. surface roughness < 3 Å as shown in Figure **2-15a**. Surface energy is greatly reduced to about 22 dynes/cm ($\theta_{H2O} \sim 110°$), as verified by contact angle measurements. This roughness is slightly larger than the 1.5 Å of a high-quality silicon dioxide, but it is smooth enough for controlled pentacene deposition.

Although OTS is expected to form a high-quality monolayer on the exposed silicon dioxide surface, sometimes impurities and small particles consisting of polymerized OTS in the commercially available OTS (purity ~ 95–98 %) could aggregate in the solution or on the substrate surface. Figure **2-15b** shows that these particles increase the surface energy ($\theta_{H2O} < 90°$) and r.m.s. roughness (> 5 Å). Although the contact angle of water indicates that the roughened surface remains hydrophobic, this degree of roughness can have a substantial effect on the growth and performance outcome of the pentacene films. Thus, the use of distilled OTS is often necessary to assure a high-quality OTS SAM, and it adds to the processing complexity. This also indicates the importance of controlling the moisture concentration in the solution and on the substrate as well as the processing time.

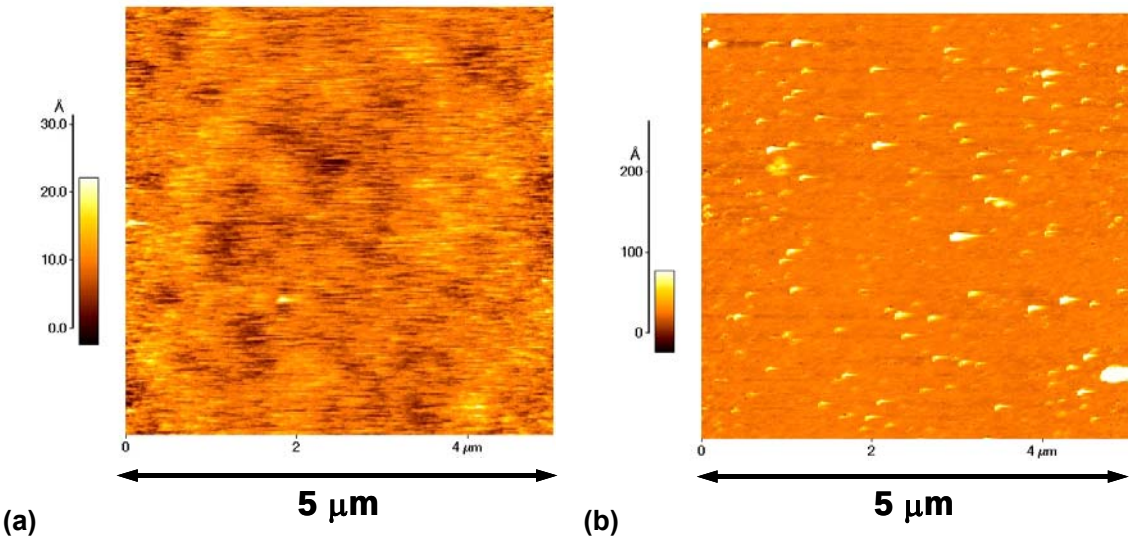

Figure 2-15: AFM micrographs of (a) carefully treated OTS surface with r.m.s. roughness < 3 Å and (b) falsely treated OTS surface with r.m.s. roughness > 5 Å.

Studies of the properties of OTS monolayers have been reported, which include those of the molecular structure and orientation, the molecule density on the surface, and the chemical bonding ratios [Ulman 1991]. In addition, because water absorption also has a strong influence on pentacene devices, the amount of water at the interface of OTS and pentacene is of interest. It was found that the major location of the absorbed water on a few alkyl silane layers, including OTS, is the defect region of these monolayers [Thomas, Rudich 1999]. Further research is required to quantify such correlation.

A silane coupling agent can also be applied through the vapor phase as an alternative way which provides some processing flexibility. One example is using vapor prime hexamethyldisilazane (HMDS) to promote the resist's adhesion by preventing water's penetration into the interfaces present in photolithography, where multiple HMDS layers are deposited. Another advantage of using a vapor prime treatment for this process is to preclude the substrate from direct exposure to the organic solvents in an OTS solution. This prevents the swelling of the flexible polymeric substrates, organic gate dielectrics as well as polymeric patterns. However, more controlled and optimization are necessary to yield a smooth, hydrophobic OTS monolayer, and thus, this

was investigated to develop a processing method for fabricating organic electronic devices.

Figure **2-16** shows the schematics of the vapor prime oven for OTS. To avoid OTS condensation on the walls, substrates, or vacuum lines, the system uses a hot-wall design, where all components exposed to the OTS vapor subsequent to the cold trap are heated to a designated temperature. The OTS source in liquid form is placed inside the system. In principle an independent hot-wall OTS vapor source and a water vapor source would allow more flexible and controlled processing. For the vacuum system's long-term operation it is necessary to protect it from the HCl from the chlorine groups' hydrolysis and damages by polymerized OTS flakes, particularly the turbo molecular pumps.

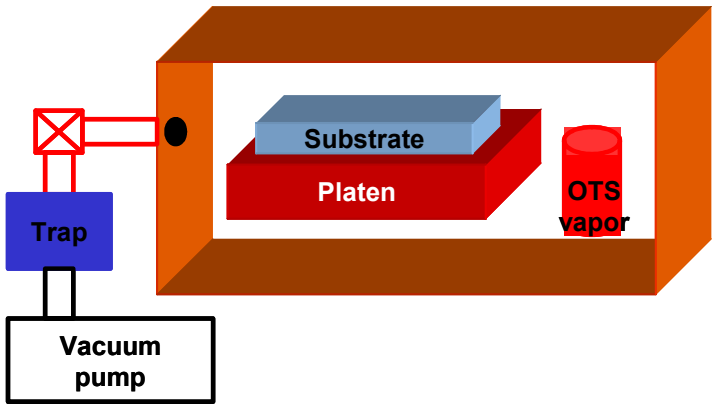

Figure 2-16**: Scheme of the vapor prime oven for OTS surface treatment.**

A low processing temperature is preferred for this vapor prime gate dielectric treatment, particularly in the case of polymeric substrates. Since only one OTS layer is needed, the required OTS vapor pressure can be low but the boiling point of OTS hasn't been reported. There have been three reports on its vapor pressure ~ 0.075 torr at 155 ºC and ~ 3 torr at 185 ºC, but there is disagreement in the data [United-Chemical-Technologies 1993; Parikh, Schivley 1997]. In addition, the corresponding temperatures are too high to process either polymeric substrates or novalac resists that are of interest, such as polyethylene naphthalate (PEN) and polyester (PET).

An experiment was carried out to measure OTS's vapor pressure at 100 ºC. Figure **2-17a** shows the measured pressure of a vacuum oven as a function of pumping time when the oven is maintained at 100 ºC with OTS supplied from a hot liquid in a bottle. The vacuum line was turned off after five minutes and the system pressure rose from the contribution of the vaporized OTS molecules and the leakage. By assuming that the system has a constant leak rate that is fitted by the red straight line, the vapor pressure of OTS is estimated as ~ 0.18 torr at 100 ºC. Because the surface is rapidly bombarded by gas molecules, 180 mtorr of the OTS vapor is enough for growing a monolayer of OTS. Moreover, because the OTS vaporization is analogous to a distilled OTS source, the issues caused by the impurity and polymerized OTS particles in the liquid is avoided. We found that with carefully controlled vapor prime OTS a good reproducibility and can be obtained.

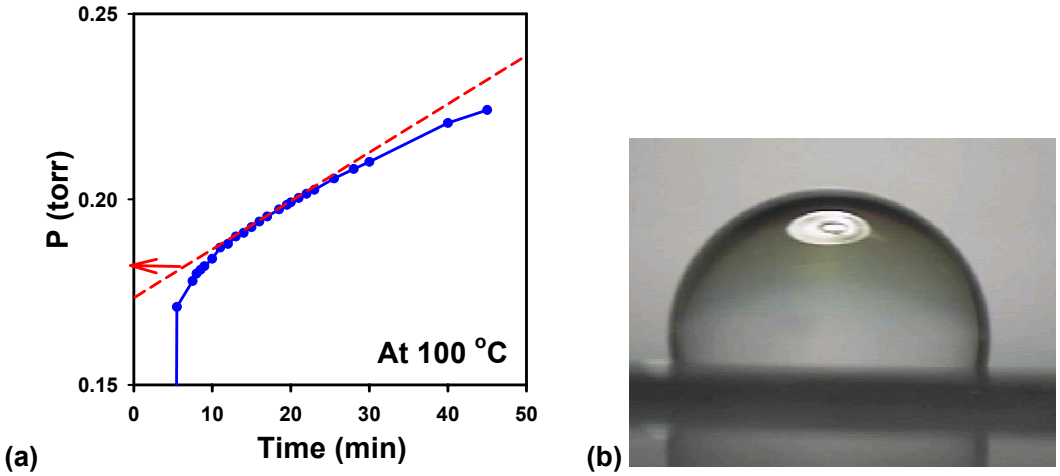

Figure 2-17**: (a) Pressure in a vacuum oven with OTS vapor source; (b) contact angle of H_2O on vapor prime OTS using 100 ºC baking.**

In such vapor prime OTS process, substrates and an OTS liquid source are loaded together when the oven remains at 100 ºC. The system is pumped down and maintained at < 10 mtorr for 15 minutes by a mechanical pump and a molecular dragging pump. Then, the system pressure is balanced at 55 mtorr for two hours using a dry nitrogen purge. Both OTS condensation on the substrate and excess moisture leakage from the ambient have to be prevented, otherwise OTS polymerization and surface roughening

will occur. Prior to venting the oven, another purge is introduced to remove excess OTS vapor and residual gases, after which a rinse in isopropyl alcohol is carried out [Gelest 2000].

The surface properties of such a vapor prime OTS layer have been established as suitable for the gate dielectric. The surface energy of vapor prime OTS is low with contact angles of water, θ_{H2O}, > 95 ° as shown in Figure **2-17b**. Figure **2-18** shows the uniformity and low r.m.s. roughness ~ 1.50 Å of a treated silicon dioxide substrate. In this case the thickness of the OTS layer measured with a spectroscopic ellipsometer is about 2 nm and thinner than the 2.5 nm obtained with a solution treatment. All these properties suggest that the criteria necessary for pentacene OTFT fabrication have been satisfied.

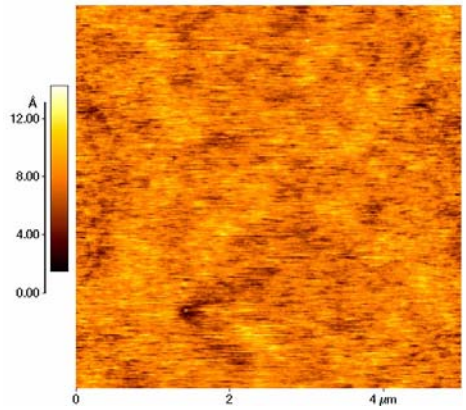

Figure 2-18**: 5 µm × 5 µm AFM micrograph of vapor prime OTS with r.m.s. roughness ~ 1.5 Å.**

OTFTs consisting of a few other types of small molecule organic semiconductors also perform better when they are vapor deposited on hydrophobic surfaces [Garnier 1998]. Based on these results, this vapor prime OTS method can be adapted in processing of different types of gate dielectrics for pentacene OTFTs as well as other organic semiconductor devices.

Pentacene Films on Chemically-Modified Gate Dielectrics

The morphology of a thin pentacene film is altered by this dramatic difference in surface energy or chemistry. This is illustrated with results shown in Figure **2-19** on two silicon dioxide substrates, where one substrate was modified by OTS, and become a smooth hydrophobic surface. A 5-nm pentacene film is deposited on each substrate under the same conditions (at a deposition rate ~ 0.5 Å/s and at a substrate temperature ~ 75 ºC). The AFM micrograph in Figure **2-19a** shows that on the controlled substrate, pentacene grows continuously in the Stranski-Krastanov type over a large area with expected more than one nucleation center, and only some voids. On the other hand, in Figure **2-19b** pentacene film is three-dimensional with more discontinuity and a large portion of voids. Because the smoothness in these voids is similar to that of silicon dioxide, they correspond to the exposed substrate. A large portion of the area has pentacene film as thick as equivalent to three or four molecular layers. A closer review of the AFM micrograph of a larger area shows that the connectivity over tens of μms exists between these curled grains, and the inter-grain connection might be also improved through thicker grain boundary (about three layers of pentacene in this film).

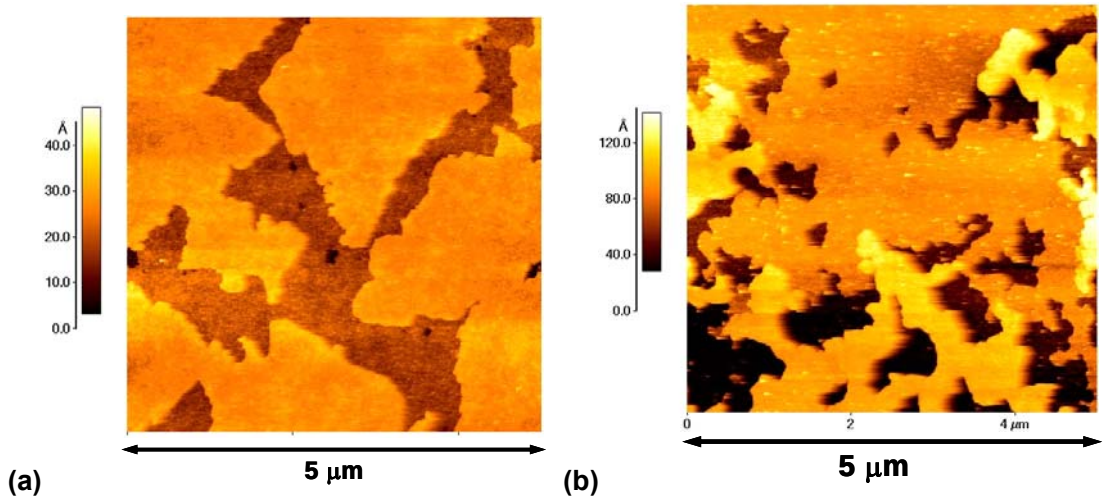

Figure 2-19**: AFM micrographs of two 5 nm thick pentacene films with deposition rate ~ 0.5 Å/s and T_{sub} = 75 ºC (a) on hydrophilic SiO_2 and (b) on hydrophobic SiO_2 surface with OTS treatment.**

The surface roughness of OTS surfaces has a strong effect on the morphology and OTFT performance of thick pentacene films. Using different processing conditions, OTS surfaces have different levels of roughness as seen in Figure **2-15**. Such levels of differences change the outcome of the pentacene thin films. Figure **2-20a** shows a typical dendritic, terraced pentacene film on a smooth, hydrophobic OTS surface. Pentacene TFTs based on this type of film have large field-effect mobilities ~ 1 cm^2/V-s. On the other hand, Figure **2-20b** shows that the film has many small, irregular pentacene grains on a rough OTS surface. Device performance from this films is poor (mobility < 0.1 cm^2/V-s). These results suggest that the essential requirement of the smooth OTS surface for fabricating pentacene TFTs with large mobilities.

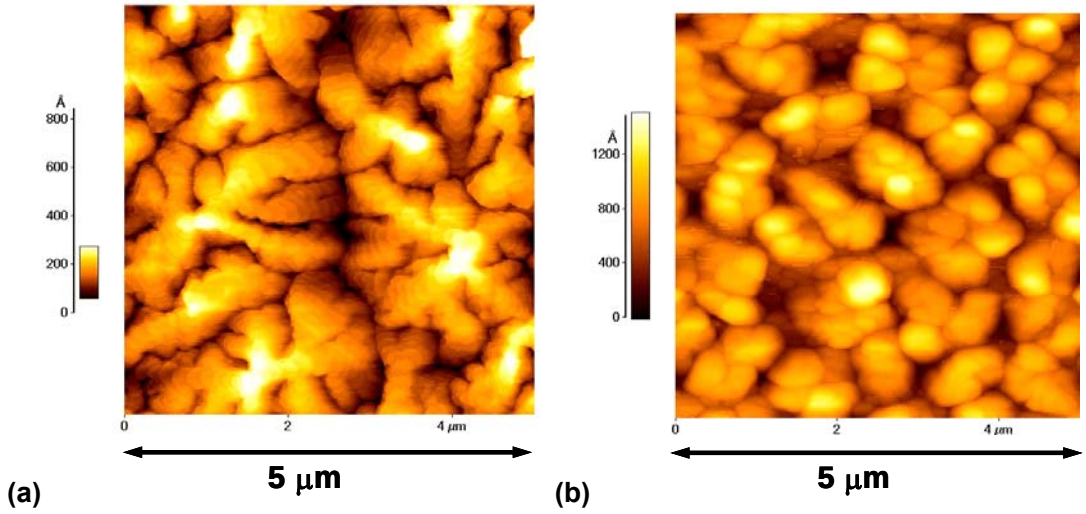

Figure 2-20**: AFM micrographs of two 50 nm pentacene films on (a) smooth "good" and (b) rough "bad" OTS with substrates held at 75 ºC.**

On a smooth vapor prime OTS surface the morphology of a pentacene thin film is similar to that on a smooth OTS surface. The AFM micrograph in Figure **2-21** shows that in a pentacene film of 50 nm on a vapor prime OTS surface, the dendritic grains are μm in sizes and molecular terraces are present in another high resolution image. Such reproducible results suggest that pentacene thin films deposited on vapor prime OTS surfaces can be used to achieve high-performance OTFTs. Indeed, field-effect mobilities larger than 1 cm^2/V-s were obtained in these pentacene TFTs, and this process has been

utilized to fabricate the first active matrix LCD driven by pentacene TFTs on polymeric substrates [Sheraw, Zhou 2002].

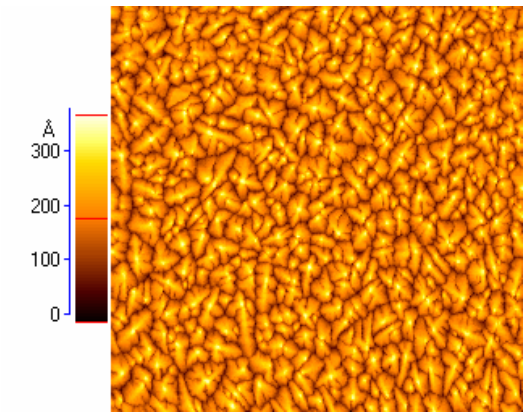

Figure 2-21**: 20 µm × 20 µm AFM Micrograph of 50 nm pentacene on a silicon dioxide substrate treated with vapor prime OTS.**

2.4.2 **Pentacene OTFTs on Silane Surfaces**

The yield and reproducibility of pentacene TFTs with mobility > 1 cm^2/V-s are improved by obtaining a reproducible OTS monolayer on gate dielectric. Based on pentacene thin films deposited at a low deposition rate on a smooth, hydrophobic gate dielectric, the largest saturation field-effect mobility of pentacene OTFTs exceeds 2 cm^2/V-s. Figure **2-22** shows the electrical characteristics of an OTFT with a pentacene thin film of 50 nm on silicon dioxide of an n-type heavily doped silicon wafer. Silicon dioxide of 250 nm and the silicon wafer served as the gate dielectric and the gate electrode, respectively. It was fabricated with top gold contacts, channel lengths L of 30 µm, and a channel widths W of 220 µm. Because this device uses evaporated gold as the source and drain electrodes, the output characteristics have a concave linear region that is often associated with proper carrier injection as depicted in Figure **2-22a**. It also has a typical saturation region where the current is linearly proportional to the square of $(V_{GS}-V_T)$.

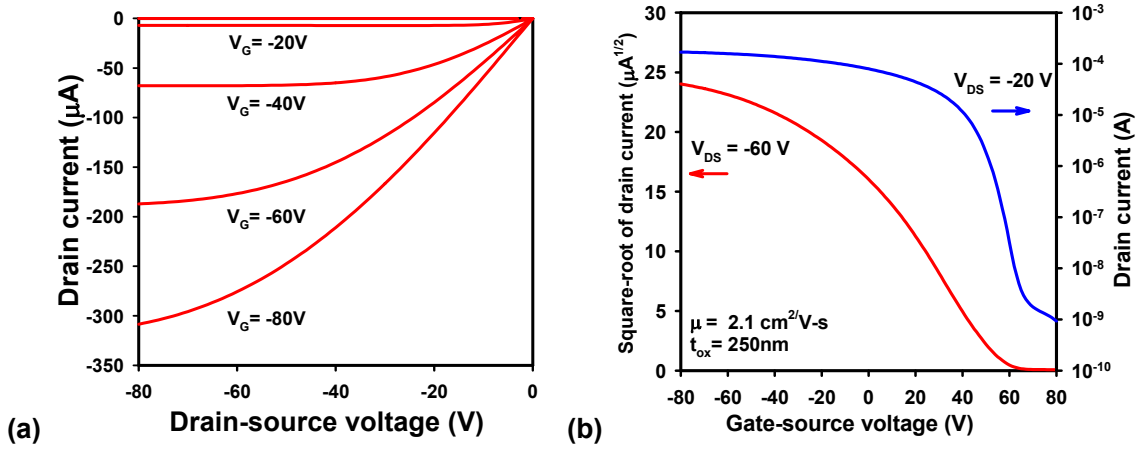

Figure 2-22: Electrical characteristics of a pentacene OTFT with a field-effect mobility of 2.1 cm^2/V-s on thermally grown silicon dioxide: (a) output characteristics (I_D-V_{DS}) and (b) transfer characteristics ($\sqrt{I_D}$-V_{GS} and I_D-V_{GS}). (W / L = 220 μm / 30 μm, t_{ox} = 250 nm, pentacene thickness= 50 nm, T_{sub}= 60 °C).

From the electrical transfer characteristics in Figure **2-22b**, a carrier mobility of 2.1 cm^2/V-s is extracted for this device. To our knowledge, this is the largest field-effect mobility reported for any organic thin-film transistor at the time when this sample was fabricated. We note that the off current of this device is near 10^{-9} A because an OTFT with shadow-masked top contacts often has poor isolation and leakage from the ungated area. The on/off current ratio for this device is near $10^{5.5}$, and the subthreshold slope is 3.5 V/dec. Using a gate dielectric with an OTS layer can improve the subthreshold slope from about 5 V/decade on silicon dioxide to a between 0.6 and 3 V/decade. This reduces the circuits' operating voltage and power consumption, and greatly enhances the practicality of such devices.

The threshold voltage is critical in the OTFT operation, but so far very little control over it has been possible to achieve. In Figure **2-22** the extracted threshold voltage of 54 V is indicated when a large gate-source voltage (V_{GS}) of ±80 V is applied. In general, large variations in the mean values of the threshold voltages occur among a group of OTFTs on either the same or different samples. Also when these pentacene OTFTs are operating continuously, additional deviation of threshold voltage is induced. An important advantage of using OTS is that it results in more stable threshold voltages,

where such drift is drastically reduced. However, an effective method for stabilizing and/or controlling the threshold voltages is still not available, thus, making it one of the major obstacles in OTFT applications.

The pentacene TFTs fabricated on a vapor prime OTS layer have a comparable device performance to that fabricated on a solution-processed OTS layer. Figure **2-23** shows the electrical characteristics of a pentacene TFT with the same device geometry as that in Figure **2-22**. The extracted saturation field-effect mobility is 1.3 cm^2/V-s, the threshold voltage of 18 V, and the on/off current ratio of $10^{4.5}$. The device parameters in such OTFTs are not distinguishable from those on solution- processed OTS layers. Thus, the vapor prime OTS process is a reliable method for chemically treating the gate dielectric in pentacene TFT fabrication.

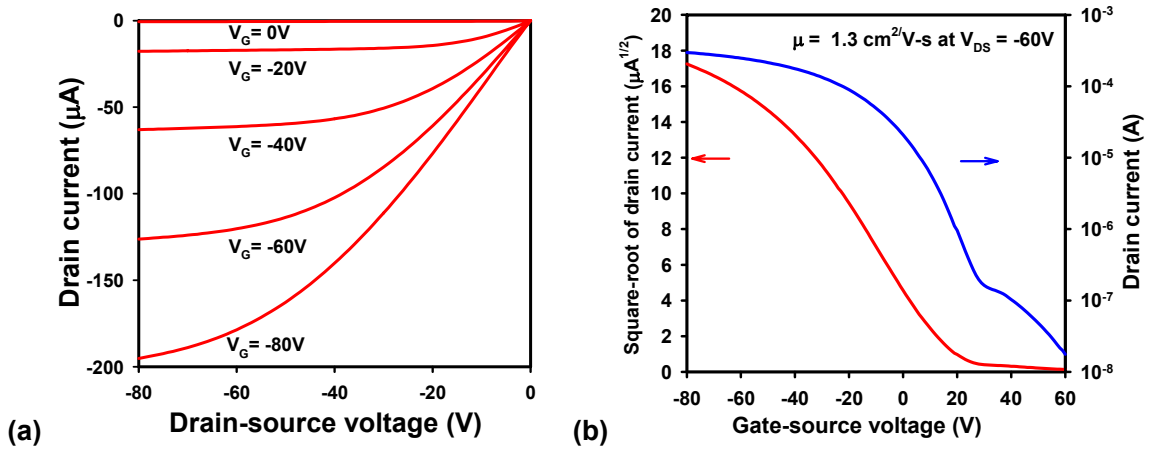

Figure 2-23**: The (a) I_D-V_{DS} and (b) $\sqrt{I_D}$-V_{GS} characteristics of a pentacene OTFT with gold bottom contacts, vapor prime OTS on silicon dioxide gate dielectric of 250-nm. The device has a channel width (W) of 221 μm and a channel length (L) of 31 μm. (Tsub= 60 °C Mobility μ= 1.3 cm^2/V-s at V_{DS} = -60 V, V_{th}= 18 V, I_{ON}/I_{OFF}= $10^{4.5}$).**

Therefore, using OTS treatments results in several fold improvement of field-effect mobilities. The reproducibility of a smooth OTS layer is improved by using anhydrous solutions or vapor prime in a vacuum oven.

2.4.3 **Source / Drain Contacts with a Thiol Layer**

Contacts play a very important role in device operation and the reduction of contact resistance is important in improving the linear region operation. Among several methods for improving charge injection into OTFT active layers, one is the introduction of a layer of thiol-based charge exchange materials that can bond to the source and drain electrodes and serve as an electron acceptor. The sulfur atom of the thiol molecule can form a dipolar bond to most noble metals that immobilize the charge withdrawing molecule. Such materials give a stable and effective method for "doping" the source and drain contacts. As a result, the effect of increasing the charge carrier density near the contact metal/organic active layer interface and reducing the width of the barrier can improve charge injection. Although many candidates for electron acceptor molecules such as cyano (CN) containing compounds, aromatic nitro (NO_2) compounds, and quinones can act as dopants, empirical comparisons of several thiols were made and applied in solution-processed OTFTs in Chapter 4.

2.4.4 **Limitations in Pentacene OTFTs**

The device structure of pentacene OTFTs limits the fabrication processes and the limits their performance. One example of such a limitation is the low carrier injection efficiency of bottom source / drain contacts. A typical OTFT used in several applications is shown in Figure **2-24a**. Such an OTFT has an inverted device geometry, having a gate electrode (~ 50 nm), a gate dielectric (~ 300 nm), and the source and drain contacts (~ 100 nm) all covered by the pentacene active layer. Because the electrical field of the gate electrode is shielded by the source and drain electrodes, where the pentacene film are not conductive, the carrier injection only replies on the edge of the channel region. Such a line contact causes the difficulty in making a low-resistance bottom contact to a pentacene OTFT. Because the typical contact resistance is large and comparable with its channel resistance, current crowding happens and the device performance is limited [Gundlach, Jia 2001]. In addition, source and drain bottom contacts must be resistant to

oxidation and other chemical effects before the pentacene deposition. For metals, this limits the choices to Pt, Pd, and Au, which are stable, high work function metals. Thus, the performance of such a pentacene TFT is limited by the contacts and the whole choice is also limited by the subsequent processing of the pentacene.

Pentacene OTFTs using top contacts have the advantage that lower contact resistances can be achieved. Because the contact resistances of these devices are in the GΩ-μm range, it is often comparable to or surpassing the channel resistance when the pentacene active layer is turned on by a gate bias and the modulation of the drain current is carried out. Thus, the device performance is often contact limited [Gundlach, Jia 2001; Klauk, Schmid 2003]. Figure **2-24** shows the two different device structures and compares their corresponding current-voltage characteristics. In the case of the bottom contacts the larger contact resistance suppresses that of the drain current at small V_{DS} and results in a concaved curve seen in the blown-up plot of Figure **2-24b**. On the other hand, OTFTs with top contacts exhibit linear regions which clearly show the improved nature of the contacts which lead to better device performance.

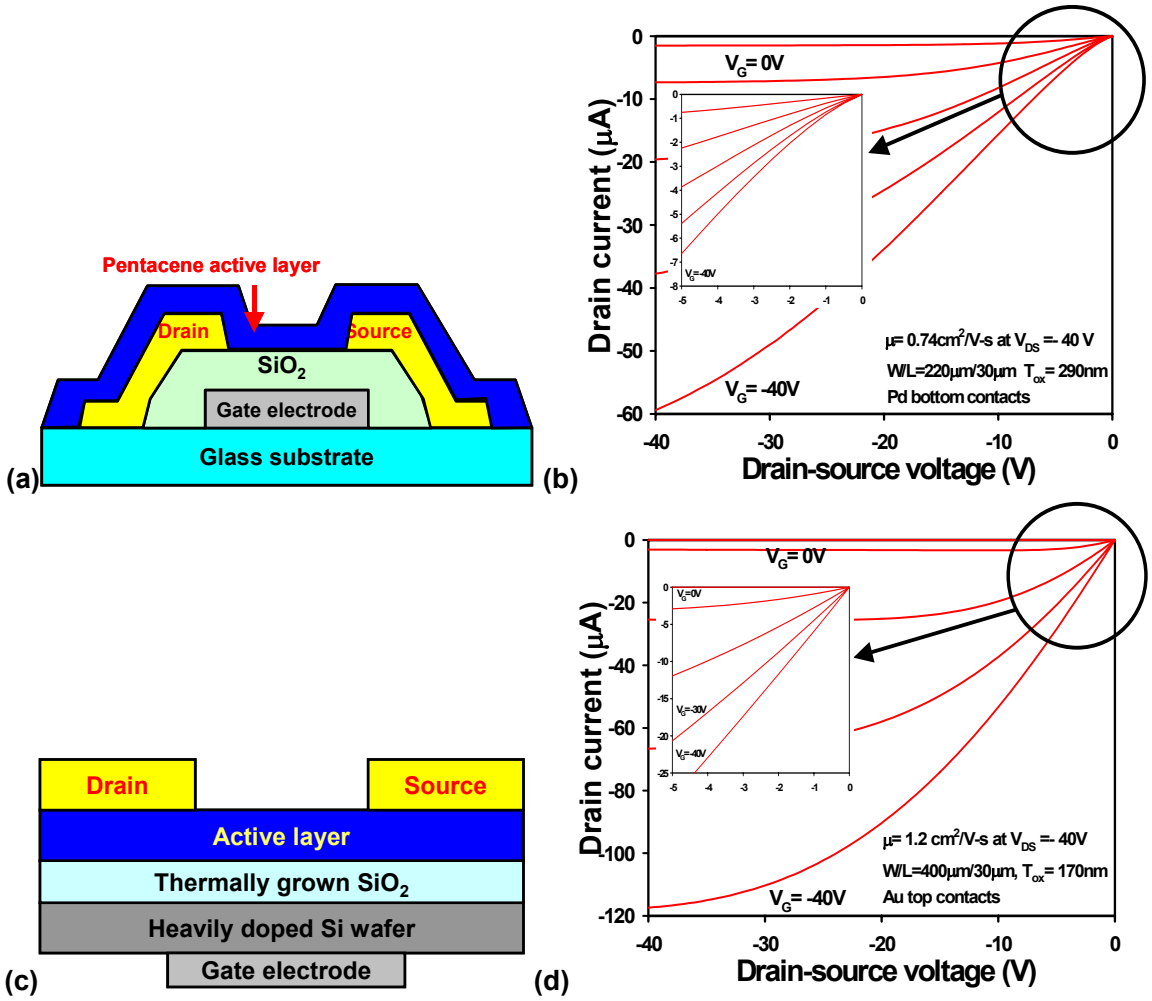

Figure 2-24: The scheme on the left are OTFTs with either (a) bottom contacts or (c) top contacts and their correspondent I_D-V_{DS} characteristics in (b) or (d) on the right. The blowups of I_D at small V_{DS} show that the bottom contact device has a larger contact resistance in the linear region, which results in the concaved curves.

The process that requires the use of thermal evaporation of pentacene limits the ultimate cost saving that can be achieved using organic electronics. A solution-processable material and the development of such solution processing are the paths to large volume production at a lower cost. However, pentacene has a low solubility and cannot be solution-processed without using a precursor and a hot processing.

These issues are addressed in Chapter 3 and 4.

2.5 **Summary**

This chapter has presented the fundamental processes for fabricating high performance pentacene OTFTs. In addition to works which have been reported, such as source and drain electrode metals and gate insulators, these investigations in the deposition parameters and the surface treatments for gate dielectrics and electrodes allow fabricating high performance OTFTs for integrated applications possible.

The molecular ordering and the purity of pentacene are essential for high performance devices. This type of thin-film growth was achieved by using thermal evaporation at a low deposition of 0.1 – 0.5 Å/s. In most cases the degree of ordering can be characterized by AFM and XRD and distinguished by the dendritic grains, molecular terraces, and the interplanar spacing in ultra-thin or thin films.

Although device stability of OTFTs on silicon dioxide is poor and difficult to control due to poor adhesion and contaminant penetration at the interface, the chemical modification of the gate dielectric which reduces the surface energy by silane coupling agents can improve the stability and increase several fold the field-effect mobility as large as 2 cm^2/V-s. Developing such a reliable silane coupling agent processing in an anhydrous environment is of importance to achieve a higher reproducibility and increase the yield.

The development of these key processes and their understanding has led to the fabrication of pentacene OTFTs with a performance comparable to that of a-Si:H TFTs. This has then allowed the demonstrations of active matrix PDLC and OLED displays using OTFT backplanes to be carried out and emerged into the OTFT technology.

Chapter 3

Direct Photolithographic Top Contacts for OTFTs

Processing organic semiconductor thin films is a challenge in developing OTFT technology. Because of the fragility and complexity of these materials and then easily induced chemical interactions, many typical processes cannot be adapted to the OTFT fabrication without some solid, systematic exploration. Developing a photolithographic process to deposit electrodes on these materials is one of the challenges.

A variety of alternative methods for depositing or attaching top contacts on the active layer are possible but not preferred [Bao, Feng 1997; Loo, Willett 2002; Brandon, West 2003]. Examples include silicon membrane masking, shadow masking, and inkjet printing, mainly for laboratorial research. These are often complicated, having a limited resolution or a degrading of device performance; such methods consequently lead to undesirable restrictions. Using OTFT technology for flat panel display applications requires a convenient, high-resolution (< 10 μm channel resolution) lithographic process for top contacts; such a key process which may lead to improved contact, new fabrication, or new device structures, has not yet been demonstrated.

3.1 Solvent-Induced Degradations in Pentacene OTFTs

Processing organic semiconductor thin films, such as pentacene is problematic. Small molecule organic semiconductors and their OTFTs have fundamentally different physical, chemical, and material properties from those of inorganic crystalline or amorphous semiconductors and devices. The electrical properties of these organic films are sensitive to chemical effects during their fabrication; such effects include exposure to organic solvents, oxygen plasma, and resist developers. So many conventional photolithographic processes cannot be directly applied. One example is that a short exposure to oxygen plasmas or strong ultra violet light simply oxidizes or photo-

decomposes and removes the pentacene film rapidly, thereby degrading device characteristics. Most common resist developers are weak ionic base solutions that can dope the pentacene film, damage the gate dielectric interface, or cause film detachment. In spite of many failed attempts, the processibility of pentacene not only limits the fabrication processes but also the device geometry and device performance.

The exposure of pentacene thin films to an organic solvent can cause some micro-transformation in the material and dramatically degrade the electronic transport in the film. For example, when a pentacene thin film is exposed to isopropyl alcohol (IPA) or acetone, frequently used in photolithography, it undergoes transformations as seen in Figures **3-1** [Gundlach, Jackson 1999]. This is often attributed to the film's weak interaction with the substrate, a strong intermolecular interaction, or a strong interaction with organic solvents. As a result, it experiences dissolving, swelling, strain relaxation, or crystal phase transition. The volume of the bulked grains estimated is similar to the increase of volume due to the relaxation of crystal spacing. This indicates that these possible effects cause film detachment, cracks, or roughened morphology, and then dramatic degradation in device characteristics.

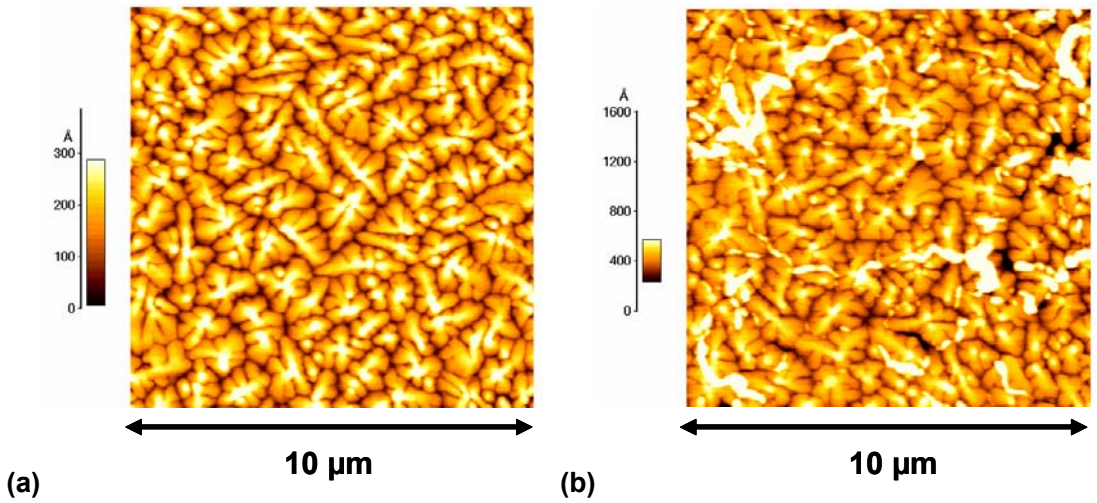

Figure 3-1**: 10 μm × 10 μm AFM micrographs of a pentacene thin film of 50 nm (a) as deposited and (b) IPA exposed. A few bulked, clustered grains indicate an explicit morphological transformation.**

The X-ray diffraction as seen in Figure **3-2** points out that the degree of the crystallinity and the inter-planar spacing between molecular layers of this pentacene thin film are altered by the solvent exposure. In spite of those high spikes in the AFM micrograph, most molecular crystals conformably transform from the "thin-film" phase into the bulk phase because of the indication of the minor decrease in the peak intensity. We tried to identify its driving force and verify three possible mechanisms of such uniform crystalline transformation: diffusion/swelling, solvent polarity, and the molecular size of solvents.

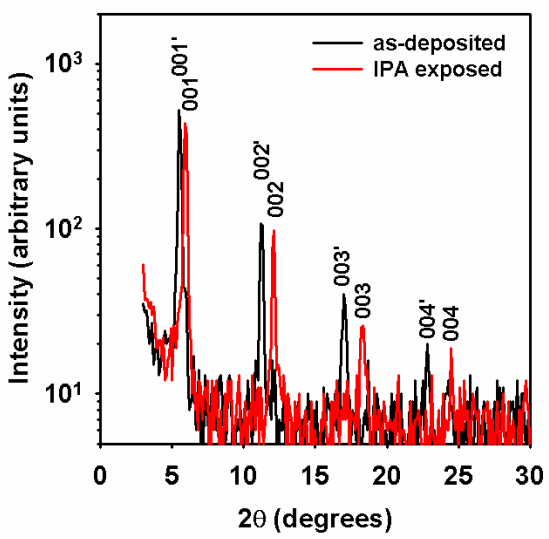

Figure 3-2**: The X-ray diffraction of a pentacene thin film as deposited (black line) and IPA exposed (red line). The peaks of the bulk and "thin-film" phases are denoted as 00x and 00x', respectively.**

Although the device degradation and the analysis of X-ray diffraction support pentacene molecular crystals in the thin film undergoing a crystallographic transformation, the driving force and mechanism are not clear. One possible reason is the swelling when an organic solvent is added onto the pentacene film. We used the following two methods and compared their results to verify this hypothesis: 1) real-time monitoring the degradation rate in the electrical properties due to the exposure to a solvent mixture that has various compositions; and 2) comparing these transitions and the solvent ratio.

The testing procedure is described here. We put down all three probes on source / drain bottom contacts and the gate electrode of a pentacene TFT and measured a set of initial device characteristics. A solvent drop is directly added on this TFT. Then, the semiconductor parameter analyzer is triggered to continuously test the device when the solvent is vaporizing. In case of the solvent with a high boiling point, the sample is baked in ambient air to remove the excess solvent and tested again.

In these solvent mixture experiments, we used water and an IPA mixture to test the association of TFT mobility and IPA ratio in volume %. We selected them for two

reasons: 1) IPA and water can be mixed uniformly over a large ratio range; and 2) water or moisture can reversibly reduce the device mobility and shift the threshold voltage to a more positive level. In fact, water by far is the only one known to be compatible with pentacene in wet processing.

Figure **3-3** shows the degree of degradation in terms of I_D-V_{DS} and I_D-V_{GS} electrical characteristics of a pentacene TFT. In this specific case, the same TFT was repeatedly tested continuously and damaged several times by the solution of IPA and water. The ratios of IPA to water were 1:10, 2:10, 3:10, 4:10, 5:10, and 15:10. We observed a dramatic change in the drain current when the IPA ratio surpasses 50 % (Here it is 60 %.)

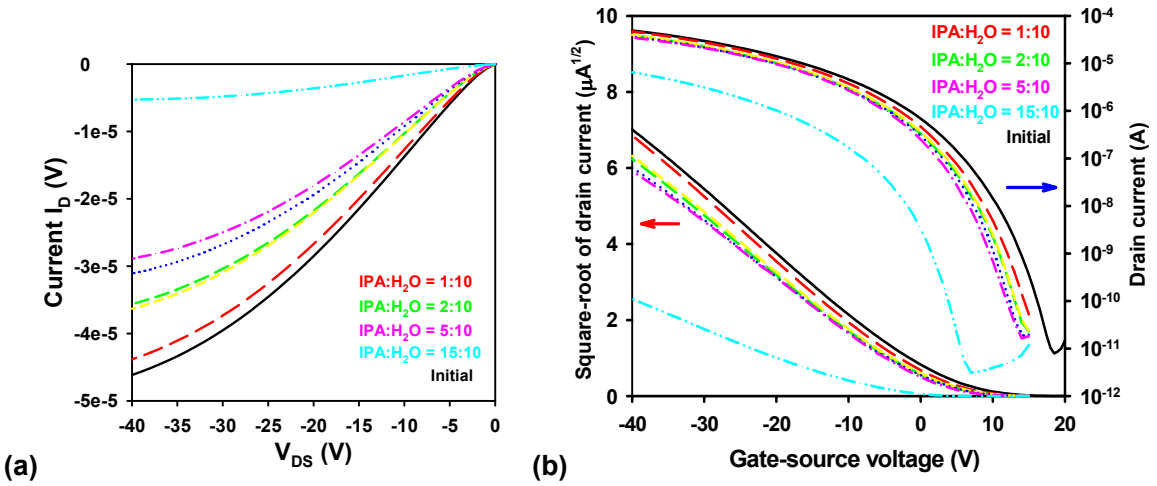

Figure 3-3**: (a) The I_D-V_{DS} characteristics of a pentacene OTFT exposed to IPA and water solutions with ratios of 1:10, 2:10, 3:10, 4:10, 5:10, and 15:10. Exposures started from the solution with a lower IPA concentration. (b) The corresponding $\sqrt{I_D}$-V_{GS} and log(I_D)-V_{GS} characteristics of (a) by color codes.**

Figure **3-4** shows the changes of the field-effect mobilities in the saturation region. When the IPA ratio is less than 30 %, the variation of the mobility in each solution exposure test is < 15 %. We also observed that when the IPA ratio is 40 %, the mobility still remains > 0.3 cm^2/V-s. Once IPA ratio reaches 50%, the mobility drops another 35 % and becomes 0.2 cm^2/V-s. The interaction between the solution and the pentacene thin film increases rapidly when the IPA volume ratio is over 50 %. This suggests that the intermolecular forces inside the solvent and between the solvent and

pentacene are important. The mechanism is likely to be swelling and experiencing a stress relaxation instead of dissolving or a chemical reaction.

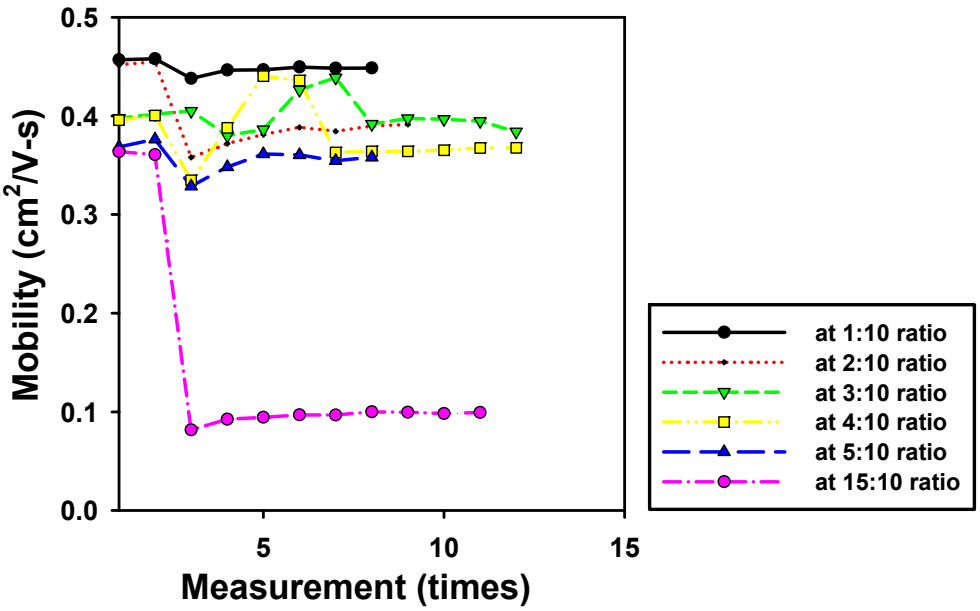

Figure 3-4**: The transition of the field-effect mobility of a pentacene OTFT prior to, during, and after six exposures to an IPA/water solution.**

Figure **3-5** shows the transition of threshold voltages and subthreshold slopes of this TFT. Again, the 60 % IPA solution causes a large change in both device parameters. The threshold voltages that drift from 1 V to -9 V and the moderately improved subthreshold slopes might be attributed to the increase in the density of deep trapping states and the decrease in the near-band edge after the displacement and relaxation of molecular crystals.

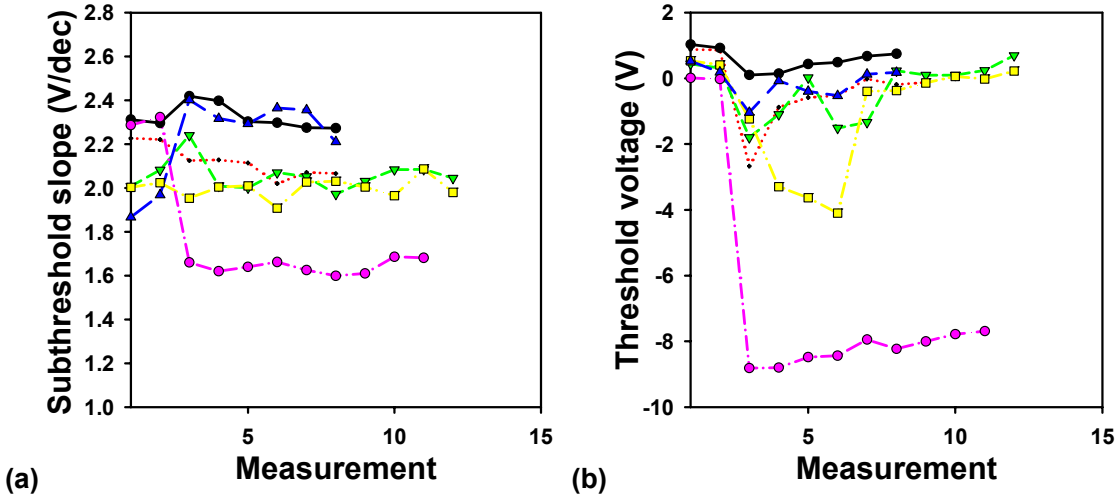

Figure 3-5**: The transition of (a) threshold voltages and (b) subthreshold slopes prior to, during, and after six exposures to an IPA/water solution. The figure's legends are the same as that in Figure** 3-4**.**

Solvent diffusion, lubricating, and swelling of the pentacene film might be the driving force of stress relaxation and phase transformation when it is exposed to a solvent. The IPA is a small molecule with a moderate polarity. Because it can form an aqueous solution with water, the rate and grade of diffusion and swelling is limited by the intermolecular force from water molecules when the IPA's concentration is low. However, when the IPA exceeds 50 % in the solution, this intermolecular constraint is not sustained and the diffusion rate increases greatly.

Figure **3-6** shows the correlation of the normalized mobility degradation and the IPA concentration. This curve suggests an abrupt drop in mobility at a threshold concentration around 45–50 %. This can be used as a reference for processing pentacene films when an IPA/water solution is used.

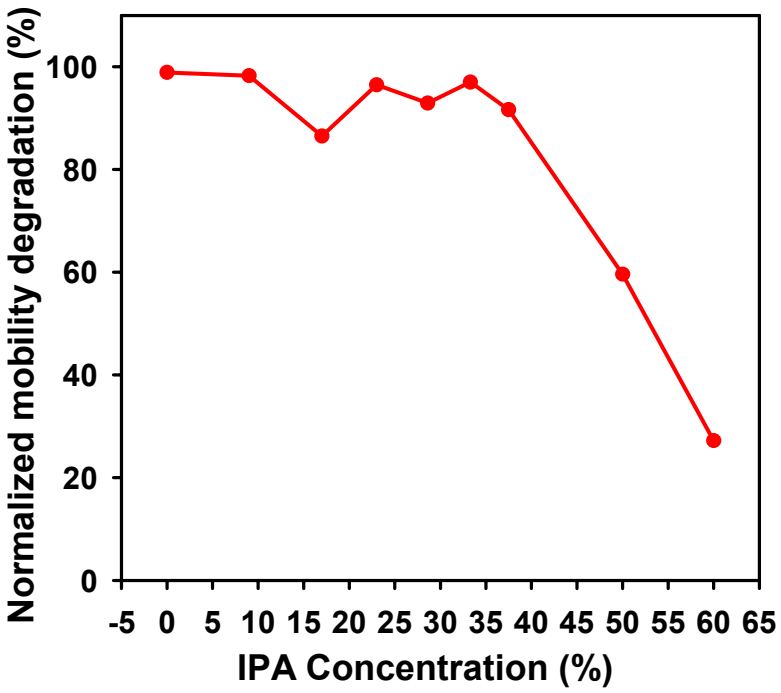

Figure 3-6**: The normalized mobility degradation as a function of IPA concentration in water.**

The possible correlation with a solvent's polarity was examined by comparing the exposure results of two polar solvents: dimethyl sulfoxide (DMSO, m.w. 78, m.p. 20 ºC, b.p. 189 ºC, molecular volume $Å^3$) and water with a dipole moment of 3.96 and 1.85, respectively. The irreversible degradation triggered by the exposure to DMSO is like that of other organic solvents. Because DMSO has a high boiling point, a short anneal for the removal of excess solvent is used to verify this effect. Figure **3-7** shows the transition of transfer characteristics of an OTFT before (black line) and after (red line) the DMSO exposure and after two periods consisting of two-minute annealing (green and yellow) at 50 ºC and 70 ºC in ambient air. Such baking does not reverse the damage to the device. Thus, the solvent's polarity is not the determining variable when comparing the results of water and DMSO exposure.

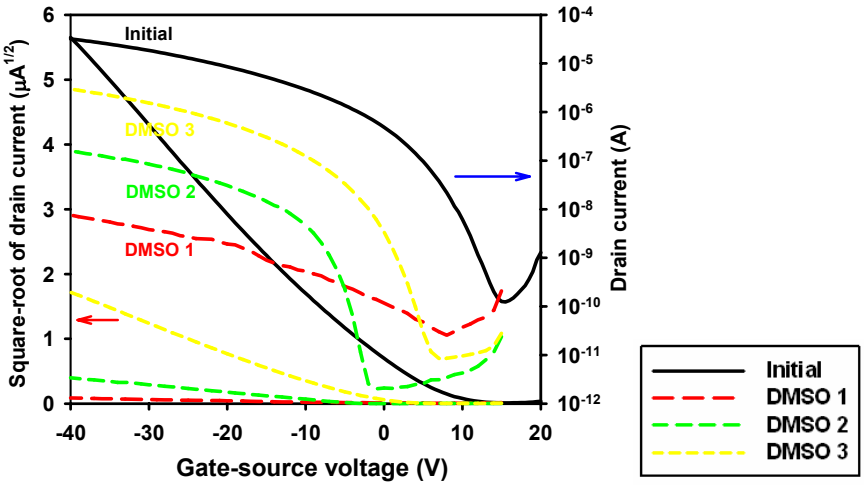

Figure 3-7**: The $\sqrt{I_D}$-V_{GS} and log(I_D)-V_{GS} characteristics of a pentacene OTFT before and after DMSO exposure "1" and two annealings at 50 ºC "2" and 70 ºC "3".**

Figure **3-8** shows the traces of three major device properties (saturation field-effect mobility, threshold voltage, and subthreshold slope) during the DMSO exposure.

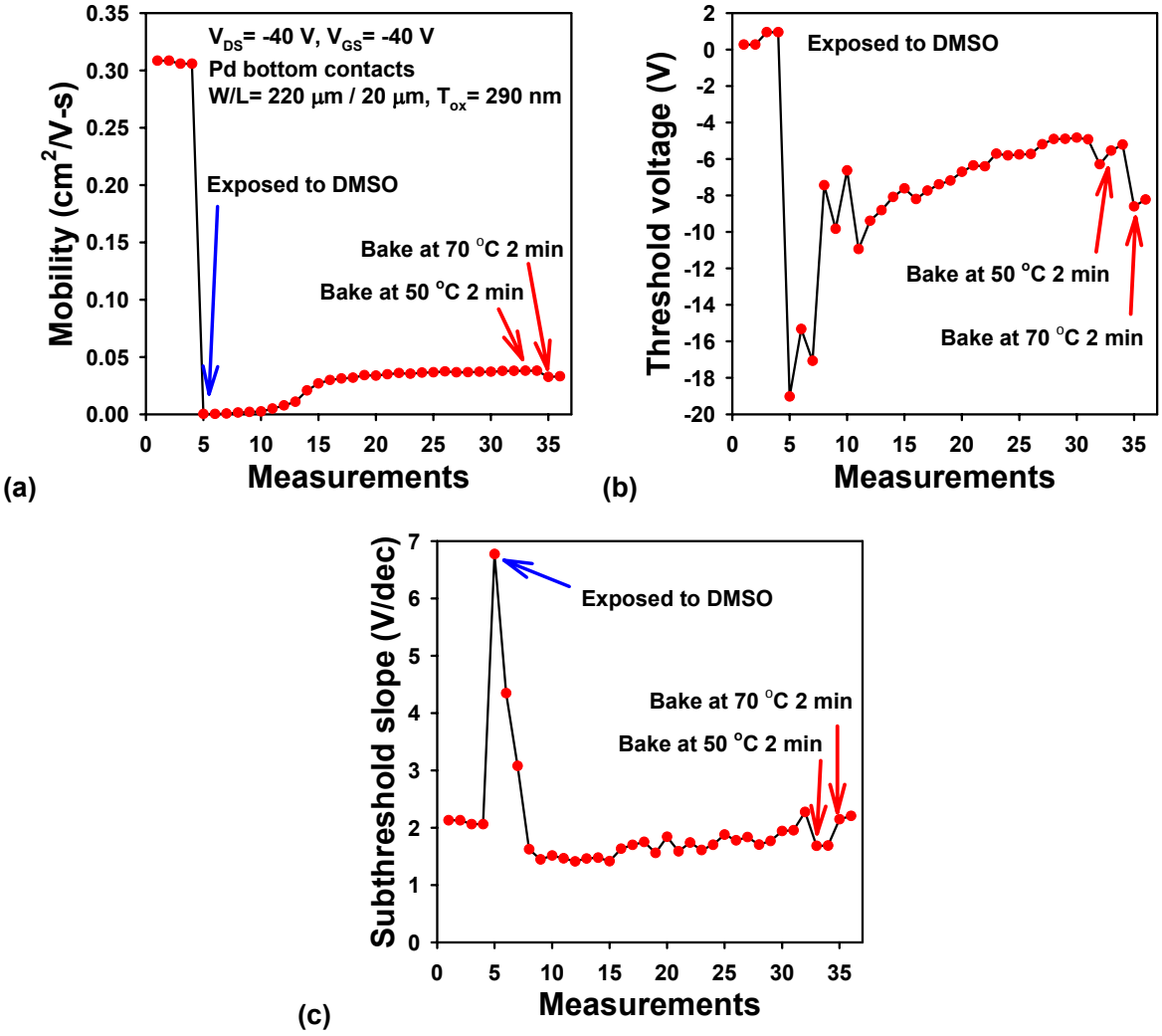

Figure 3-8**: The transition of (a) saturation field-effect mobility, (b) threshold voltage, and (c) subthreshold slope of a pentacene OTFT after exposed to DMSO and two two-minute annealings in ambient air at 50 ºC and 70 ºC, respectively.**

In addition, we used a linear large molecule, n-hexadecane (m.w. 226, b.p. 287 ºC) to test the effect of the dimension of solvent molecules. We found similar device degradation after a few minutes of exposure although the initial change in I-V characteristics is less aggressive. Because hexadecane has zero polarity, this illustrates the case of a non-polar solvent.

Table **3-1** shows the overall effects of solvents on the electrical characteristics of pentacene OTFTs with bottom source and drain electrodes. However, we could neither

determine the decisive solvent parameter nor understand the driving force of the kinetics. According to these preliminary results, water remains the only solvent that does not cause severe damage to pentacene thin films and their device performance. Most wet processes require aqueous materials and solutions, and protection barriers are required when organic solvents and basic or acid solutions can directly contact with pentacene films. Therefore, there is still a difficulty with using wet processing on pentacene films.

Table 3-1**: The degradation of pentacene TFTs as a result of exposure to solvents. The result of acetone was on a published paper [Gundlach, Jackson 1999].**

Solvent (m.w.)		Before		After		Reversible
	Dipole moment / Dielectrics	Mobility	V_{sub}	Mobility	V_{sub}	
H_2O (18)	1.86 / 80	0.45	2.3	0.44	2.2	> 90 %
Chlorobenzene (112.5)	1.69 / 5.69	0.49	1.40	< 0.09	1.53	N
DMSO (78)	3.96 / 47.2	0.4	2.0	< 0.05	1.9	N
2-Propanol (60)	1.58 / 20.18	0.36	2.3	< 0.1	1.6	N
Hexadecane (226)	0.13 / 2.05	0.43	1.3	< 0.08	1.2	N
Acetone (58)	2.88 / 20.7	0.45		< 0.1*		N

3.2 **Fabrication of Direct Lithographic Top Contacts**

With the complexity of the pentacene active layer in mind, a multi-layer photolithography process, when each layer serves a different purpose, would allow direct lithographic top contacts to be fabricated for pentacene OTFTs. We successfully developed a suitable layer combination with photosensitized and bare polyvinyl alcohol (PVA), a conventional photoresist and developed a successful process for patterning lift-off structures on pentacene thin films.

A Tetra-Layer Lithographic Process

We developed a metallization process that uses multiple photoresist layers to form a reentrant profile for lifting off the metal in the unwanted area. The tetra-layer

lithographic process is shown schematically in Figure **3-9**. For simplicity, we started from a blank pentacene thin film on an oxidized silicon wafer treated with a silane coupling agent. Four polymer layers were applied using spin casting and drying in ambient air for few minutes, including a 0.4 μm thick polyvinyl alcohol (PVA, m.w. 30 – 50 kD, 87 % hydrolyzed, Sigma-Aldrich), a 0.2 μm thick polymethylmethacrylate (PMMA), a 0.2 μm thick PVA (m.w. 86 – 146 kD, 87 % hydrolyzed) photosensitized with 1 w.t.% ammonium dichromate (ADC), and a 1.7 μm thick negative photo resist (ma N-440 by MicroResist). Because PVA becomes insoluble at elevated temperatures, only a four- minute baking at 75 ºC is used to remove the excess solvent in the ma N-440 layer. In terms of functionality, the bottom PVA layer is a detachable barrier; the PMMA layer prevents the resist developer, a weak base, from penetrating, doping, or hindering the adhesion and the functionalized gate dielectric. The third layer, PVA(ADC), which is cross-linked when heated to more than 50 ºC, prevents a strong intermixing between PMMA and ma N-440 and renders a stable processing condition for the ma N-440 resist. Then ma N-440 was exposed to 2.5 J/cm^2 i-line UV light and developed in a weak base to form the reentrant profile. A controlled reactive ion etching (RIE) etched the transferred pattern through PVA(ADC), PMMA, and partially through the bottom PVA. The remaining bottom PVA in the patterned area was removed by water etching. The lithographic top contacts were completed by metal deposition and lift-off using water.

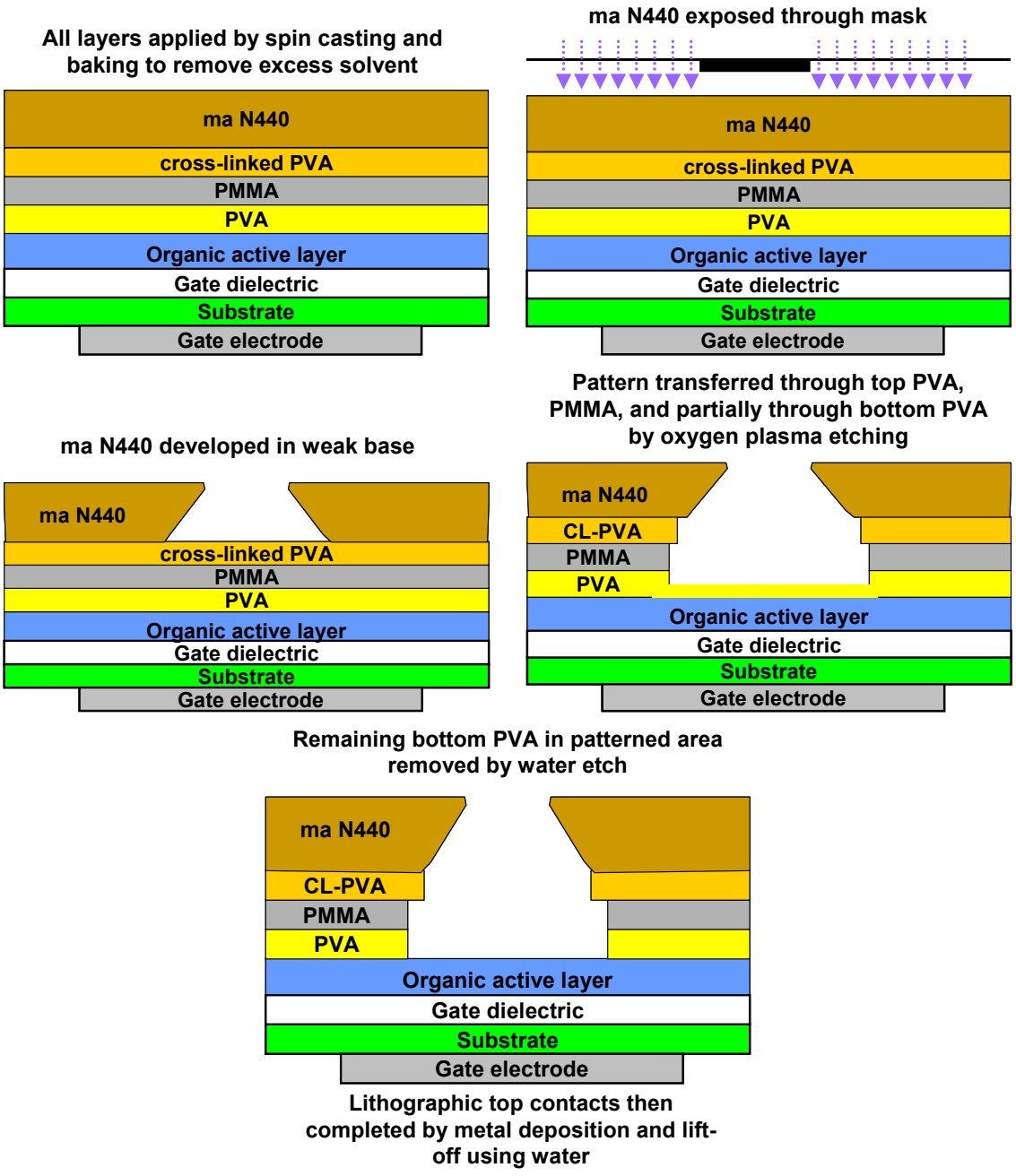

Figure 3-9: **Processing scheme of direct photolithographic top contacts to pentacene thin films.**

Figure **3-10** shows a field emission scanning electron microscopy (FESEM) micrograph of a contact window (the right-bottom portion) and the field region after the thermal evaporation of 50 nm gold. The overall resist edge is unswerving and the undercut is upright and explicit. The grainy shapes of the gold film reflect the morphology of the rough pentacene grains. It indicates this four-layer process is feasible for making lithographic top contacts using lift-off on pentacene thin films. A few lumps near the center are possibly a PVA residue underneath the metal layer but their negative effect on contact over the essential area is negligible. Because the commercial available PVA from Sigma-Aldrich often has a large polydispersity (a large deviation in molecular weight), the control over thermal or developing processes is reduced. Polydispersity is defined as the ratio of weight-average molecular weight (M_w) over number-average molecular weight (M_n),

$$\text{where } M_w = \frac{\sum_{i=1}^{\infty} n_i M_i^{\,2}}{\sum_{i=1}^{\infty} n_i M_i} \text{ and } M_n = \frac{\sum_{i=1}^{\infty} n_i M_i}{\sum_{i=1}^{\infty} n_i}$$

Thus, a high quality PVA with a lower polydispersity can improve the reproducibility. Using another type of photo-sensitizer instead of ADC may also improve the process.

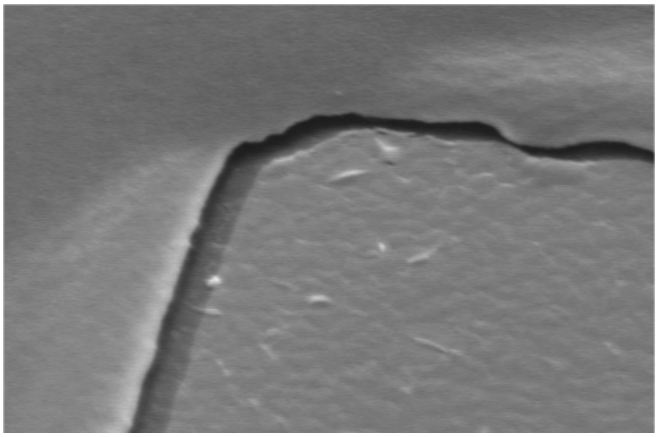

Figure 3-10**: Micrograph by FESEM of a source / drain window after metallization. The reentrant profile stacked by this multiple-layer lithographic process is clear.**

Figure **3-11a** shows an optical micrograph of an array of finished OTFTs with lithographic top source and drain contacts. The channel width is either 300 or 340 µm, and the channel length ranges from 6 to 20 µm in this mask. Because the lift-off process requires at least 1 µm of undercut on each side, the minimum channel length is limited to about 4 µm. A better yield was found when it was longer than 8 µm. Another problem is that certain parts of the four layer stack may detach from the surface during the buffer PVA etching (the last step). This causes defected patterns and missing electrodes. Figure **3-11b** is a zoom-in micrograph of a device with a channel length of 12 µm and shows that this level of resolution can be achieved by this new process.

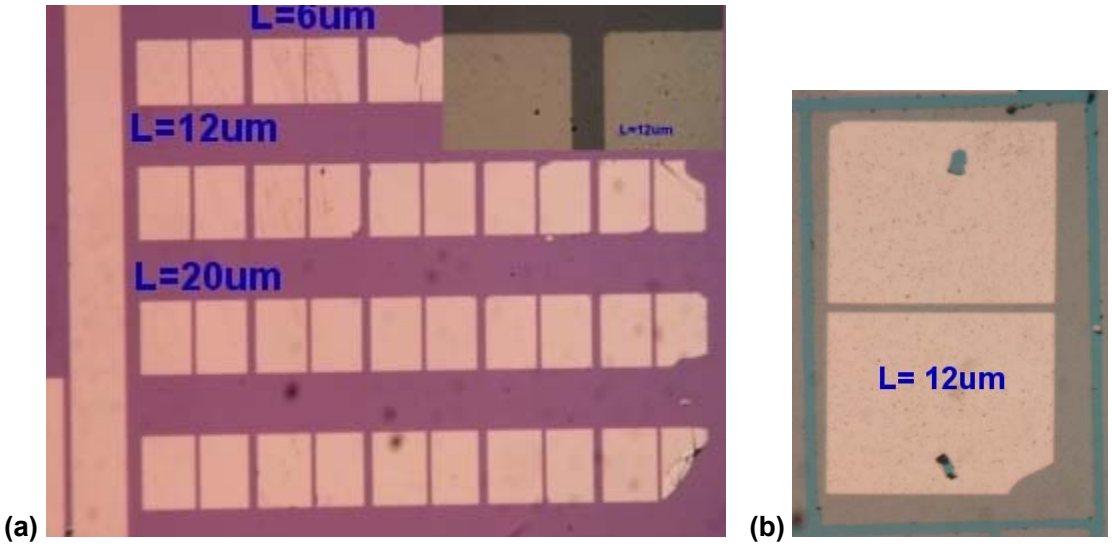

Figure 3-11**: Optical micrographs of finished OTFT arrays with top source and drain contacts, having channel length range from 6 to 20 µm in (a) and channel length L= 12 µm in (b).**

Attempts to Use Other Multiple-Layer Processes

Attempts to use different combinations of two to four layers were also tested, and the results were not acceptable. We tried a few double-layer PVA processes using PVA with molecular weight between 30 k to 146 k Daltons and various combinations of ADC concentrations (0 % to 3 %), another double-layer with PVA and Shipley 1811 resist,

three triple-layer processes (PVA, PMMA, and 1811, or PVA, PMMA, and ma N-440, or PVA, PMMA, and PVA), and one tetra-layer processes (PVA, PMMA, PVA(ADC), and 1811). Although none of them were successful, we gained enough knowledge to develop working process.

We encountered several issues in these attempts. Several of them can be solved, but some of them appear insoluble. Examples of these issues include the following: 1) Because the inter-diffusion of ADC between two adjacent PVA layers is rapid, it is difficult to spin cast one pure PVA layer adjacent to one with ADC. 2) Polymerized PVA remains permeable to water, which dissolves the non-polymerized PVA underneath. 3) Polymerized PVA is too soft to form the cap layer with an undercut, and its patterned edge is not trim. 4) Because a pure PVA layer is permeable to toluene or chlorobenzene, using PMMA as the sacrificial layer for undercut is not possible, which requires organic solvents as the etcher. 5) When the process temperature is limited to less than 90 ºC, the intermixing of PMMA with 1811 or with ma N-440 results in non-uniform, incomplete exposure and poor developing.

Figure **3-12** shows a tri-layer process (PVA, PMMA, and 1811). It takes one minute of wet etching by toluene to form a 1 μm undercut at the PMMA layer. As a result, the toluene penetrates through the bottom PVA layer and degrades the devices. The field-effect mobility of pentacene OTFTs drops to 0.08 cm^2/V-s from 1.0 cm^2/V-s.

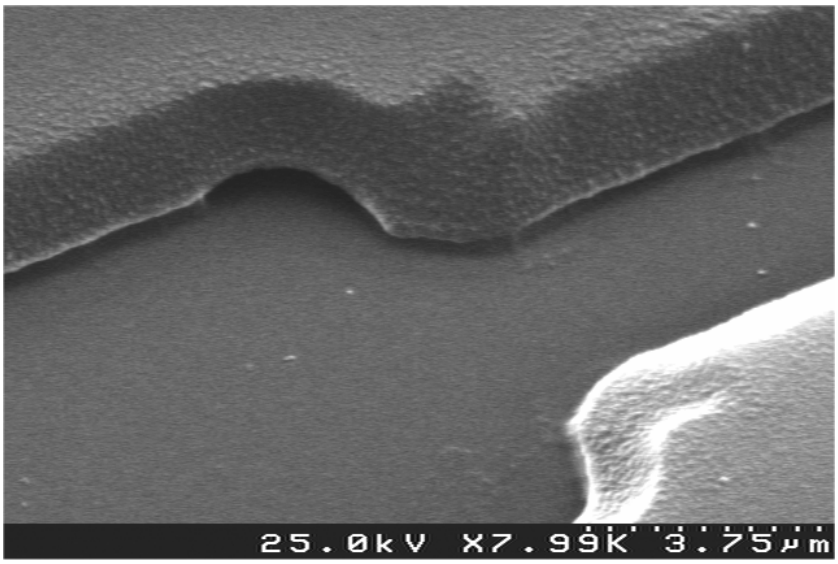

Figure 3-12**: FESEM micrograph of a reentrant profile formed by PVA, PMMA, and Shipley 1811 resist.**

Additionally, the processing parameters depend on the properties of these polymers, including molecular weight, thickness, hydrolyzation ratio, and concentration of the photosensitizer. A few tables of the processing data (Table **A-1**) are listed in the Appendix.

3.3 **Characteristics of OTFTs with Lithographic Top Contacts**

For convenience, pentacene OTFTs were fabricated on thermally oxidized silicon substrates using a structure such as that shown in Figure **2-24c** except for the top contacts that were made by this new direct lithographic process. These devices were dried in ambient air and tested in a dry glovebox. We tested devices with channel lengths ranging from 4 μm to 40 μm. Most devices have a mobility between 0.2 to 0.3 cm^2/V-s at V_{DS}= -40 V. Here we show two typical device characteristics.

Typical $\sqrt{I_D}$-V_{GS} and I_D-V_{DS} characteristics of such devices are shown in Figure **3-13**. Extracted device properties are a field-effect mobility of μ= 0.3 cm^2/V-s at V_{DS}= -40 V, a threshold voltage of V_T= -0.7 V, a subthreshold slope of V_{sub}= 1.6V/dec, and a

on/off current ratio of $I_{ON}/I_{OFF}= 10^{6.5}$; these indicate that these devices received neither drastic damage nor experienced a strong degradation in comparison with that of pentacene OTFTs exposed to organic solvents. The linear region of the drain current for small V_{DS} does not appear concave, and suggest that the contact resistance is reduced as observed in devices with shadow-masking top contacts.

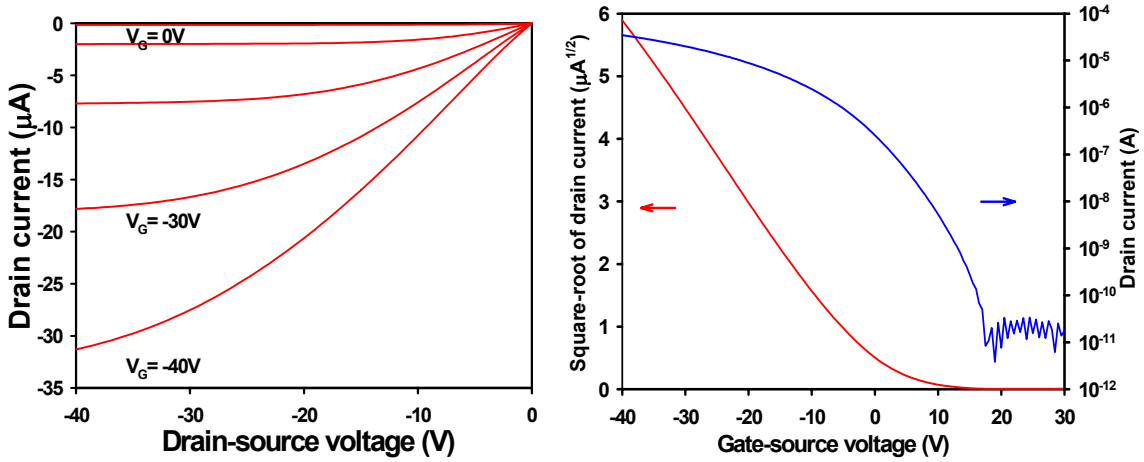

Figure 3-13: The I_D-V_{DS} and $\sqrt{I_D}$-V_{GS} characteristics of a pentacene OTFT with gold top contacts, a silicon dioxide gate dielectric of 400 nm, a channel width (W) of 340 μm, and a channel length (L) of 20 μm. Mobility μ is 0.32 cm^2/V-s at V_{DS} = -40V, V_{th}= -0.7V, V_{Sub}= 1.6V/dec, and $I_{ON}/I_{OFF}= 10^{6.5}$. This device was tested in a dry glovebox.

Because the OTFT is exposed to water or moisture for a long time during the process, the threshold voltage becomes more positive. After a few hours of storage in a dry environment, the threshold moves to a more negative level and the mobility remains at the same level as in Figure **3-13**. Most devices actually exhibit a near-zero threshold voltage, which is a desired property for OTFT circuits.

In addition, 4 μm short-channel OTFTs with a field-effect mobility of 0.2 cm^2/V-s were also tested as seen in Figure **3-14**. It also has a threshold voltage of near zero volt, a subthreshold slope of 1.3 V/decade, and the on/off current ratio of 10^7. The characteristics in the linear region are comparable with that of long-channel devices. Thus, it is evident that this direct photolithographic process is feasible and the channel resolution can be less than 10 μm.

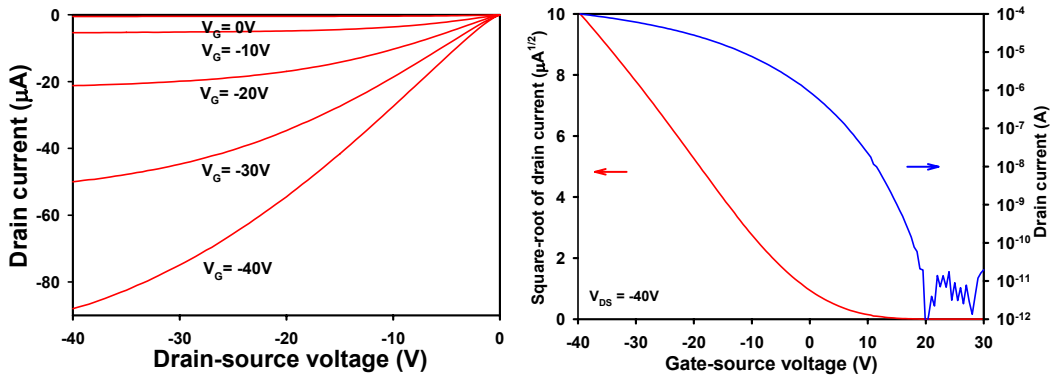

Figure 3-14: The I_D-V_{DS} and $\sqrt{I_D}$-V_{GS} characteristics of a pentacene OTFT with gold top contacts, a silicon dioxide gate dielectric of 400nm, a channel width (W) of 300 μm, and a channel length (L) of 4 μm. The mobility μ is 0.21cm^2/V-s at V_{DS}= -40V.

The mobility remains at a moderate level of 0.3 cm^2/V-s after this new process, but the degradation still exists. In comparison with devices with shadow-masked top contacts and using the same pre-process pentacene thin films, the mobility of OTFTs using this new process decreases from 1.0 to 0.3 cm^2/V-s. Although the device performance was moderately degraded, such performance has potential in applications. This degradation may arise from the organic solvent exposure through small pinholes, the thermal processes, the UV exposure of the lithography or the plasma etching, or the effect of PVA as a residue or a source of mechanical stress. Further investigation may solve this problem and reduce the degradation.

3.4 **Contact Resistances of OTFTs with Top Contacts**

The contact effect is manifested in OTFTs for small drain-source voltage V_{DS}, and the drain current I_D increases linearly with V_{DS}. A plot of the drain current I_D at low V_{DS} shows this linear correlation. We used the transmission line model to extract the contact resistance. In the presence of the high source and drain resistance (R_{SD}) in typical OTFTs the measured resistance defined as V_{DS}/I_D can be expressed as Eq. **3.1**

$$R_m = R_{ch} + R_{SD} \approx \frac{L}{W C_{ox} \mu (V_{GS} - V_T)} + R_{SD} \qquad (3.1)$$

where R_{ch} is the channel resistance and C_{OX} is the gate dielectric capacitance in the channel region. Then, the extracted normalized source/drain resistance $R_{SD}W$ and the normalized contact resistance R_C is given by Eq. **3.2**

$$R_C = \frac{R_{SD}}{2} W \qquad (\mathbf{3.2})$$

We measured and analyzed a group of pentacene TFTs with direct lithographic top contacts. The measured resistance, R_m, is a series combination of the OTFT channel resistance and the resistance of the source and drain contacts. It was extracted from the linear region characteristics for OTFTs with different channel lengths and channel widths (W = 300 µm for L= 4, 6, and 12 µm and W= 340 µm for L= 20 µm). Measured resistance is plotted as a function of V_{GT}, where $V_{GT} = V_{GS}-V_T$ for L = 4, 6, 12, and 20 µm as seen in Figure **3-15**. The measured resistance drops quickly and evenly to a minimum as the V_{GT} ramps up. Thus, these consistent curves illustrate the uniformity across the devices and validate the consequent analysis.

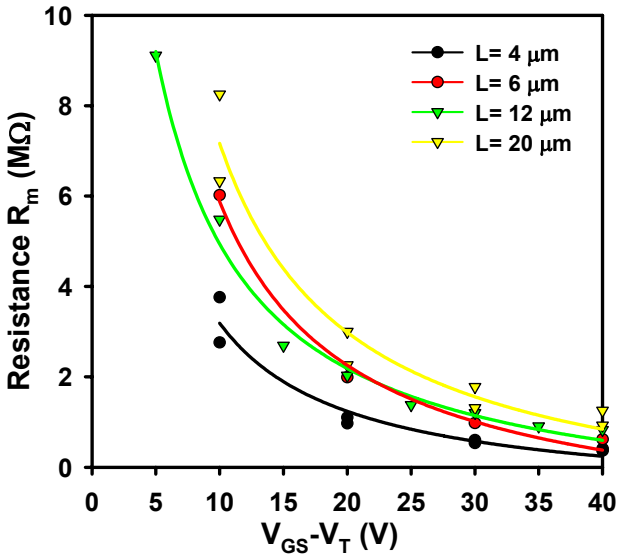

Figure 3-15: **Measured resistance R_m as a function of V_{GT} for L = 4, 6, 12, and 20 µm.**

Figure **3-16** shows the normalized measured resistance as a function of the channel length range from 4 to 20 µm for four levels of gate bias (V_{GT}= -10, -20, -30, and -40 V) with V_{DS}= -10 V. The intersection point of the fitting lines with a channel length

of zero corresponds to the series combination of the source and drain contact resistance. All normalized joint contact resistances of these devices fall within 0.06 - 0.8 GΩ/μm, where the max/min ratio is 13. These results are about 50% lower than the typical result (~ 1 GΩ/μm) of pentacene TFTs with bottom contacts. The crossing point of the extrapolated lines with X-axis at zero resistance gives the value of twice the transfer length, T_L. The transfer length is a characteristic distance that carriers travel under a contact before being collected. Its range of 2 to 4 μm is much smaller than that of bottom contact or shadow-masked top contact devices (15–25 μm) [Gundlach, Jia 2001; Klauk, Schmid 2003; Necliudov, Shur 2003]. The fluctuation of the fitting lines is also smaller and suggests that the contact correlation across devices is homogeneous.

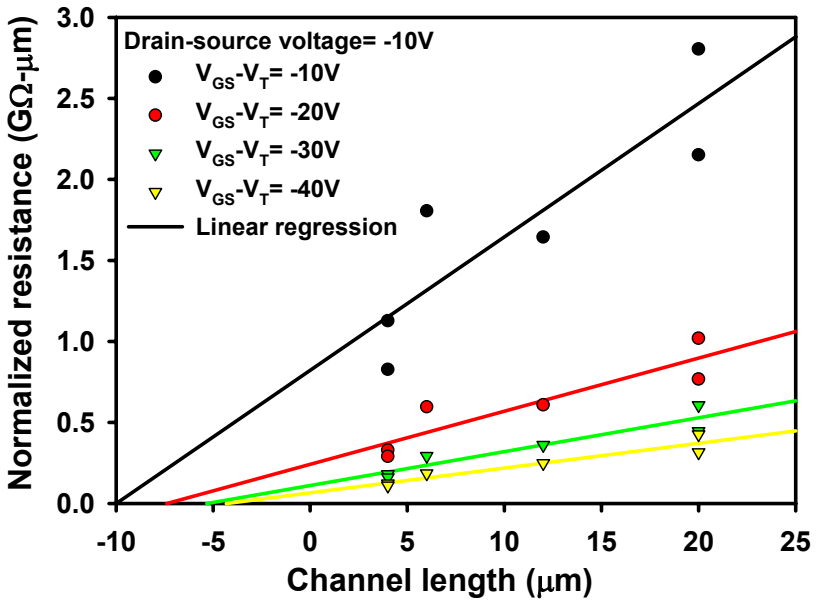

Figure 3-16**: Normalized contact resistance as a function of the channel length in devices with lithographic top contacts.**

Figure **3-17a** and **b** show the normalized contact resistance R_C as a function of V_{GT} on a linear and log-log scale. The linear fitting line in Figure **3-17b** shows R_C varies with $V_{GT}^{-1.8}$. This exponential correlation between contact resistance and V_{GT} also indicates that the possible mechanism or origin of the contact resistance is the space charge barrier built up at the interface of the source electrode. This is in agreement with

the results of studying contact to pentacene films using Scanning Kelvin Probe Microscopy and X-ray Photoelectron Spectroscopy (XPS) [Schroeder, France 2002; Koch, Kahn 2003; Nichols, Gundlach 2003].

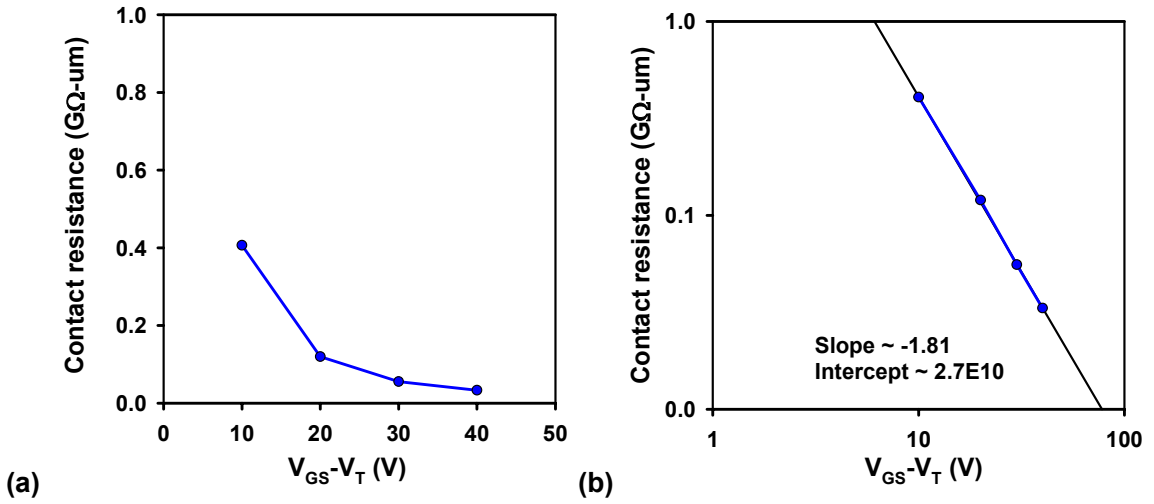

Figure 3-17**: Normalized contact resistance as a function of V_{GT} on (a) a linear and (b) log-log scale.**

We compared these results with the published results in Figure **3-18**. The contact resistance Rc varies as V_{GT}^{-1} and V_{GT}^{-2} for bottom contact and top contact OTFTs, respectively. Fr bottom-contact pentacene OTFTs because the film growth is disrupted at the contact edge, as suggested by AFM micrographs in Figure **3-19**, and the source and drain electrodes shield the gate potential from the pentacene film on top of the electrodes, the film can only form a line contact with the film in the channel region, which is more fragile. Consequently, the modulation of the carriers in the contact area by the gate bias is smaller, as well as the dependence of R_C on V_{GT} when compared to OTFTs with top contacts. Thus, it is reasonable that the dependence of OTFTs with lithographic top contacts is close to that of OTFTs with top contacts.

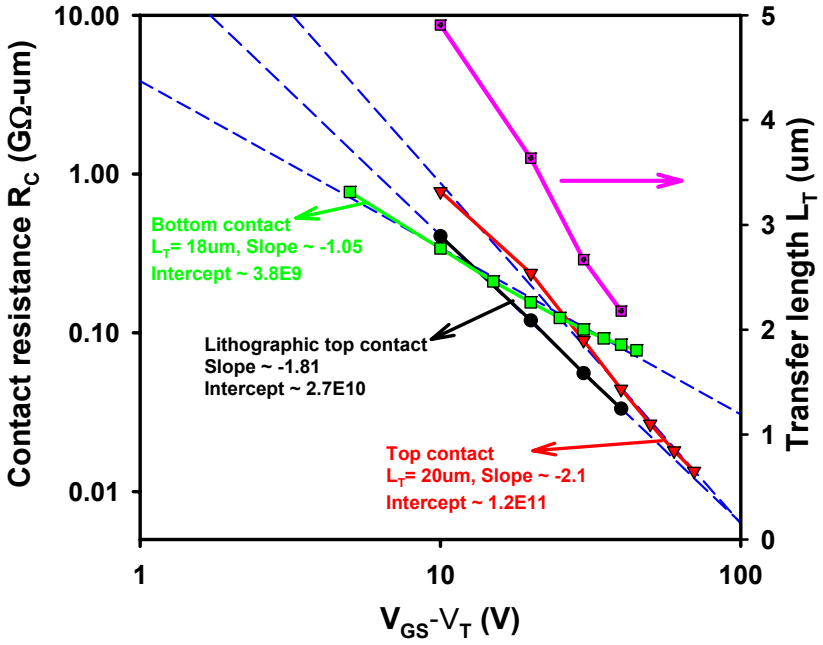

Figure 3-18: **Normalized contact resistances of OTFTs with three types of contacts as a function of V_{GT} on a log-log scale. Transfer length of lithographic top contact OTFTs as a function of V_{GT} on a semi-log scale.**

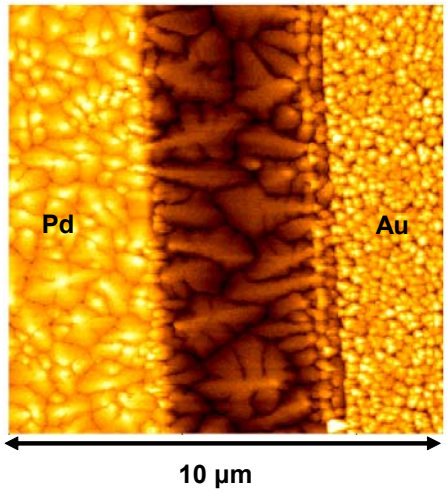

Figure 3-19: **10 µm × 10 µm atomic force microscopy micrograph of a TFT channel region with pentacene of 50 nm thick, deposited on a thermally oxidized silicon substrate with lithographically-defined Pd and Au contacts.**

The ratio of the combined contact resistance R_{SD} to the measured resistance can demonstrate the dominant factor of device performance in a TFT other than the channel resistance. Because an OTFT often has an undesirably large contact resistance, the reduction of this ratio signals a larger tunable switch. Figure **3-20** shows such ratio of these devices as a function of channel length with a reference curve from a group of bottom contact pentacene TFTs [Gundlach, Jia 2001]. In comparison, the ratio of those with direct lithographic top contacts is about one half lower. Thus, we infer that the objective of using top contacts to reduce the contact resistance is feasible. In addition, the rapid rising of the ratio for a short channel device in either case represents the dominant contact resistance. This indicates the difficulty of improving device performance, including drain current or field-effect mobility, by only scaling down the channel length and the importance of solving contact problems for improving OTFT performance.

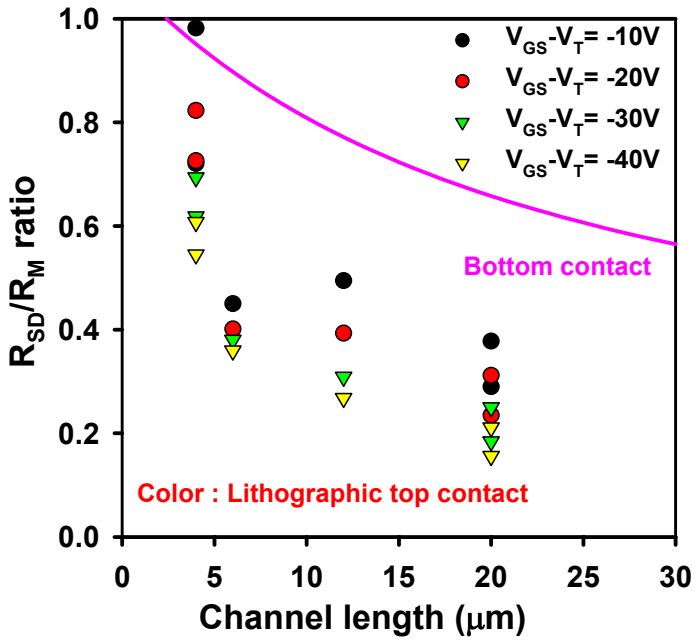

Figure 3-20**: The ratio of the series contact resistance R_{SD} to the measured resistance R_M as a function of channel length and V_{GT} with a reference curve from bottom contact OTFTs [Gundlach 2001].**

3.5 **Summary**

Processing pentacene or other organic semiconductors is not easy. We showed that a variety of organic solvents cause large device degradation and render device unusable. Water remains the only solvent that does not introduce much damage to pentacene films. The possible mechanisms are briefly discussed but need further investigations.

We have shown a new fabrication method to directly pattern top contacts to pentacene OTFTs with a channel resolution of less than 10 μm. 4 μm Short- and 20 μm long-channel devices were characterized and found to have field-effect mobilities of 0.2 and 0.3 cm^2/V-s at V_{DS}= -40 V, respectively. To our knowledge, this is the first process available for fabricating direct lithographic source and drain electrodes on pentacene OTFTs with sufficient device performance and resolution for integrated circuits. Based on this new process, we can explore new possibilities. These include a new method for patterning pentacene without leaving a polyvinyl-alcohol (PVA) layer behind, a method of making contact vias when using source and drain top contacts, as well as the electrical characteristics of pentacene TFTs with either a double source and drain (bottom and top) or double gates.

The benefit of lowering the contact resistance by about 50% in these devices relative to OTFTs with bottom contacts was confirmed through the contact resistance analysis. However, the device performance still remains contact limited where the contact resistance is linearly and inversely proportional to V_{GT} in the log-log scale. This lithographic method has demonstrated the practicality of fabricating lithographic top electrodes on organic semiconductor thin films with desired resolution, and can expand a wider possibility of new device structures for further development of OTFTs.

Chapter 4

High Performance Solution-Processed OTFTs

We are interested in solution-processed devices because they may allow large-area electronic applications to be manufactured in high volumes on arbitrary substrates by printing or other low-cost fabrication techniques. Most solution-processed OTFTs have used polymeric organic semiconductors such as alkyl-substituted polythiophenes. Polymeric semiconductor OTFTs typically have field-effect mobility < 0.1 cm^2/V-s, compared to > 1 cm^2/V-s often reported for vapor-deposited small molecule organic semiconductors [Ebisawa, Kurokawa 1983; Tsumura, Koezuka 1986; Assadi, Svensson 1988; Burroughes, Jones 1988; Sirringhaus, Tessler 1998; Dimitrakopoulos and Mascaro 2001; Salleo, Chabinyc 2002; Kline, McGehee 2003; Paul, Wong 2003; Gelinch, Huitema 2004]. In spite of the lower mobility in polymeric organic semiconductors, a high-temperature annealing is usually required to regain molecular ordering for electronic transport [Stolka and Abkowitz 1993; Sirringhaus, Tessler 1998]. Additionally, solution precursor routes to pentacene OTFTs also have been demonstrated with mobility near 0.9 cm^2/V-s [Afzali, Dimitrakopoulos 2002]; however, this approach requires a high-temperature conversion step (~200 ºC), which precludes the use of low-temperature plastic substrates.

Before we start this chapter, a few abbreviations of the functional groups and backbone molecules are listed in Table **4-1** for easy understanding. We collaborated with Professor John Anthony, Department of Chemistry, University of Kentucky, who leads the synthetic work of these novel molecules.

Table 4-1: Abbreviations of a few functional groups and backbone molecules discussed in this chapter.

Name	Chemical structure	Abbreviation
Trimethylsilylethnyl	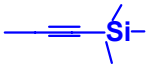	TMS
Triethylsilylethynyl	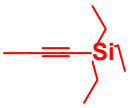	TES
Triisopropylsilylethynyl	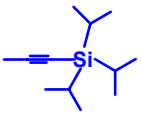	TIPS
Anthradithiophene (two isomers)	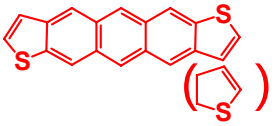	ADT

In this chapter we present further work after the discovery of TIPS pentacene TFTs with a mobility near 0.2 cm^2/V-s without high-temperature processing [Shankar, Sheraw 2003]. Although solution-processing technology has been utilized for many polymer organic semiconductors since early 1990s, many challenges remain. In addition, there are few studies for small-molecule organic semiconductors which have different material properties. Thus, assuming that the solution process can be analyzed in terms of independent variables, we investigated a few typical solution deposition methods, their working principles, and the thin film quality. Then, thin film fabrication and analysis and device characterization of a few small molecule organic semiconductors, particularly TES anthradithiophene and TIPS pentacene, are discussed. Based on these results, we conclude some preliminary directions of improving molecules by molecular engineering.

4.1 **Solution Processing for Electronic Device Fabrications**

Solution processing has been proven to be an effective way of printing or spreading coating materials onto flexible substrates such as paper, plastic, or metal foil for a host of applications. The idea of using printable semiconductor circuits was

demonstrated in 1967 for II-VI devices [Sihvonen, Parker 1967]. However, the real utilization did not take off due to a lack of applications. Now using solution processing technology in semiconductor fabrication is revisited for large-area electronics. In conventional semiconductor fabrication using inorganic semiconductors, it is not possible to use solution processing because a very high processing temperature is required and most materials are not soluble or cannot be converted from solutions or gels. However, many organic semiconductors are soluble and make solution processing possible. This has the advantages of non-batch processing on large substrates with high production throughput, which may alleviate the financial difficulty in high equipment and manufacturing costs and the difficulty of scaling up the substrate area.

Nevertheless, extensive effort is still needed to implement a solution-processing technology. Depending on the use and properties of the selected material for electronic devices, either vapor phase or wet coating techniques have been developed. At present for most of the films, the solution-processing technique is not the one that is preferred method at present. In addition to the lack of solution-processable materials, one major reason is the lack of standards in equipment and the coating materials [Schmidt and Mennig 2000]. Although in many cases, the materials are not standardized and the process has to be developed by users using the specific equipment, many companies have focused on this technology such as Infineon, 3M, SiPix Imaging, and FlexIC. Here we describe a roll-to-roll process to illustrate the potential merits of solution processing.

Roll-to-roll (R2R) process, a typical example of low-cost solution processing, has drawn a lot of interest for its potential of cost reduction in semiconductor processing, and a schematics of such a process is shown in Figure **4-1**. A long sheet of flexible substrate is continuously passed over rollers and chambers. In such a course, the solution-processable organic semiconductor is deposited using dip casting, and layout patterns are printed by stamping or three-dimensional structures are created by an embossing roller. Thermal or radiative curing by a hot roller or a lamp is commonly used. At the end of this process, substrates are recollected into a roll. Although the real processing system can be much more complicated than the schematics, the cost of a manufacturing facility is still much cheaper than traditional semiconductor fabrication facilities, such as

lithographic tools, furnaces, and many sophisticated deposition or etching systems. In addition, R2R is suitable for higher-volume production at a faster speed. The substrate handling is minimal, and the numerous and intricate steps involved in batch processing are avoided. Thus, R2R and other low-cost processing techniques enabled by solution processing have great potential in manufacturing electronics cheaply.

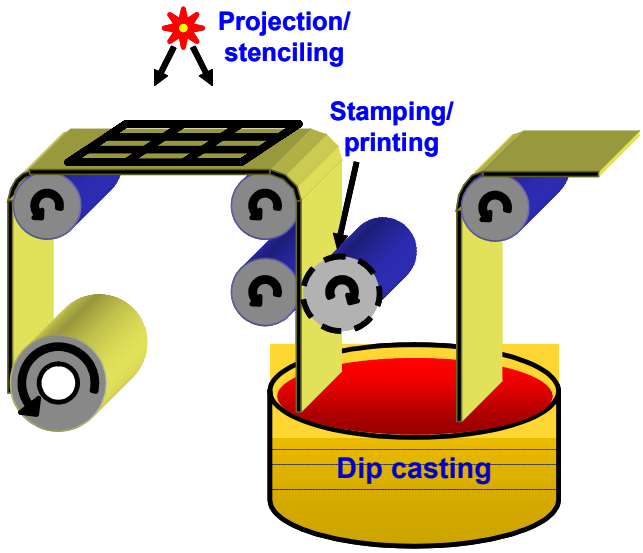

Figure 4-1**: Schematics of a roll-to-roll process for low-cost solution processing.**

4.2 **Fabrication of Solution-Processed OTFTs**

Assuming that the fabrication process can be analyzed in terms of independent variables, such variables are separately in the approach, several main steps are investigated and analyzed independently: 1) the deposition methods and the number and sources of forces in the action, that are involved and often predetermined by the selection of a deposition method; 2) the formation or reformation of the thin film, including the kinetics; 3) the manipulation of these types and sources of forces whose levels and even dominance can be altered; 4) the modification of the substrate surface that have much joint influence with the previous module; 5) the analysis and prediction of the

intermolecular force between each pair of the semiconductor molecule, the solvent molecule, and the surfactant that can provide the input of the third module; 6) the mass transportation and solubility of the organic semiconductor, particularly at the location where the film densifies or crystallizes; 7) the changes of physical conditions of the system, such as temperature, heat flow, and photonic energy, which can also alternate the third module and subsequently effect the kinetics of the film formation; and 8) the criteria for improving device performance. We will focus on the first variable in this section, cover a small portion of the third and forth variables, and report the possible criteria of achieving high-performance devices.

We presented the substrate fabrication and four solution-processing methods, including dip casting, bar coating, slide coating, and spin casting, and the preliminary results.

For simplicity of device testing in this work, we exclusively used heavily doped n-type silicon wafers (0.015 ohm-cm) with 370 nm of thermally grown silicon dioxide as a convenient substrate, gate electrode, and gate dielectric for fabricating OTFT test devices as seen in Figure **4-2**. 100 nm thick gold or platinum source and drain contacts were deposited by ion beam sputtering and patterned by photolithography and wet etching. These contact metals are smooth with r.m.s. roughness of less than 6 Å for gold and 4 Å for platinum. Prior to the active layer deposition, substrates were cleaned using oxygen plasma. Certain samples were treated with pentafluorobenzenethiol in an attempt to improve the OTFT contacts. Thin films of a small molecule organic semiconductor with a thickness of 30 – 100 nm were deposited on samples from 0.5 – 4 wt % solutions (with toluene as major solvent) using one of four methods. Then, the samples with active layers were either simply dried at room temperature or annealed at a temperature between 75 and 90 ºC in air for two minutes to remove the bulk of the solvent.

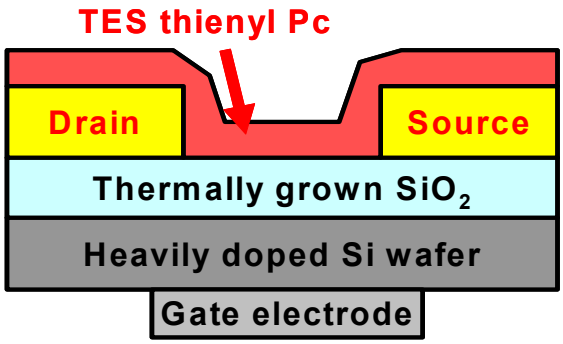

Figure 4-2: Schematic cross section of an OTFT with lithographically defined source and drain.

Deposition Methods and Basics of Fluid

When a thin fluid film is dragged by an object moving through a fluid, the induced resistance is called fluid friction. This viscous drag, called viscous resistance, is approximately proportional to the velocity. For a sphere falling through a liquid in a velocity regime where viscosity is the dominant effect and turbulence can be neglected, the viscous drag is $F_{drag} = -6\pi a \eta v$, where a is the sphere radius, η is the viscosity, and v is the partial velocity. Fluids in which the viscosity is independent of pressure are called Newtonian fluids. And the solutions used in our processing have these Newtonian attributes. If the conditions for laminar flow are met, Poiseuille's law can be used to describe the flow.

In our preliminary experiments, each method provides individual merits either for thin film uniformity, device performance, or reproducibility. Thus far, we have found fabricating thin, uniform, and reproducible active layer films from solution-processable small-molecule organic semiconductors is difficult, and the limitations of each method are discussed here.

Dip casting

In dip casting, a substrate to be coated is immersed in an organic semiconductor solution for a given time, and then withdrawn at a well-defined speed under controlled temperature and atmospheric conditions. A thin layer of solution adhering to the substrate dries to form a layer of semiconductor thin film. The liquid coating thickness is mainly defined by these criteria: the withdrawal speed, the solid content, and the viscosity of the liquid. If the withdrawal speed, denoted as v, is chosen such that a sheer rates keep the system in the Newtonian regime, the coating thickness can be calculated by the Landau-Levich equation (Eq. **4.1**) [Landau and Levich 1942]:

$$h = 0.94 \cdot \frac{(\eta \cdot v)^{2/3}}{\gamma_{LV}^{1/6} (\rho \cdot g)^{1/2}} \qquad \textbf{(4.1)}$$

where h is the coating thickness, η is the viscosity, γ_{LV} is the liquid-vapor surface tension, ρ is the density, and g is the gravity. Figure **4-3** shows a schematics representative of the three stages in dip casting and a detailed sketch of possible fluid regions and kinetics during the densification. Thus, a slower pulling rate results in a thinner solution and a resulting thinner organic thin film. It is also possible to withdraw the substrate in a solvent-rich ambient which slows the film densification and may assist film ordering. By choosing an appropriate pulling rate and solution viscosity, dip casting can be easily controlled to form thin films ranging from 20 nm to 50 μm that are macroscopically uniform and reproducible.

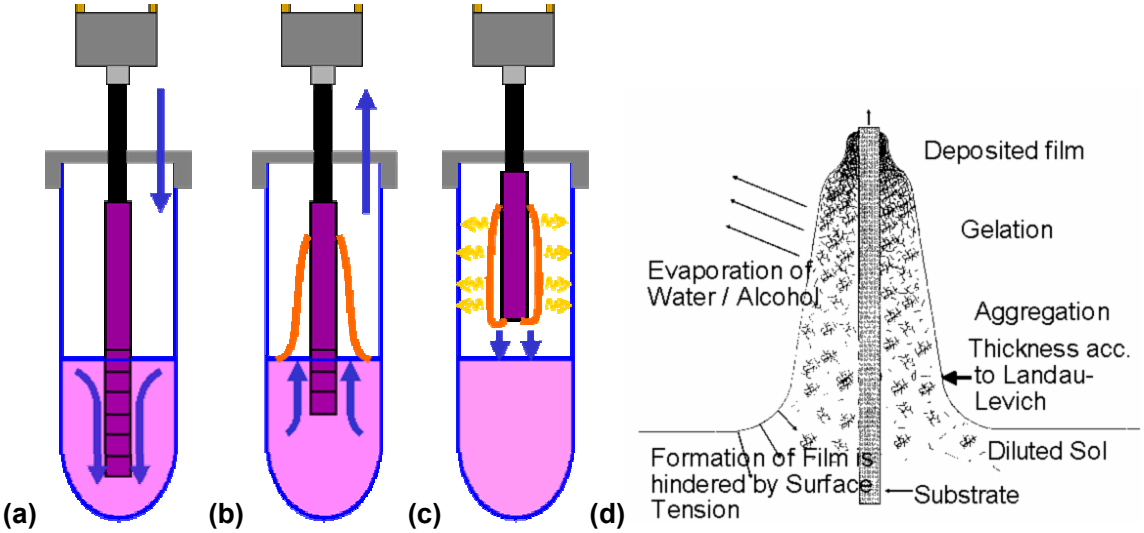

Figure 4-3**: Dip casting has three stages: (a) dipping, (b) wet film formation, (c) solvent evaporation and densification, and (d) detailed fluid regions and kinetics during densification.**

However, in the cases studied here controlling the film thickness and uniformity at the microscopic level is not as simple as the theory predicted. These solutions of small molecule organic semiconductors have a relatively low viscosity that is predetermined by the solvent used. As a result, it limits the ability to control the film thickness by varying the viscosity. We established the deviation from Equation **4.1**, which predicts a slope of 2/3 in log plot of thickness and pulling rate. 1 w.t. % TES ADT solution in toluene and deposited thin films on silicon dioxide using dip casting with various pulling rates as shown in Table **4-2**.

Table 4-2**: The pulling rates of the dip casting set up.**

Controller position	Pulling rate (mm/s)	(cm/min)	Pulling rate ratio
1	1.54	9.24	20
2	0.794	4.76	10
3	0.312	1.85	4
4	0.155	0.93	2
5	0.079	0.475	1

Figure **4-4** is a plot of thin film thickness versus pulling rate on a log-log scale. The linear fitted line has a slope of 0.49 and indicates that the correlation is lower than

the theoretical prediction. We also found such a relatively small thickness of these films in fabricating bottom contact OTFTs with 100 nm source and drain metal, which may affect the contact and their electrical properties. Thus, the ability to increase the film thickness in dip casting is also an important issue.

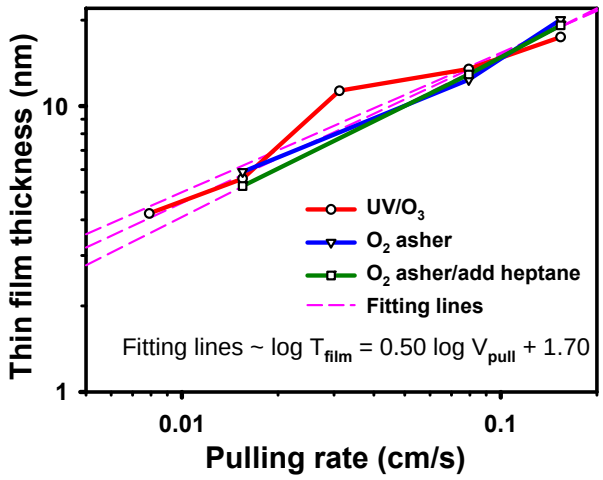

Figure 4-4**: Film thickness plotted as a function of the pulling rate from 1 w.t. % TES ADT solution by toluene on silicon dioxide substrates cleaned by UV ozone or oxygen plasma. The third line with squares is for the solution with 10 % of heptane.**

Figure **4-5** shows the film thicknesses using concentrations of 1 and 5 w.t. %. at various pulling rates. It reveals that the thickness scales up with the concentration increases, but is not exactly linearly proportional to the concentration. The measurements were carried out assuming that the film is uniform based on spectroscopic ellipsometry results, which were obtained for thinner films.

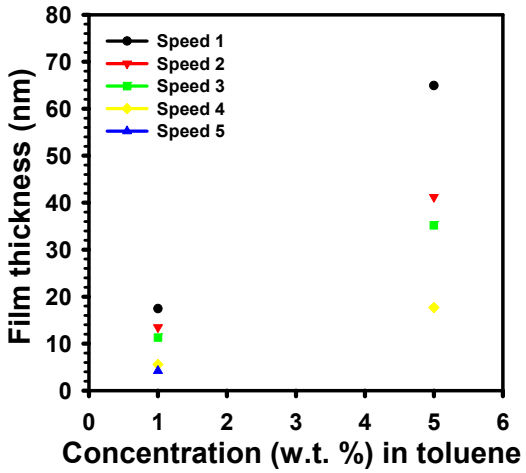

Figure 4-5**: Film thickness as a function of TES ADT concentrations of 1 and 5 w.t. % in toluene at various pulling rates.**

The morphology of the TES ADT films deposited by dip casting transits from a uniform flat layer into a three-dimensional films with complicated micro structures when the film is greater than about 30 nm. Figure **4-6** shows the optical micrographs of a thin film of 20 nm thickness (on the left) and a thick one on silicon dioxide substrates using dip casting. The right side of both pictures corresponds to the upper part of the substrates during the dip casting as the solution retreats from the right to the left of the micrograph. The right edge of Figure **4-6a** is the bare substrate. Such a thin TES ADT film on a silicon wafer is uniform and almost indistinguishable from a bare surface until the ellipsometry measurements are carried out or a scratch is drawn on it. Ellipsometry measurement results indicate films with thicknesses in a range of 5 to 30 nm have this character. Because the thin film wets the whole surface, a total dewetting in the cases of thicker films are not possible. On the other hand, a 40 nm thick film has a lot of structures as shown in Figure **4-6b**. The fractal-like structures of Figure **4-6b** reflects the kinetics of the film formation and indicates that the dynamics of the densification of the bottom and top layers are different. Because the solution has a low viscosity and can flow freely, the solvent withdrawn from the bottom layer can draw TES ADT molecules upward, unlike the case of a large heavy polymeric molecule. As a result, the densification in both layers is closely coupled. When the top layer film densifies, the

surface energy of the substrates is overridden by the bottom TES ADT so that the morphology is quite different from the bottom layer. The domains of the various microstructure sizes suggest a sequentially time-dependent film growth and reflect the complicated evolution of film growth that is associated with the individual local environments. Thus, this increases the difficulty in depositing uniform thin films of a desired thickness between 40 and 100 nm.

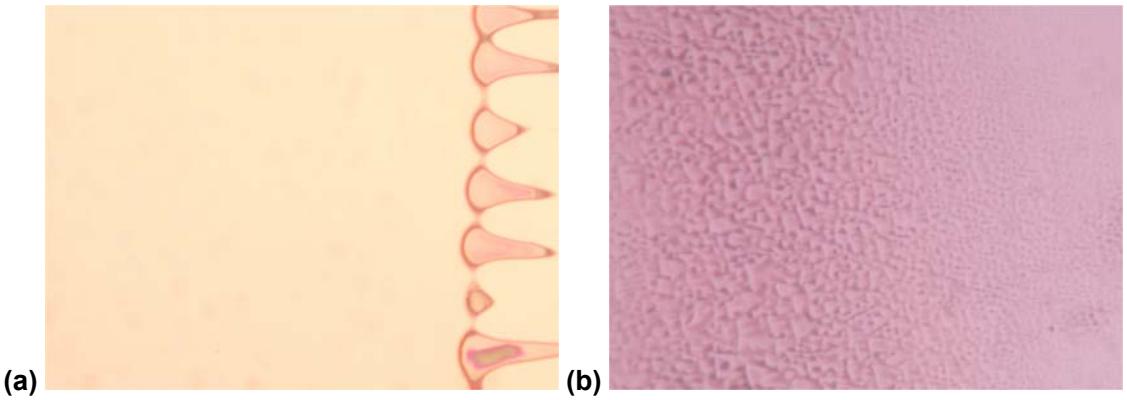

Figure 4-6**: Two 0.5 mm × 0.4 mm optical micrographs of TES ADT films on silicon dioxide substrates using dip casting: (a) a 20 nm uniform film (The right side with horn shape patterns is the top edge of the film.) and (b) a 40 nm film with periodic patterns of various sizes and domains like scales from the deposition. The right side is the upper part of the substrates during the dip casting in both cases.**

The morphology of these fractal features were further studied by atomic force microscopy. Figure **4-7** shows an atomic force micrograph of a dip-coated TES ADT film of about 800 nm on a smooth platinum surface (r.m.s. roughness ~ 0.3 nm). The film is macroscopically uniform but has a non-uniform microstructure, which includes a high density of film voids. Although the cross section analysis of a hole in Figure **4-7b** shows that the hole's depth is 80 nm with a smooth morphology at the bottom of it, the substrate in the hole should be covered by a thinner film according to the as indicated by the uniform 20 nm film as seen in Figure **4-6a**.

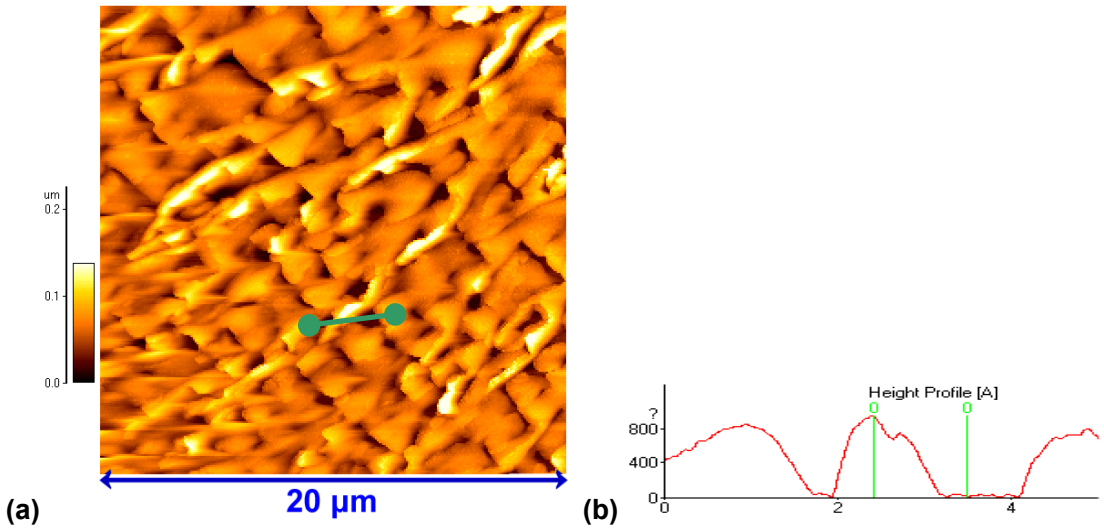

Figure 4-7: (a) Atomic force micrograph of a TES anthradithiophene thin film of 100 nm on platinum surface, deposited by dip coating. (b) The cross section analysis of a hole in the image.

Blade coating

The conventional blade coating method was adopted. In the conventional blade coating, also known as Doctor Blade, a mechanical aid, which is often a knife blade, is pressed to a moving surface to smooth the coating material on the surface. It is often used in industrial processes in cast coatings with film thicknesses above several microns with materials having a relatively high viscosity. The overall condition is not as simple as under the conventional condition. For example, the contact pressure from the blade to the patterned substrate is more restricted. Because the molecular dimension is small and the molecular weight and the concentration are low, the coating solution has a much lower viscosity, which allows it to flow freely. In addition, the desired thickness is one order of magnitude thinner (~100 nm) and the organic solvent vaporizes quickly. We modified the method to satisfy these differences and used solutions with concentrations between 0.5 and 2 w.t.%.

A plastic film is used to distribute the organic semiconductor solution over the substrate with a gap of about 0.5 mm. As shown in Figure **4-8**, the blade is placed with its edge close to the substrate. The semiconductor solution is inserted behind the blade and forms a solution reservoir in the triangular gap. By drawing the blade across the substrate a thin organic active layer is coated onto the substrate at a rate of about 2 cm/min manually.

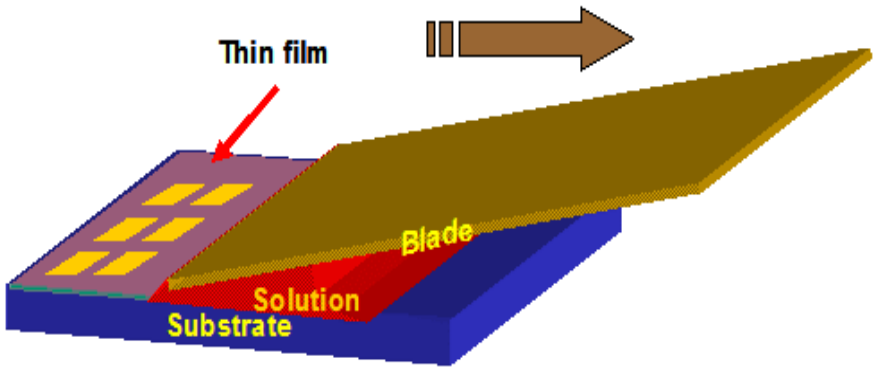

Figure 4-8**: Blade coating film deposition technique.**

We have found that such blade coating often results in films with improved wetting and reduced void density; however, the macroscopic uniformity of blade-coated films using this simple approach is often poorer than that with dip coating as seen in Figure **4-9**. This can be attributed to the difficulty of keeping the blade edge parallel to the surface with a constant height in such a simple setup. Nevertheless, the device performance is improved in many cases in comparison with that using dip and spin casting.

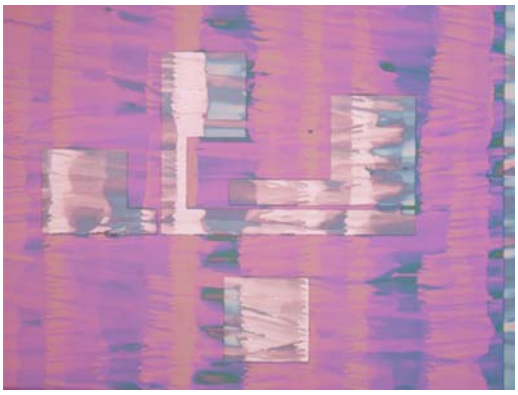

Figure 4-9: Optical micrograph of a TIPS pentacene thin film using our modified blade coating. The blade edge is along the y-axis and is moving from the right to the left.

Bar coating

A bar-coating machine consists of a coating bar sitting above a substrate, with a moving mechanism that drives the substrate to move against the bar. The moving part can be either the substrate or the coating bar. Figure **4-10** illustrates a typical coating bar with wire coils and the coating patterns before the fluid flows out and redistributes itself across the surface. Although the coating bar does not rotate in a typical setup, it can be rotated to reduce the fiction and the damages to the micro patterns on the substrate. The speed used is 3 cm/min or higher. The diameter and line density of wire coils can control the volume of the fluid drawn on the substrate. The selection of various wire coils allow us to examine the deposition conditions for a variety of thread spacings, thread depths, as well as coil materials and surfaces.

The film uniformity was improved, and it was found that bar coating results in thin TES anthradithiophene films with improved macroscopic uniformity compared to that of blade coating.

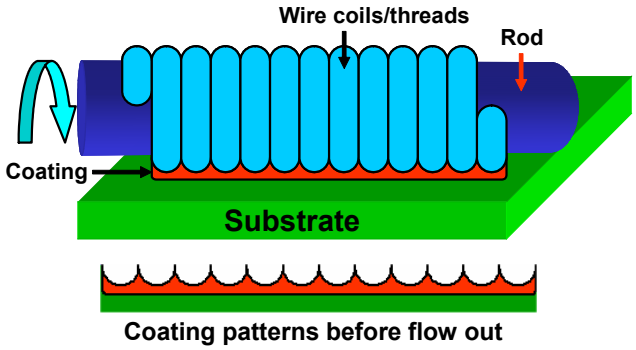

Figure 4-10: **Scheme of a** coating bar in bar coating. The wire coils guide the formation of this type of coating patterns.

Spin coating

Spin casting is a common method for depositing uniform films over a large area such as drawing resist on silicon wafers. Many processes for fabricating polymer OTFTs use spin casting. The spun-on polymer semiconductor is often more disorderly than those that with desired electrical properties; an annealing is also used to promote an ordered thin film. Because of the nature of this quick removal of solvent and rapid fluid flow from the rotation and mass exchange with the ambient, a rapid film growth often results in a less ordered film. Even in this situation some pentacene derivatives or anthradithiophene derivatives still can form dendrites on the substrates. This suggests a possible existence of good molecular ordering and a strong intermolecular $\pi-\pi$ interaction. Previously we only can get OTFTs with moderate performance (0.2 cm2/V-s) from a slow spin of about 700 rpm under conditions like drop casting. More recently, TIPS pentacene TFTs with a mobility larger than 1.5 cm2/V-s were fabricated from spin casting from a low concentration solution [Park, Kuo 2005]. This could lead to a renewed interest in using spin cast for small molecule OTFTs.

Blade and bar coating resulted in better devices with yields acceptable for which need further studies. Dip casting gives macroscopically uniform films and the device performance is in the moderate range. Spin casting offers better film uniformity, but the

performance is poor. Drop cast, another method not introduced above, yields a wide range of results. Table **4-3** shows a few methods' results of film morphology, uniformity, and device performance.

Table 4-3**: A list of deposition methods and their major characters.**

Methods	**Film morphology & uniformity**	**Dev. performance by mobility (cm^2/V-s)**
Dip casting	Macroscopically uniform, complicated micro film morphology	0.001 – > 0.1
Blade coating	Non-uniform, varying along the blade's moving direction	0.001 – 1.0
Bar coating	Non-uniform (better than blade coasting)	0.01 – 0.6
Spin casting	Uniform, micro dendrites (in some cases)	0.001 – 0.05
Drop casting	Non-uniform, many types of morphologies	0.001 – > 0.3

In addition to the device performance that is often evaluated by a few numbers from numerical measurements, the differences of I-V characteristics are dramatic and found to be impacted by the deposition methods. Figure **4-11** shows two output characteristics (I_D-V_{DS}) of two TIPS pentacene OTFTs with identical device structures and parameters using blade coating and dip casting, respectively. Figure **4-11a** has a typical curve features of a solution-processed OTFT which also includes the effect of poor device contact in the linear region and current crowding in the saturation region. On the other hand, a device with a dip-casted active layer as seen in Figure **4-11b**, has a linear region and a knee near the saturation. In stead of having a current crowding in the saturation region, the current continue to increase with V_{DS}. This may be attributed to the different kinetics of these two deposition methods and result in different film morphologies at the device contact or the differences in molecular ordering. Thus, substrates' surface energy and chemistry and solutions' wettability are crucial in developing the fabrication process, and such investigation are discussed later.

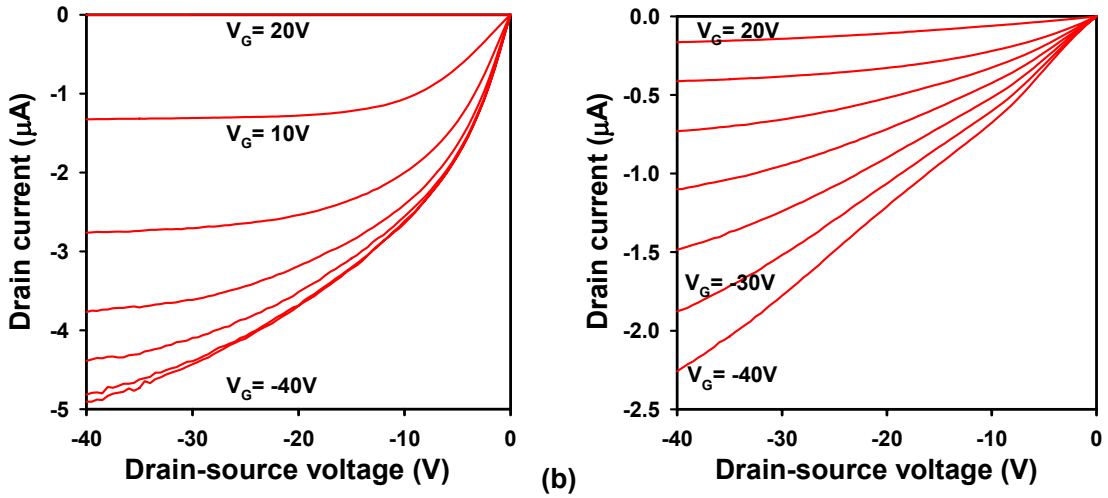

Figure 4-11**: These two I_D – V_{DS} characteristics of TIPS pentacene OTFTs were using (a) blade coating and (b) dip casting, respectively. The field-effect mobilities are 0.17 and 0.02 cm^2/V-s. The device structure and parameters are identical: Pt bottom contacts, a channel length and width of 22 and 340 μm and the SiO_2 gate dielectric thickness of 370 nm.**

Organic solvents are a key parameter in the solution processing. These derivatives have a high solubility in hexane, chlorobenzene, toluene, dichlorobenzene, xylene, etc. They are also soluble in common solvents, such as acetone and IPA. Thin films deposited from solvents with an aromatic group often have better semiconducting properties for transistors. However, because of the complexity in several of the few key factors, we have not been able to identify the solvent property responsible for the differences.

4.3 **Improvements of Solution-Processed OTFTs**

In order to increase the device performance, it is desirable to improve the film for its electronic transport. Although the molecular stacking of a few types of organic semiconductor crystals can assist the electronic transport, the methodology for making such type of films is not known. In addition to the diverse film uniformity that originates from the selection of a deposition method, the key factors of the film formation of small molecule organic semiconductors from solutions are not identified. The desired

properties of the thin films are not well established from the experimental results. Using the simple variable approach, we investigated the third and fourth variables (the manipulation of these types and sources of forces and the modification of the substrate surface) by modifying the gate dielectric surface (which is a high quality and of smooth dry thermally-grown silicon dioxide) and the contact surface.

Improving the Wettability and Thin Film Deposition

Because the film dewetting or localized drastic variations in morphology are a common problem in all deposition methods, the investigation of the wettability of the solution was selected as our focus. We can categorize the types of forces involved in the action into three groups: a) the capillary and centrifugal forces associated with the deposition method and b) the intermolecular forces and the substrate's surface tension corresponding with the solution (including the solvent and semiconductor molecules), the surface energy of the substrate (and also the blade), as well as the ambient.

The method of depositing a semiconductor solution often predetermines the types, the sources, and the levels of these two forces in the interaction. For example, the centrifugal force dominates the interaction in spin casting. The capillary force is only from one side (the substrate) in dip coating but from both sides in our modified blade coating using a flexible plastic blade. The capillary force can promote the wettability and the film coverage. Although some of these forces can be changed in order to study the film formation, we did not attempt to control them in our experiments.

Surface treatments by silane coupling agents were used to manipulate the surface energy of the gate dielectric and consequently the film formation. The silanes we selected were all shorter than 2 nm. Processing and ellipsometry characterization were carefully done to avoid silane polymerization or roughening the gate dielectric surface.

Table **4-4** shows the water contact angles and the thicknesses of TIPS pentacene films on silicon dioxide from dip coating to indicate the uniformity of films. The thicknesses are the average of a 3 mm^2 area of each film using the ellipsometry. The variation in the film thicknesses is small (less than 3 nm) for a substrate surface yielding

a contact angle less than or around 50 º. But the film thickness quickly reduces to almost zero if the contact angle is around 70 º. This indicates the strong correlation between the wettability of the toluene solution and the surface energy, where the change in thickness is rapid at the critical surface energy.

Table 4-4**: The film thickness of TIPS pentacene on substrates treated with four types of surfactants and on bare silicon dioxide, using dip coating from a 3 % toluene solution. (Surface tension of water, toluene, and SiO_2 are 71.8, 28.4, and > 120 dyne/cm, respectively.)**

Surface Treatment	Water contact angle (º)	Average film thickness (Å)
t-Butyldiphenylchlorosilane	25	392
Dimethylphenylchlorosilane	50	374
10-carbomethoxydecyl dimethylchlorosilane	50	377
Octyldimethylchlorosilane	70	10
Native SiO_2	< 5	367
Native SiO_2 (2 × pulling speed)	< 5	690

In addition, their film morphology varies with the types of surfactants. The average film thicknesses on SiO_2, SiO_2 with t-butyldiphenylchrolosilane or 10-carbomethoxydecyl-dimethylchlorosilane are approximately the same (~37 nm) but the morphological features have some similarities as well as distinctive differences as seen in Figure **4-12a, b, and c**. All three films have complicated fractal dendrites and a high surface coverage. The solution recedes from the bottom to the top, and this may explain why most of the dendrites mainly grew along the same direction. But the surface condition at each local region may also have a strong influence to change the evolving direction. Moreover, at certain locations the surface contaminant, such as particulates, can create a range of domain. The optical micrograph in Figure **4-12d** shows a dewetted film with round clumps on SiO_2 with octyldimethylchlorosilane.

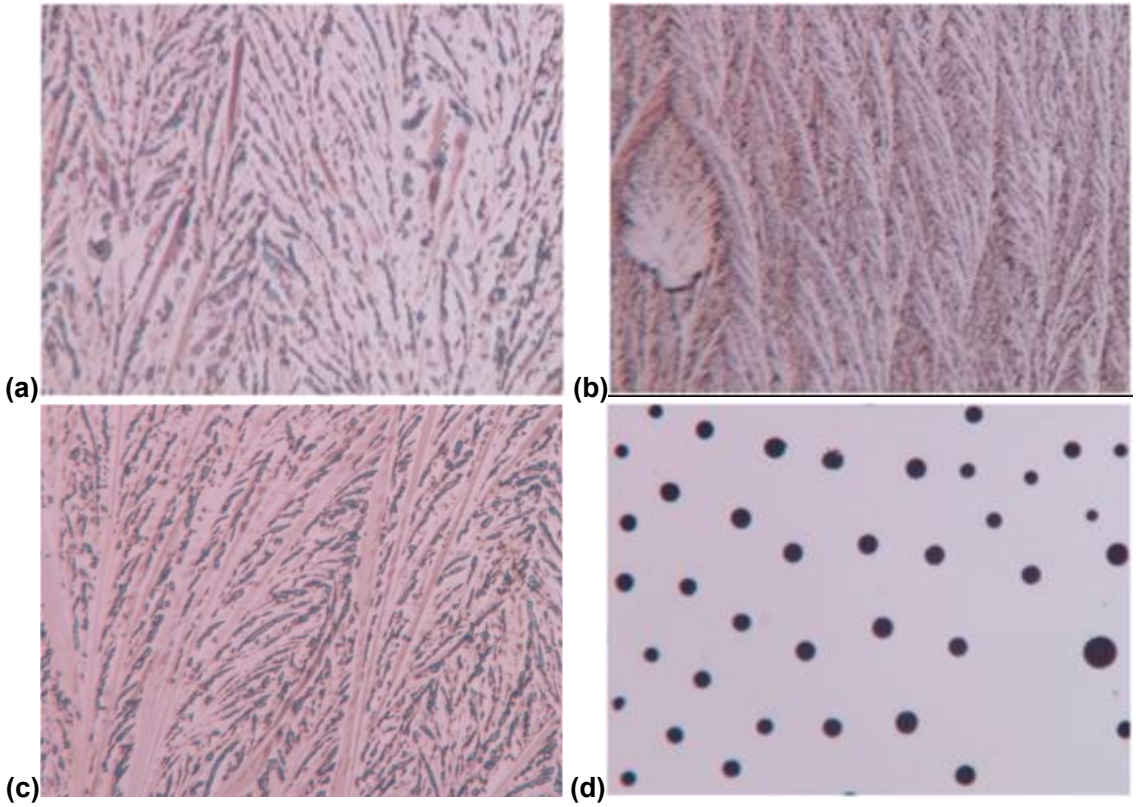

Figure 4-12**: Fractal dendrites of TIPS pentacene with dramatic variation of thickness (a) on SiO_2, (b) on SiO_2 with t-butyldiphenylchlorosilane, and (c) on SiO_2 with 10-carbomethoxydecyl dimethylchlorosilane. (d) A dewetted film on hydrophobic SiO_2 with octyldimethylchlorosilane. The solution recedes from the bottom to the top during the dip coating.**

The variation of the film thickness can be heightened at the border of different regions. The FESEM micrograph in Figure **4-13a** shows that several step edges forms among these parallel platelets and certain areas of the film becomes much thinner, estimated thickness of about 10 - 20 nm, than the flat platelet. Such step edges suggest the possible existence of micro or molecular ordering. The upper part of the image is the gold electrode, which is 100 nm thick. At the border of the gold electrode and silicon dioxide, the thin film is thin and does not have proper step coverage. As a result, the step coverage is poor and may cause poor electronic contact. Additionally, the surface's property transition and the height variation may cause strange morphological structures as seen in Figure **4-13b**. The film is dewetted on the silicon dioxide with OTS but it

forms a thick layer at the border and some three-dimensional bulges on the platinum. These are typical examples of the thin films obtained in depositions from solution.

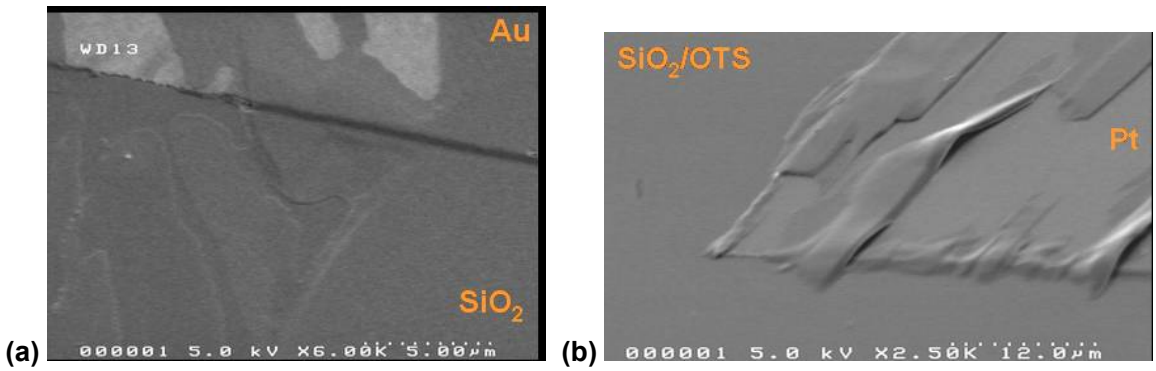

Figure 4-13**: FESEM micrographs of TIPS pentacene films (~ 40 nm thick) using dip casting from a toluene solution. (a) A few parallel platelet structures have step edges. (b) The film is thicker at the border of 100 nm Pt electrode. A few areas have bulges.**

These results demonstrate the importance of the surface which allows a control of the film formation in certain cases. The silane treatments, including contact treatments described in the next part, have been used to improve the properties of the films. However, the figures of these films (Figures **4-12** and **4-13**) all indicate the complicated nature of the film formation. More work is required in order to further understand and improve the film formation.

Contact Treatments

A common problem in a solution-processed OTFT is drain current crowding and large contact resistance. Organic contact treatments can be used to improve OTFT contacts. For example, source and drain contacts treated with 4-nitrobenzenethiol resulted in improved contact and linear region characteristics for pentacene OTFTs [Gundlach, Jia 2001]. But the performance enhancement can be different for different organic semiconductors. Thus, we compared the performance improvement using four thiolates with the control group applied to bare gold electrodes, including **1**) 3,4-

dichlorobenzenethiol, **2**) pentafluorobenzenethiol, **3**) 4-nitrobenzenethiol, and **4**) 2-mercaptobenzimidazole, shown in Figure **4-14**.

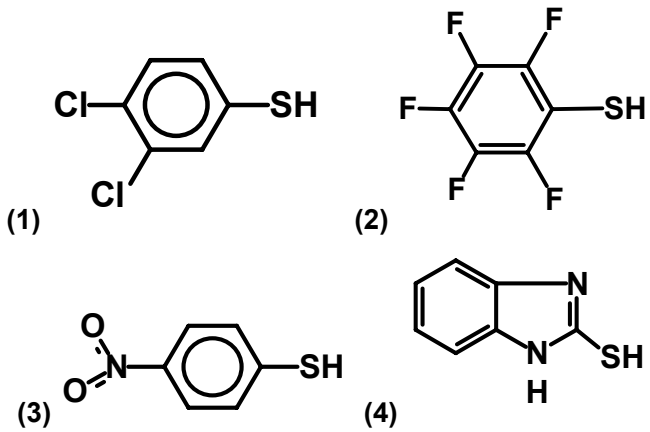

Figure 4-14**: Metal source and drain contacts (gold) were treated with these four thiolates for improving the contact performance: 1) 3,4-dichlorobenzenethiol, 2) pentafluorobenzenethiol, 3) 4-nitrobenzenethiol, and 4) 2-mercaptobenzimidazole.**

Figure **4-15** presents the current-voltage characteristics measured at a low drain-source voltage range to show the large variation associated with these contact treatments when the OTFT is operating in the linear region (V_G= -40 V). The curves for thiol **1** and **2** have a strong current ramp up and become larger than that of the bare gold electrode and the other two thiols, **3** and **4**. This suggests that pentafluorobenzenethiol and 3,4dichlorobenzenethiol and treatments can improve contact. The deep concave-down curves for thiol 3 and 4 correspond to an increase of the contact resistance. This can be attributed to the formation of an injection barrier at the interface or a growth of unfavorable film structures or molecular orderings for electronic transport. The initial I-V curve of the control group is adequate but the resistance increases rapidly, indicating the effect of drain current crowding.

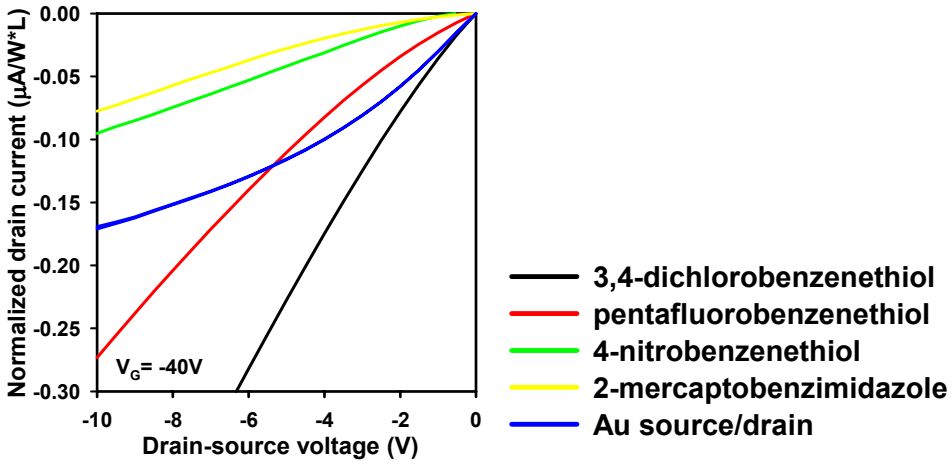

Figure 4-15: The I_D-V_{DS} characteristics of a TIPS pentacene TFT for small V_{DS} show a strong current modulation by the gate bias for treatments of thiol 1 and 2.

The overall I_D-V_{DS} characteristics of these devices using contact treatments as seen in Figure **4-16** also support the conclusions drawn from the characteristics of Figure **4-15**. Those two improved devices with thiol treatments **1** and **2** have a maximum drain current up to seven times larger than that of the lowest one and preserve the performance in the large drain-source voltage region. Such improvement may also be shown by the extracted saturation field effect mobilities of 0.3 cm^2/V-s of **1** and **2** which are about two times larger. Thus, the saturation drain current and the OTFT mobility are affected by the contact treatments which points to these contact treatments having an effect on other solution-processable organic semiconductors, such as TES ADT.

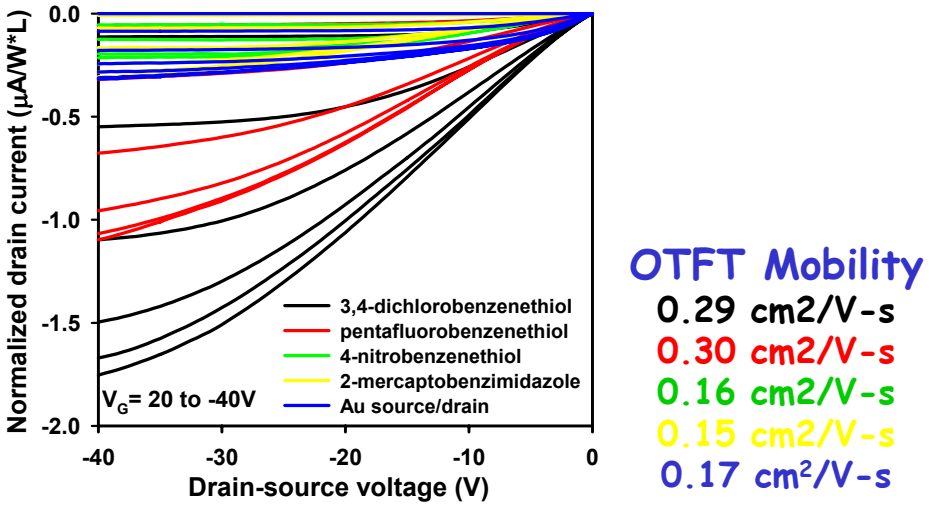

Figure 4-16**: The complete I_D-V_{DS} characteristics of Figure** 4-15**. The device contact difference results in as large as seven times difference of the drain current. Their field-effect mobilities are at the right side. The channel widths are either 300 or 340 μm and the channel lengths are between 14 and 22 μm.**

In addition to this general improvement, OTFTs based on TIPS pentacene were found to have a high device performance as seen in Figure **4-17**. The OTFT demonstrated here has a channel length of 22 μm, a channel width of 340 μm, and a silicon dioxide gate dielectric thickness of 370 nm and the active layer was deposited using the blade coating. Figure **4-17 a** and **b** show $I_D - V_{DS}$ characteristics for several gate voltages, $\log(I_D - V_{GS})$, $\sqrt{I_D} - V_{GS}$ characteristics. A saturation field-effect mobility of 0.8 cm^2/V-s and a threshold voltage of -40 V are extracted from the slope and intercept of the $\sqrt{I_D} - V_{GS}$ characteristics with V_{DS} = -40 V. The on/off current ratio is about 10^4 and the subthreshold slope is about 1.6 volts/decade. This was then the highest device performance of TIPS pentacene OTFTs.

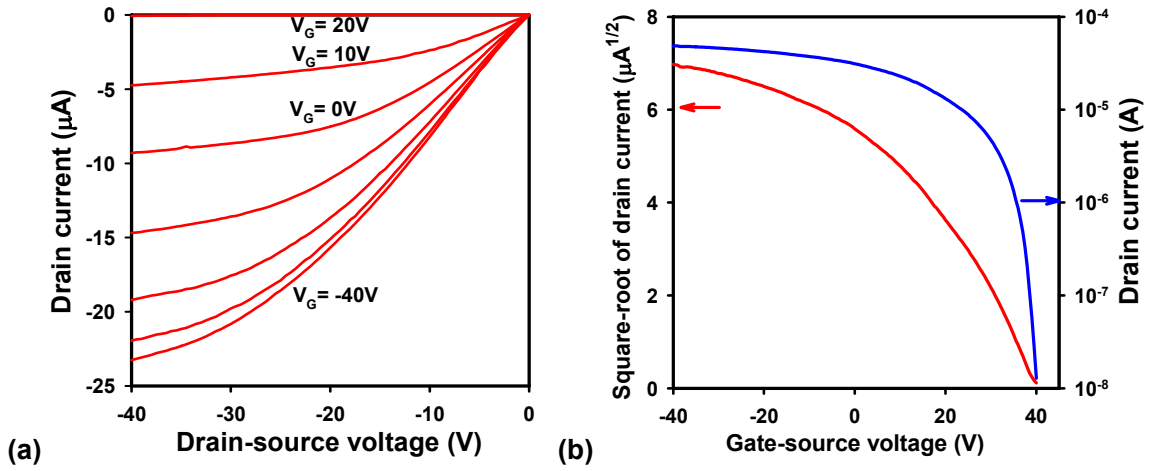

Figure 4-17: (a) I_D – V_{DS} characteristics and (b) log(I_D – V_{GS}) and $\sqrt{I_D}$ – V_{GS} characteristics of TIPS pentacene OTFTs with 3,4-dichlorobenzenethiol treated gold contacts. The channel length and width are 22 and 340 μm and the SiO_2 gate dielectric thickness is 370 nm. The extracted field-effect mobility is about 0.8 cm^2/V-s.

These thiol contact treatments have improved the OTFT device performance. OTFTs' field-effect mobility is a few times larger than that of the controlled group using thiol modified contacts. Nevertheless, the carrier injection in the linear region remains poor. This suggests the critical problem of carrier injection in this type of devices still need to be solved.

4.4 **Anthradithiophene Derivatives**

This section focuses on the derivatives with an anthradithiophene (ADT) backbone. A new class of materials, TMS, TES, TIPS ADT, are introduced, particularly TES ADT, which has shown interesting electronic properties.

TES anthradithiophene

Triethylsilylethynyl anthradithiophene (TES ADT), as seen in Figure **4-18**, is one of several small molecule materials that have been investigated in an effort to improve π-

orbital coupling in pentacene-like organic semiconductors. TES anthradithiophene is readily synthesized in two steps from commercially available starting materials and is soluble in a variety of common organic solvents. The synthesis does not require the use of transition metal catalysts and is easily scalable with the potentials for low material cost and flexible solution processibility.

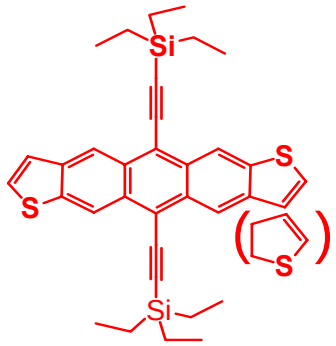

Figure 4-18**: Molecular structure of triethylsilylethynyl anthradithiophene (TES ADT) which has two isomers.**

The resulting product which is recrystallized repeatedly from hexanes to improve purity forms red crystals of mm in size as shown in Figure **4-19a**. TES anthradithiophene not only has two bulky groups but, compared to TIPS pentacene, has a modified backbone structure with one benzene ring replaced by a thienyl at each end. Single crystals of TES anthradithiophene have a close stacking structure, with 3.2 Å or 3.3 Å spacing between adjacent backbones depending on which of the two possible thienyl allotropes is involved as seen in Figure **4-19b**.

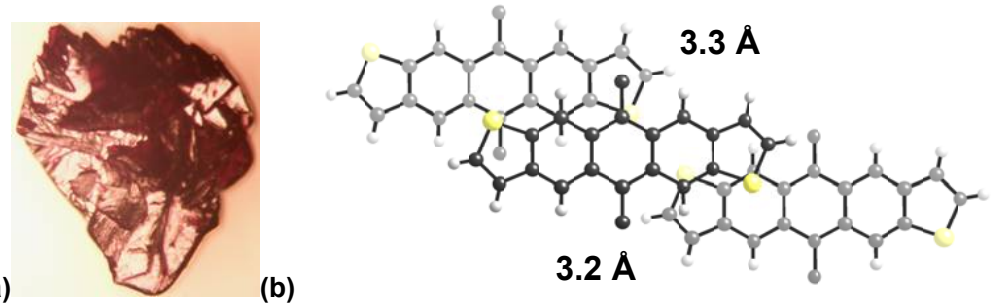

(a) (b)

Figure 4-19: (a) Optical micrograph of a 2 mm × 2 mm TES ADT crystal. (b) The structure of TES ADT molecular crystals is a two-dimensional slip stacking with slipping of 3.2 and 3.3 Å on either side.

Figure **4-20** shows two other anthradithiophene derivatives which were tested. A trimethylsilylethynyl ADT crystal shows a herringbone arrangement with no π-stacking as a result of a molecular order dominated by edge-to-face interactions. Triisopropylsilylethynyl ADT packs in a one-dimensional slip stacking with a distance of 3.46 Å between the π-faces. The electrical properties obtained with their OTFTs were poor having field-effect mobilities less than 10^{-4} $cm^2/V\text{-}s$. Hence, the prediction from the crystal arrangement is in agreement with the results of devices. This also validates the importance of increasing the π-interaction and reducing the interplanar spacing in the design.

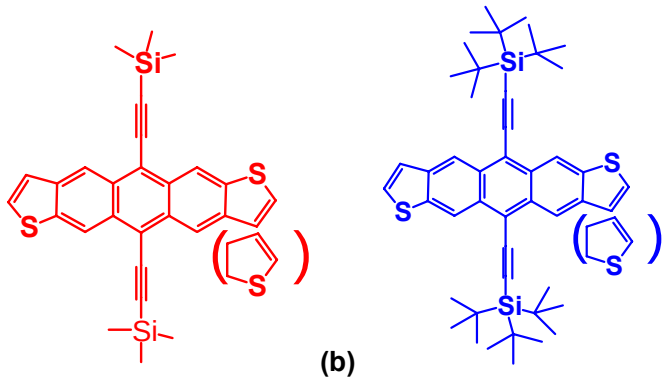

(a) (b)

Figure 4-20: The molecular structures of (a) TMS ADT and (b) TIPS ADT.

4.5 **Characteristics of TES Anthradithiophene OTFTs**

The solution-processed OTFTs described here had a channel length of 22 μm, a channel width of 340 μm, and a silicon dioxide gate dielectric thickness of 370 nm. Figure **4-21** shows $I_D - V_{DS}$ characteristics for several gate voltages, $\log(I_D - V_{GS})$, $\sqrt{I_D} - V_{GS}$ characteristics for an OTFT with TES anthradithiophene (ADT) active layer deposited by the blade coating. A saturation field-effect mobility of 0.3 cm^2/V-s and a threshold voltage of ~30 V are extracted from the slope and intercept of the $\sqrt{I_D} - V_{GS}$ characteristics with V_{DS} = -40 V. The on/off current ratio is about 10^6 and the subthreshold slope is about 1.6 volts/decade.

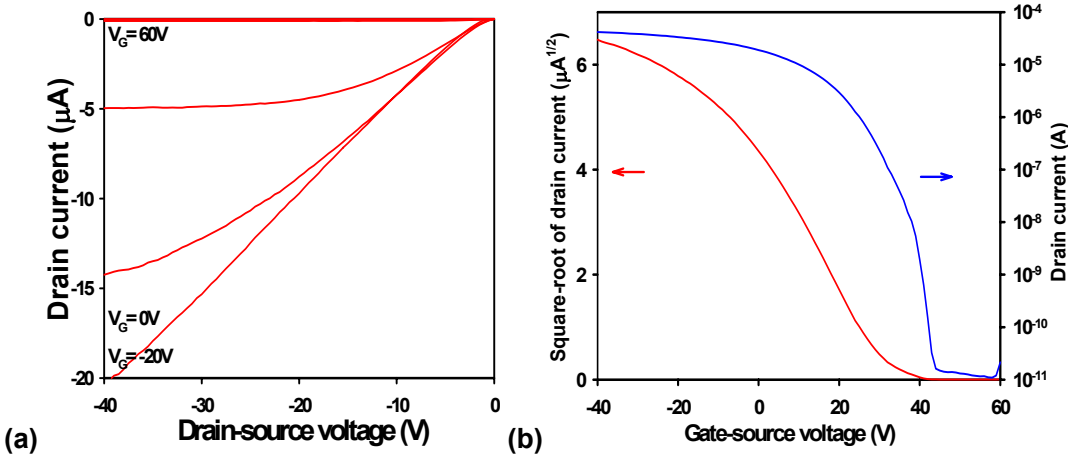

Figure 4-21: (a) $I_D - V_{DS}$ and (b) $\log(I_D - V_{GS})$ and $\sqrt{I_D} - V_{GS}$ characteristics of TES anthradithiophene OTFTs with untreated gold contacts. The channel length and width are 22 and 340 μm and the SiO_2 gate dielectric thickness is 370 nm. The extracted field-effect mobility is about 0.3 cm^2/V-s.

The linear $I_D - V_{DS}$ characteristics for the device shown in Figure **4-21a** indicate the presence of serious contact problems. There is a concave down region at small V_{DS} for some V_G curves and the channel resistance also appears to saturate for large negative V_G (that is, for the device in strong accumulation).

We used a contact treatment of pentafluorobenzenethiol to modify gold source and drain contacts for TES anthradithiophene OTFTs, and the device characteristics are improved. Figure **4-22** shows $I_D - V_{DS}$ characteristics for several gate voltages, $\log(I_D -$

V_{GS}), $\sqrt{I_D} - V_{GS}$ characteristics for an OTFT with TES ADT active layer deposited by blade coating and gold source and drain contacts treated with pentafluorobenzenethiol. A saturation field-effect mobility of 1 cm^2/V-s and a threshold voltage of ~5 V are extracted from the slope and intercept of the $\sqrt{I_D} - V_{GS}$ characteristics with V_{DS}= -40 V. The on/off current ratio is about 10^7 and the subthreshold slope is about 1 volt/decade.

The linear $I_D - V_{DS}$ characteristics for the device shown in Figure **4-22** indicate a moderate improvement in the OTFT contact characteristics. However, significant contact problems still remain and the device performance is probably contact limited so that further device improvements may be possible with further contact optimization.

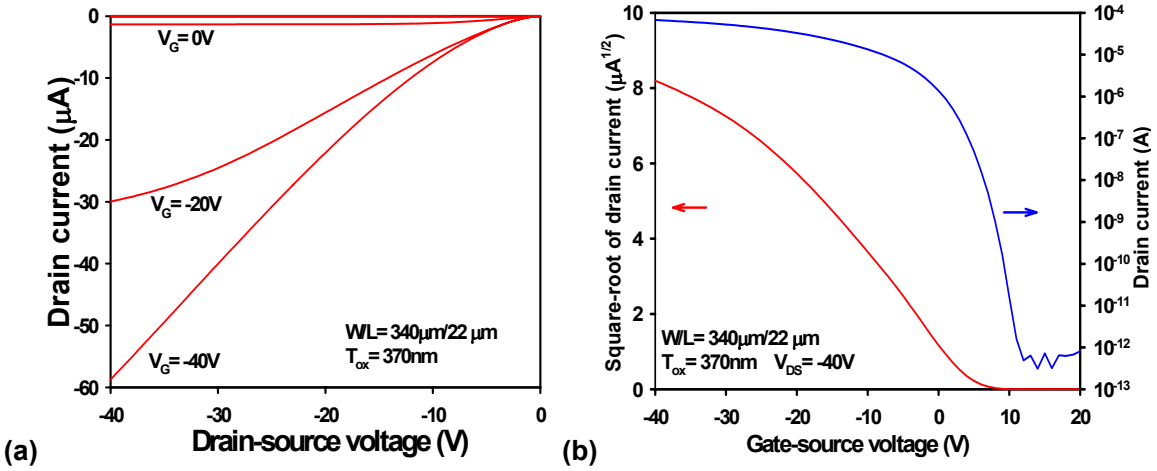

Figure 4-22: (a) $I_D - V_{DS}$ and (b) $\log(I_D - V_{GS})$ and $\sqrt{I_D} - V_{GS}$ characteristics of TES anthradithiophene OTFTs with pentafluoro-benzenethiol treated gold contacts. The channel length and width are 22 and 340 μm and the SiO_2 gate dielectric thickness is 370 nm. The extracted field-effect mobility is about 1 cm^2/V-s.

Figure **4-23** shows that the saturation field-effect mobility decreases with temperature where this OTFT has the same device dimensions reported above and an initial saturation field-effect mobility of 1.0 cm^2/V-s at room temperature. The mobility drops to 0.1 cm^2/V-s when the substrate is cooled down to about -100 ºC and it recovers to 0.6 cm^2/V-s at room temperature. This indicates the electronic transport in the solution-deposited film is like band transport. This would support the possible existence of molecular ordering in the thin film indicated by the presence of the dendritic

morphology seen in AFM and optical micrographs together with the platelet structures and terraces seen in the FESEM micrograph.

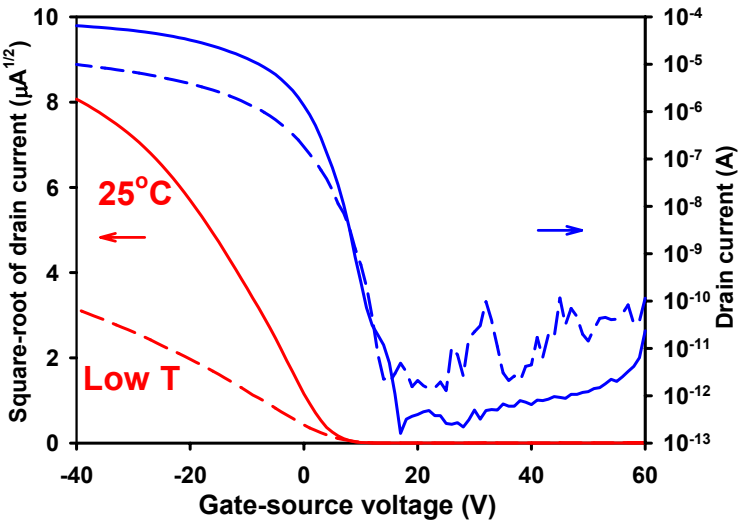

Figure 4-23**: The log(I_D – V_{GS}) and $\sqrt{I_D}$ – V_{GS} characteristics of a TES ADT OTFT with pentafluorobenzenethiol untreated gold contacts. The saturation field effect mobility varies with the testing temperature. The carrier mobility changes from 0.95 to 0.1 and back to 0.6 cm^2/V-s at 25 ºC, about -100 ºC, and 25 ºC, respectively.**

Although the device characteristics described here are not fully optimized and the contacts appear to limit device performance, these are the first reported solution-processed OTFTs using only low-temperature processing with performance that is similar to devices fabricated using vapor-deposited small molecule organic semiconductors. The availability of high-mobility solution-processable semiconductors can simplify device fabrication and in particular device patterning. This increases the likelihood that organic semiconductors will find applications in low-cost and large-area electronic applications.

4.6 **Molecular Designs and Improvement of Organic Semiconductors**

After the OTFTs' device performance dramatically improved in the last decade, there was a wide interest in newly-synthesized organic semiconducting materials. Many

approaches for achieving a high device performance were partly understood from the experience gained during the development of OTFTs based on organic semiconductors such as pentacene and α-6T. These include the material selection, the requirements on high purity, the deposition methods and their important parameters, the surface treatment of the gate dielectric, and the selection of electrodes. The small molecule organic semiconductors in the earlier studies were found often to have strong crystal forming properties and their ordered structure which could contribute to their large carrier mobilities. On the other hand, because these molecules have large anisotropy, their crystalline structures are not symmetric which may not assist carrier transport. However, the molecular stacking can be better controlled by modifying various molecular parameters. This offers the potential for synthesizing new molecules with desirable properties. In addition to the development of known organic semiconducting materials, which are commercially available, extensive knowledge was gained about the design and synthesis of new candidates.

We have discussed earlier the significant progress in utilizing new small molecules for OTFTs and confirmed our design hypotheses after fabricating and characterizing devices based on more than ten solution-processable small molecule organic semiconductors in collaborative research with University of Kentucky.

Improving the molecular stacking

A significant objective of designing new small molecule organic semiconductors is to improve the π-orbital overlap between molecules in molecular crystals. This requires manipulating the molecular stacking into an appropriate one. Organic molecular crystals of conjugated organic molecules often have a low-symmetry crystal structure (often monoclinic or triclinic) because of the large asymmetry of the molecules. Although pentacene OTFTs have thus far demonstrated the best OTFT device performance, pentacene molecular crystals have an open herringbone structure with a combination of face-to-face and edge-to-face interactions that result in minimal π-orbital

overlap and poor electronic transport. The 001 plane spacing for single crystal pentacene is 14.49 Å and the interplanar spacing is 5.7 Å as illustrated in Figure **4-24**. This interplanar spacing is much larger than the spacing of 3.4 Å of graphite. Thus, carrier transport in electrical field-induced channels is dominated by the difficulty of moving carriers from one molecule to the next and across grain boundaries.

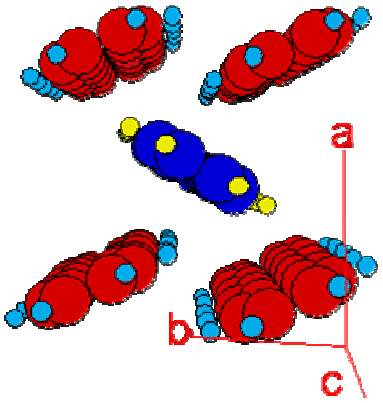

Figure 4-24**: A scheme of pentacene crystal structure – herringbone stacking.**

By substituting the bulky groups at the 6, 13 positions of pentacene, as seen in Figure **4-25**, it is possible to dramatically change the molecular crystal structure. Such improved molecular stacking is expected to result in a higher degree of π-orbital overlap between adjacent backbones and assist in carrier intra-grain and inter-grain transport.

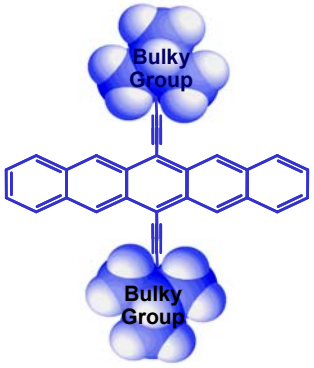

Figure 4-25**: Two substituted bulky groups at 6, 13 positions of a pentacene molecule.**

Triisopropylsilylethynyl pentacene (TIPS pentacene), as an example, adopts a two-dimensional slip-stacked structure and its interplanar spacing is 3.43 Å, a value close to that of graphite, as seen in Figure **4-26**. A few theoretical studies have focused on the correlation between the interplanar spacing and the HOMO and LUMO bandgap and bandwidth [Deng and Goddard 2004]. Because TIPS pentacene has a large anisotropy in structure, its conductivity depends on the crystalline orientation, where a single crystal shows significant anisotropy in conductivity [Anthony, Brook 2001; Wijsa, Mattheusa 2003]. Differences in conductivities due to differences in orientation are as large as four orders of magnitude. This suggests the possibility of new applications, such as an Electro-Optics material.

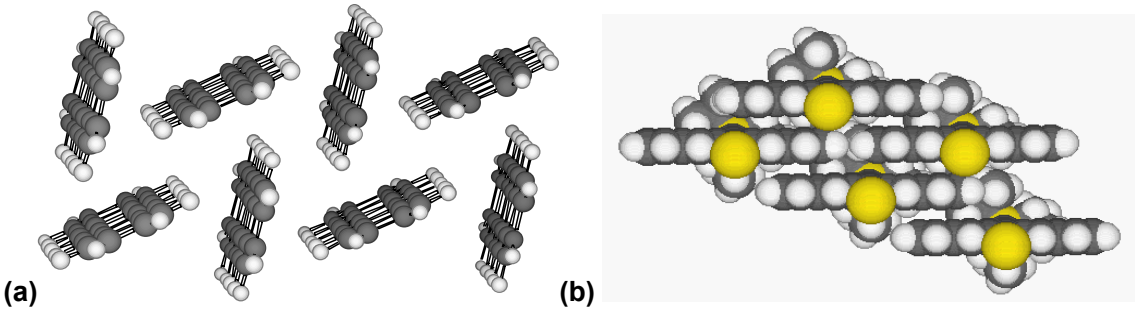

Figure 4-26**: Two substituted TIPS groups at pentacene's 6, 13 positions causes a dramatic change from (a) herringbone to (b) slipped-stack structure [Haddon, Chi 2002; Chen, Martin 2004].**

A small change in the size of the substituent group dramatically alters the arrangement of anthradithiophene derivatives. The TMS, TES, and TIPS groups cause the ADT derivatives to pack in herringbone, two-dimensional slipped-stack, and one-dimensional slipped-stack arrangements, respectively. Such slightly dimensional change of these bulky heads has a strong effect on the intermolecular interaction, the molecular stacking, and the interplanar distance of the backbone. Preliminary results show that OTFTs from the second one, TES ADT, can have few orders of magnitude higher mobilities. Both TES ADT and TIPS pentacene have a similar two-dimensional slipped-stacking and their solution-processed OTFTs have a high device performance with mobilities of ~ 1cm ^{2}/V-s. This clearly indicates the dominant or deterministic effect of a crystal structure on the thin film morphology, the molecular ordering, and the device

performance. Thus, significant improvements could be possible by changing the structure of the molecule. In addition, quantum mechanical simulation based on Marcus theory also predicts the mobility of oligoacenes to be as large as 15 cm^2/V-s [Marcus 1993; Deng and Goddard 2004]. Therefore, designing molecules with an appropriate arrangement for carrier transport has a practical advantage.

Molecular ordering in thin films

The molecular crystals are obtained from the vapor-deposited thin films of several newly synthesized organic semiconductors, particularly TIPS pentacene and TES ADT, both of interest for their electronic properties. Figure **4-27** shows the AFM micrograph and the X-ray crystallography of a thin film of TIPS pentacene that is purified by multiple recrystallizations. The film was deposited under high vacuum with the substrate holder held at 90 ºC. This figure shows the improved ordering with the d spacing of about 16.8 Å, that corresponds to the long axis of the molecule (c = 16.835 Å from the data of X-ray Crystallography) [Sheraw 2003]. The saturation field-effect mobility of OTFTs based on vapor deposited TIPS pentacene film can be as large as 0.4 cm^2/V-s, which indicates the potential of TIPS pentacene for a desirable active layer.

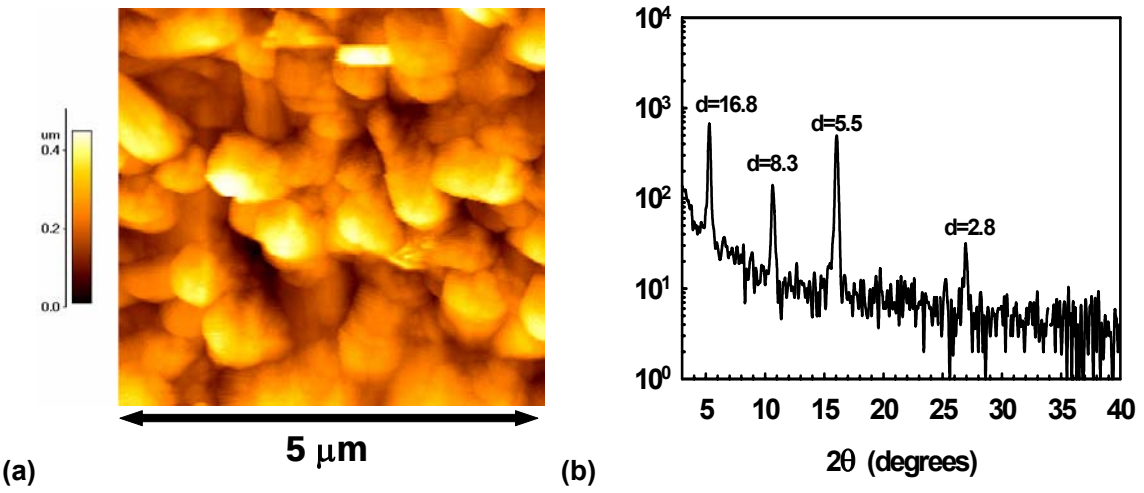

Figure 4-27: (a) AFM micrograph and (b) X-ray crystallography of a TIPS pentacene thin film from purified material using multiple recrystallizations [Sheraw 2003].

Thermally-evaporated TES ADT thin films were also found to have ordering that can be correlated with surface energy and other factors. Figure **4-28a** and **b** are 10 μm × 10 μm AFM micrographs of two vapor-deposited TES ADT thin films of 800 Å on vapor OTS treated SiO_2 and on untreated SiO_2, respectively. The substrate temperature is room temperature and the deposition rate is about 0.3 – 0.6 Å/s. Figure **4-28a** shows that several large molecular crystals micron in sizes are present with explicit molecular terraces that are as remarkably like those of typical small molecule organic semiconductor thin films. The step height is about the same as the long axis of the molecule and indicates the film is highly ordered on the "low surface energy" OTS surface. Although the other film is on the "high surface energy" SiO_2, it does not have such the same morphology, but the uniform grain formation and the ordered features suggest that it also has adequate molecular ordering. Thus, TES ADT also has a strong tendency to form molecular crystals and its growth morphology is strongly influenced by the surface energy. However, the electronic properties of vapor-deposited TES ADT are much poorer than solution-processed OTFTs in our initial attempts. The field-effect mobility is in the 10^{-3} $cm^2/V\text{-}s$ range. And further studies are necessary on evaporated thin films.

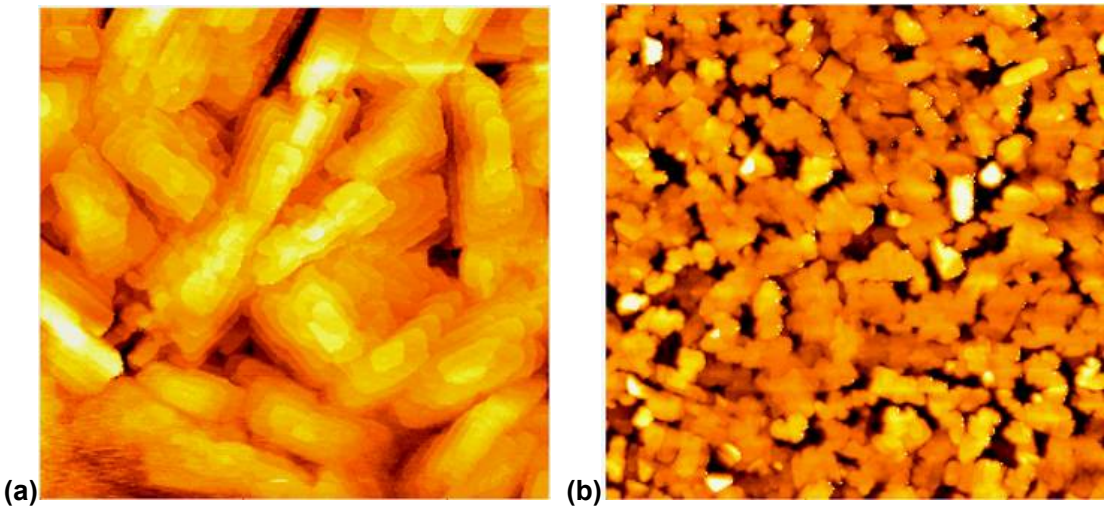

Figure 4-28**: Two 10 μm × 10 μm AFM micrographs of two TES anthradithiophene thin films that were thermally-deposited (a) on SiO_2 with OTS layer ("low surface energy") and (b) on SiO_2 ("high surface energy").**

Some of these molecules have a strong tendency to form molecular crystals from their solutions. Figure **4-29** shows a TIPS pentacene film with platelet morphology and an X-ray Diffraction of a TIPS pentacene thin film deposited from solution. The spacing of 16.8Å on the left corresponds to the TIPS pentacene's c-axis length, which shows that the high ordering present in these thin films results in their OTFT large field-effect mobilities. Thus, this property of self-organizing the structure into a molecular crystal from solution not only enhances the carrier transport in the two-dimensional stacking but also eliminates the high-temperature annealing process that is generally required to promote ordering in the film using a solution process.

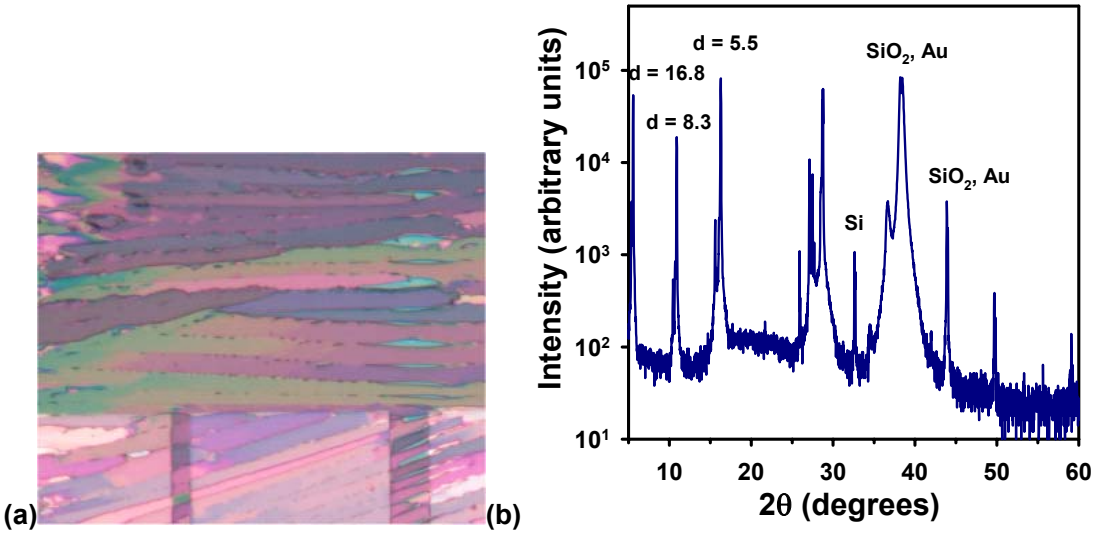

Figure 4-29**: X-ray diffraction of a TIPS pentacene film using solution processing.**

Improved solubility

From the early stages of development there has been the problem that the high device performance of many types of small molecule OTFTs have a low solubility. Because several types of these small molecule organic semiconductors are not soluble, they require a vapor deposition technique to achieve an active layer yielding high device performance. Because the molecular ordering of the thin films is essential for acceptable

OTFT characteristics, a good molecular design requires improved solubility which does not lead to a loss of the molecular ordering.

By substituting non-conductive but soluble functional groups on these molecules, it may be possible to increase the solubility and maintain a molecular stacking with a good or improved electron transport. Because these functional groups do not have a structure for assisting with electronic conduction, a limited but adequate molecular dimension is important in achieving acceptable solubility and a film formation with a preferred backbone stacking. An oversized functional group may cause much unnecessary interaction and problems in forming a conductive structure in the backbone [Halik, Klauk 2003]. Such a non-conductive group certainly has a negative effect on charge injection from the source electrode so the novel materials investigated typically have two functional groups. Each group has a short bulky alkane head (trimethyl, triethyl, or triisopropal) and a silylethynyl chain that links to the backbone. These bulky alkane heads affect their solubility, which varies between 0.5 % and 4 %. Higher solubility is desirable in developing a practical solution process but this has not been further investigated.

Additionally, these functional groups change the phase transformation of these materials; thus, offering further possibilities for processing. Most pentacene and anthradithiophene derivatives melt first prior to they vaporizing at a given elevated temperature which is different from the sublimation present in pentacene. Because the melting temperatures of these materials are lower than 200 °C, melting of these materials can be introduced as an alternative method for processing of thin films for applications.

Conducting backbones

Promoting of the intermolecular interaction of π-electrons could also assist with the charge transport. As we know, one π bond with two π electrons in a benzene molecule has a high probability of moving between any two adjacent carbon atoms by orbital coupling. Such coupling can assist with the intramolecular transport of electrons

inside an individual molecule, particularly for a long coupling network. Graphite's high conductivity is a clear example of this type of conduction by π electrons, as are the many conducting or semiconducting polymers. However, this type of network is much shorter in small molecule organic semiconductors where for example the intramolecular transport in an oligothiophene molecule (α-6T) is discretely limited to each pentagonal ring. Oligoacenes with a few fused benzene rings which act like a conductive molecular rod are limited to their lengths. Although it is difficult to separate the effect of the backbone from that of the crystalline structure and thin film morphology, the number of π electrons and their degree of intramolecular coupling is expected to have a strong effect on the electron transport. Although it is not clearly established, results on OTFTs published in peer-reviewed journals indicate that 15 % of the best field-effect mobilities in oligoacene OTFTs are about five times larger than those with oligothiophenes with similar fabrication and reproducibility. This suggests the importance of the backbone in improving and extending intramolecular transport.

We used molecules with either pentacene or anthradithiophene to form backbones. Compared to pentacene, the thiophene's bulky sulfur atom has two pairs of unbonded electrons and can cause an extra compression on the sulfur's bond angle and the rest of the thienyl ring. As a result, the thienyl plane is twisted and induces more delocalized electrons which influence the π-orbital overlap for a backbone with thienyl rings. However, whether this improve the performance has not been established and has to be investigated.

The recent OTFT results suggest that when the thin films of two molecules (TIPS pentacene and TES ADT) have stacking that favors the electron transport and a backbone of a similar size, the difference in the backbone (pentacene versus anthradithiophene) may not be the dominant difference in affecting field-effect mobility in the OTFTs. Solution-processed OTFTs of TIPS pentacene and TES ADT have mobilities of 1 cm^2/V-s but at the same time suffer from the two drawbacks of having a lower stability and higher insolubility. Both of these cause difficulties in a solution-based fabrication. Nevertheless, a longer backbone with fused acene- or thienyl- rings may raise the carrier mobility and studies are currently being carried out. The effect of the backbone serving

as a manipulator for achieving appropriate stacking is equally important to that of the functional groups. So an investigation of this remains crucial.

Improvement and suggestions

The material characterization and device measurement of these four materials support the proposed design rules and directions for new molecules. Figure **4-30** and Table **4-5** briefly summarize four of our molecular designs and their electrical properties. Although all three ADT derivatives have the same backbone, their field-effect mobilities have a difference of several orders. The majority of this difference is attributed to either the ability to form a thin film or the effect of the dramatic changes in their molecular stacking on the electronic transport. Both compounds **3** and **4** have the same bulky group (TIPS) where the difference between these backbones also results in two dissimilar stacking structures. This is also responsible for the difference in electrical properties. The backbones of the best two materials (**1** and **4**) are not similar in chemical structure but their dimensions and shapes are similar with comparable device performance. This suggests the intramolecular transport of the backbone does not have the dominant role if the backbones have similar elemental rings and sizes.

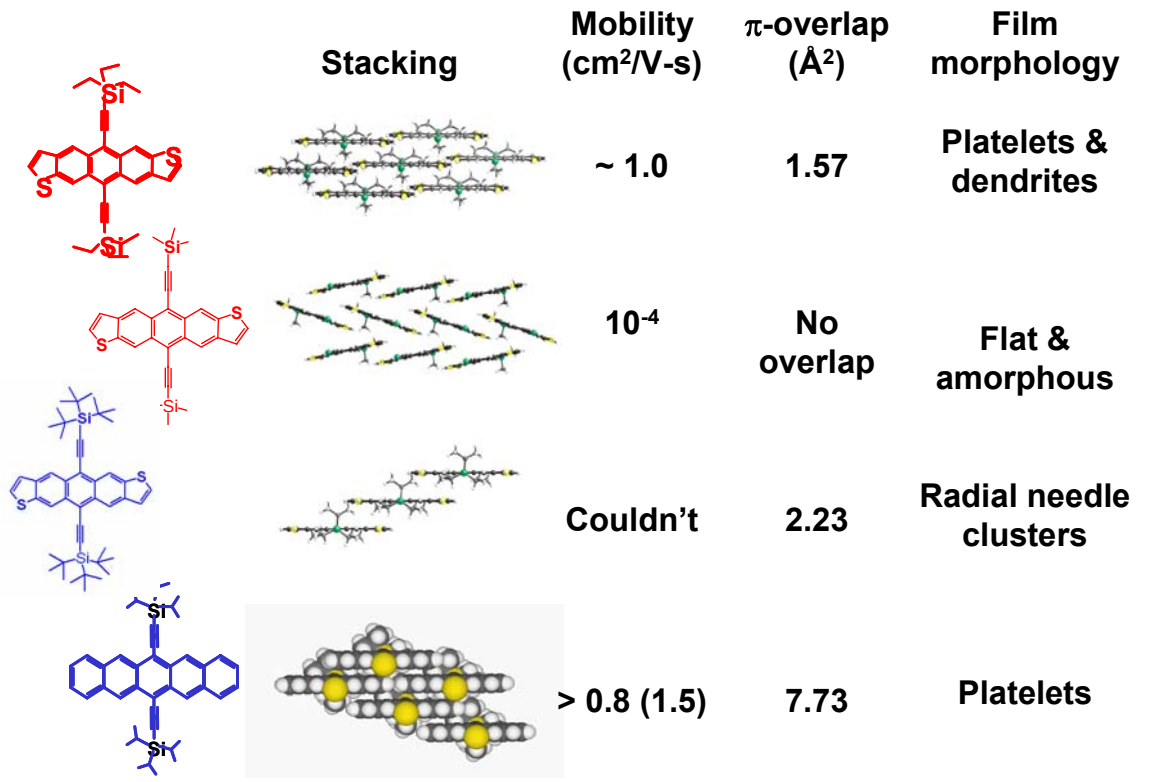

Figure 4-30**: A summary of four new small molecule organic semiconductors, their crystal structures and π-overlap in bulk crystals, thin film morphology using solution process, and OTFT performance.**

Studies using solution processing does not provide sufficient understanding of these molecules so no concrete conclusions can be drawn. These molecules have different properties when deposited from their solution or vapor sources. The performance differences in devices fabricated with the two techniques are often large so that the results presented here are preliminary. For example, TIPS ADT deposition from its solution failed to form a film so that it does not behave like an organic semiconductor. Nevertheless, it does have certain π-overlap and one-dimensional slip stacking which indicate that it still have the potential to be an organic semiconductor using other deposition techniques.

Table 4-5**: Device parameters for functionalized pentacene and anthradithiophene field-effect transistors and degree of p-overlap.**

Cpd	Compound name	Deposition methods	Mobility (cm^2/V-s)	I_{On}/I_{Off} ratio	π-overlap (Å^2)	Lateral slip (Å)
1	TES ADT	blade	1.0	10^7	1.57	2.75, 1.76
2	TMS ADT	blade	NA	NA	no overlap	no π-overlap
3	TIPS ADT	blade	$< 10^{-4}$	10^3	2.23	1.2
4	TIPS Pentacene	blade (drop)	0.8 (1.5)	10^6	7.73	0.9, 1.7

So far pentacene OTFTs still outperform the new designs discussed here. This maybe due to the limited research but it raises interesting question. The lack of adequate processing and poor electrical contacts to these materials are two possible causes for this. Based on some of the results on TES ADT, the device performance appears to be largely limited by the contacts. This points to the urgency of finding a solution for improving carrier injection in further development of organic electronics.

In addition to these design directions, hypotheses, and conclusions that were discussed in this section, the directions for synthesis of organic semiconductors should also include: 1) improving the charge injection from the source electrode by these functional groups; 2) extending the backbone to a larger size and testing their effect on intramolecular transport; and 3) improving the long range ordering or the alignment of molecular crystals in the thin film.

4.7 **Summary**

Based on the assumption that many of the variables in fabricating OTFTs from solution are independent and can be addressed separately, we have illustrated several aspects for achieving high performance solution-processed OTFTs based on TIPS pentacene and TES anthradithiophene. This includes the basic processes, the electrical characteristics of OTFTs, and the possible correlation between device performance and their molecular structures. This has led to OTFTs with a new record performance and

also draws attention and leads to a new approach for developing solution-processed OTFTs. In spite of these exciting results, it should also be noted that the assumptions, processing techniques, understanding, and conclusions are all preliminary.

Nevertheless, we have demonstrated low-temperature solution-processed OTFTs based on TIPS pentacene and TES anthradithiophene have field-effect mobilities as large as 0.8 and 1.0 cm2/V-s, respectively, where the first two types have comparable performance with either vapor-deposited pentacene OTFTs or a-Si:H TFTs. This is significant progress for solution-processed OTFTs in the development of organic electronics.

A few techniques for improving the OTFT device performance are presented and discussed. Using pentafluorobenzenethiol and 3,4-dichlorobenzenethiol to treat the source and drain metal, OTFTs based on either TIPS pentacene or TES anthradithiophene, with higher performance were achieved. The field-effect mobilities are several times larger and the carrier injection characteristics are improved, as well as the current crowding in the saturation region is reduced. But the performance still remains limited by the device contacts. The fabrication process is critical but the ability for achieving thin, uniform films remains low.

The properties and electrical characteristics of four newly designed molecules were analyzed and discussed. Based on two molecules which exhibit desirable electrical characteristics, two dimensional slip stacking is identified as a favorable molecular structure for carrier transport. The tendency to form an ordered film from a solution is an important factor. Our strategy of molecular design appears encouraging for creating novel organic semiconductors with device performance having a potential in future applications.

Chapter 5

Future Work

Organic electronics is becoming solidly rooted in the electronics industries. Currently, the production lines of flat panel displays using OLEDs are on the mark to ramp up and the shipping dates are written on the manufacturers' calendar. On the other hand, a variety of laboratory prototypes using OTFTs remain in the development stage and need to be greatly improved for commercial development. A fundamental understanding of organic devices remains incomplete or lacking, and standards and protocols of organic electronics are not well-recognized or undefined. Future work in developing OTFT technology can be separated into the following categories:

(1) General OTFT technology,
(2) Fundamental research and characterization of both small-molecule and polymer organic semiconductors,
(3) Organic synthesis for new organic semiconductors,
(4) Exploration of new applications and new types of devices such as flexible electronics, sensor and detector arrays, and diodes,
(5) Solution-processing technology for OTFTs, particularly printing,
(6) The establishment of OTFT standards and protocols, and
(7) The development of manufacturing capability for commercial products or prototypes.

A few of these are briefly described below.

General OTFT Technology and fundamental research

To reach the goal of practical applications, a few common challenges and problems of developing general OTFT technology need to be identified and solved.

Of great importance for continued advancement is forming “ohmic” source and drain contacts to the organic active layer. The results in Chapter 3 indicate that a large portion of the measured resistance in an OTFT is contact resistance. Such resistance dominates the device impedance in “short channel” OTFTs and limits the circuit density and complexity and the switching speed. The contact treatment process reported in Chapter 4 using thiols can improve carrier injection, reduce contact effects, and improve device operation in the linear region. Selection of metals by their workfunction only provides a partial solution and has limitations because most metals grow a barrier-like non-conductive oxide during fabrication or their effective workfunctions vary in a mixture of metal and organic semiconductors in the case of deposition of contacts on top of the organic semiconductors [Watkins, Le 2001; Crispin, Geskin 2002; Watkins, Yan 2002]. Selectively doping the narrow region between the channel and electrodes is also attractive. Making lithographic top contacts on the active layer is another way of reducing contact effect but such a device structure has proven difficult to fabricate and the contact improvement is thus far not dramatic. The likelihood of commercial OTFT applications would be significantly improved by an effective solution of the contact issue.

The electrical characteristics of pentacene TFTs, like those of OTFTs fabricated using similar small-molecule organic active materials, are often sensitive to environmental conditions. The source of the degradation in OTFTs has been attributed to oxygen doping where oxygen intercalates between organic layers and increases the measured film conductivity [Gundlach 2001]. The effect of oxygen doping is often reversible and the original device characteristics can be recovered by placing devices in a vacuum or an inert ambient [Laquindanum, Katz 1998; Herwig and Mullen 1999; Gundlach 2001; Maliakal, Raghavachari 2004]. Room humidity can also affect the measured device characteristics [Gundlach 2001]. The cause of such degradation is likely related to the adsorption of polar water molecules on the silicon dioxide surface where the carrier channel is accumulated. Instabilities in the electrical characteristics and device degradation with environmental exposure strongly limit the range of applications useful for OTFTs and greatly complicate circuit design. Ion beam sputtered barrier layers, aqueous-based photoresists, vapor-polymerized parylene, barrier-layers deposited

by plasma polymerization, or plasma-enhanced chemical-vapor-deposition at low temperatures may provide the needed environmental passivation.

Many characteristics of pentacene OTFTs cannot be controlled or optimized to achieve high reproducibility. For example, reproducibly obtaining a negative threshold voltage in p-channel OTFTs is of importance for improved circuit performance. Such an improvement would greatly simplify circuit design and improve circuit performance. The use of SAMs to chemically-modify the gate dielectric and controllably shift the threshold voltage is one conceivable method to achieve a negative threshold voltage.

To demonstrate utility for real applications, more studies of the processability and endurance of pentacene should be carried out. We have shown lithography using water soluble photosensitized PVA for patterning organic active materials. Further development may prove useful for patterning contacts and structures on the active layers and for designing new structures. Studies like these will expand a wider possibility of new device structures as well as processing flexibility.

Organic Synthesis for New Organic Semiconductors

The molecular design of TES ADT and TIPS pentacene and their large field-effect mobility of $\sim 1\ cm^2/V\text{-}s$ were described in Chapter 4. These materials are interesting because they exhibit a favorable two-dimensional molecular stacking for carrier transport. A tendency to pack with a high degree of π-orbital overlap from solution or vapor deposition is a useful criterion for organic semiconductor development. Current examples include hexacene, pentadithiophene, and their derivatives [Payne, Odom 2004; Zhang, Cote 2005]. Chemical stability can also be improved by molecular designs, such as substituted or twisted polyacenes, with further progress likely as understanding of OTFT degradation mechanisms improves [Maliakal, Raghavachari 2004]. Another interesting property of a few materials is low melting point. Melting may be used to assist the film deposition or recover the degraded devices due to stress and instability.

Solution-Processing Technology for OTFTs

We demonstrated low-temperature solution-processed OTFTs with performance comparable to that of vapor deposited pentacene OTFTs and a-Si:H TFTs. Advanced solution-processing techniques should be investigated to exploit the potential of these materials. At this point the process conditions for each material are like unique, and effort must focus on a specific material such as TES anthradithiophene and TIPS pentacene. Ultimately general techniques must be developed that allow a range of material types to be used in low-cost processing, such as printing technology and especially scaled to large substrates.

The OTFT standards and protocols and the manufacturing capability

The fabrication and performance of OTFTs have advanced to a level where conceptual demonstrations are regularly presented in industrial and university laboratories. OTFTs are no longer a laboratory curiosity but rather an emerging technology. So far pentacene OTFTs remain the most widely-studied for high performance OTFTs.

A systematic effort on pentacene OTFT technology is required to develop an adequate technology for real applications. One example is the control and optimization of device performance in large-scale fabrication. Although high performance devices can be repeatedly fabricated and performance variation is acceptable for simple demonstrations, the knowledge of tuning and control parameters for process optimization is incomplete. Device passivation is also of great importance but without a proper solution and reliability in real world applications is not known.

Conclusion

OTFT technology is very likely to be a part of future electronics. Though many problems remain, early device, circuit, and application demonstrations provide strong evidences that OTFT technology deserves serious investments to overcome the problems and explore opportunities in commercial electronic applications.

Bibliography

[Afzali, Dimitrakopoulos 2002] A. Afzali, C.D. Dimitrakopoulos, and T.L. Breen, "High-Performance, Solution-Processed Organic Thin Film Transistors from a Novel Pentacene Precursor," *J. Am. Chem. Soc.*, **124**, pp.8812-8813 (2002).

[Angst and Simmons 1991] D.L. Angst and G.W. Simmons, "Moisture Absorption Characteristics of Organosiloxane Self-Assembled Monolayers," *Langmuir*, **7**, pp.2236-2242 (1991).

[Anthony, Brook 2001] J.E. Anthony, J.S. Brook, D.L. Eaton, and S.R. Parkin, "Functionalized pentacene: improved electronic properties from control of solid-state order," *J. Am. Chem. Soc.*, **123**, pp.9482-9483 (2001).

[Assadi, Svensson 1988] A. Assadi, C. Svensson, M. Willander, and O. Inganas, "Field-effect mobility of poly(3-hexylthiophene)," *Appl. Phys. Lett.*, **53**(3), pp.195-197 (1988).

[Bao, Feng 1997] Z. Bao, Y. Feng, A. Dodabalapur, V.R. Raju, and A.J. Lovinger, "High-Performance Plastic Transistors Fabricated by Printing Techniques," *Chem. Mater.*, **9**, pp.1299-1301 (1997).

[Bednarz 2004] A. Bednarz, "DoD pumps up RFID effort." *NetworkWorld,* April 19, 2004, p 19.

[Bierbaum, Kinzler 1995] K. Bierbaum, M. Kinzler, C. Woll, M. Grunze, G. Hahner, S. Heid, et al., "A Near Edge X-ray Absorption Fine Structure Spectroscopy and X-ray Photoelectron Spectroscopy Study of the Film Properties of Self-Assembled Monolayers of Organosilanes on Oxidized Si(100)," *Langmuir*, **11**, pp.512-518 (1995).

[Borkan and Weimer 1963] H. Borkan and P.K. Weimer, "An analysis of the characteristics of insulated-gate thin-film transistors," *RCA Rev.*, **24**, pp.153-165 (1963).

[Brandon, West 2003] E.J. Brandon, W. West, and E. Wesseling, "Carbon-based printed contacts for organic thin-film transistors," *Applied Physics Letters*, **83**(19), p.3945 (2003).

[Brzoska, Azouz 1994] J.B. Brzoska, I.B. Azouz, and F. Rondelez, "Silanization of Solid Substrates: A Step toward Reproducibility," *Langmuir*, **10**, pp.4367-4373 (1994).

[Burroughes, Jones 1988] J.H. Burroughes, C.A. Jones, and R.H. Friend, "New semiconductor device physics in polymer diodes and transistors," *Nature*, **355**, p.137 (1988).

[Campbell, Robertson 1992] R.B. Campbell, J.M. Robertson, and J. Trotter, *Acta Crysallogr*, **15**, p.289 (1992).

[Carraro, Yauw 1998] C. Carraro, O.W. Yauw, M.M. Sung, and R. Maboudian, "Observation of Three Growth Mechanisms in Self-Assembled Monolayers," *Journal of Physical Chemistry B*, **102**(23), pp.4441-4445 (1998).

[Chen, Martin 2004] J. Chen, D. Martin, and J. Anthony, "Thin Film Morphology and Crystal Structure of Tips Pentacene," *American Physical Society, March Meeting 2004*, Montreal, Quebec, Canada, (2004).

[Chuman, Ohta 2004] T. Chuman, S. Ohta, S. Miyaguchi, H. Satoh, T. Tanabe, Y. Okuda, et al., "Active Matrix Organic Light Emitting Diode Panel using Organic Thin-Film Transistors," *SID*, **2004**, p.45 (2004).

[Crispin, Geskin 2002] X. Crispin, V. Geskin, A. Crispin, J. Cornil, R. Lazzaroni, W.R. Salaneck, et al., "Characterization of the Interface Dipole at Organic/Metal Interfaces," *J. Am. Chem. Soc.*, **124**, pp.8131-8141 (2002).

[Deng and Goddard 2004] W.-Q. Deng and W.A. Goddard, "Predictions of Hole Mobilities in Oligoacene Organic Semiconductors from Quantum Mechanical Calculations," *J. Phys. Chem. B*, **108**, pp.8614-8621 (2004).

[Dimitrakopoulos and Mascaro 2001] C.D. Dimitrakopoulos and D.J. Mascaro, "Organic thin-film transistors: A review of recent advances," *IBM J. Res. & Dev.*, **45**(1), pp.11-27 (2001).

[Ebisawa, Kurokawa 1983] F. Ebisawa, T. Kurokawa, and S. Nara, "Electrical Properties of Polyacetylene/Polysiloxane Interface," *J. Appl. Phys.*, **54**, p.3255 (1983).

[Emin 1970] D. Emin, "Correlated small-polaron hopping motion," *Phys. Rev. Lett.*, **25**, p.1751 (1970).

[Emin 1971] D. Emin, "Lattice relaxation and small polaron hopping motion," *Phys. Rev. B*, **4**, p.3639 (1971).

[Garnier 1998] F. Garnier, "Thin-film transistors based on organic conjugated semiconductors," *Chem. Phys.*, **227**, p.253 (1998).

[Gelest 2000] Gelest, *Silicon Compounds: Silanes & Silicones*, 1st ed, Morrisville, PA, (2000).

[Gelinch, Huitema 2004] G.H. Gelinch, H.E. Huitema, E.V. Veenedaal, E. Cantatore, L. Schrijnemakers, J.B.d. Putten, et al., "Flexible active-matrix displays and shift registers based on solution-processed organic transistors," *Nature Materials*, **3**, pp.106-110 (2004).

[Greenham and Friend 1995] N. Greenham and R.H. Friend, *An Electrophoretic Ink for All-Printed Reflective Electronic Displays*, ed, pp.1-149, Academic Press, San Diego, CA, (1995).

[Gundlach 2001] D.J. Gundlach. *Small-Molecule Organic Thin Film Transistors*. Penn State University, University Park, 2001.

[Gundlach, Jackson 1999] D.J. Gundlach, T.N. Jackson, D.G. Schlom, and S.F. Nelson, "Solvent-Induced Phase Transition in Thermally Evaporated Pentacene Films," *Applied Physics Letters*, **74**(22), pp.3302-3304 (1999).

[Gundlach, Jia 2001] D.J. Gundlach, L. Jia, and T.N. Jackson, "Pentacene TFT with improved linear region characteristics using chemically modified source and drain electrodes," *IEEE Electron Device Letters*, **22**(12), pp.571-573 (2001).

[Gundlach, Kuo 1999] D.J. Gundlach, C.C. Kuo, S.F. Nelson, and T.N. Jackson, "Organic Thin Film Transistors with Field Effect Mobility > 2 cm2/V-s," *57th Annual Device Research Conference Digest*, p.164 (1999).

[Gundlach, Lin 1997] D.J. Gundlach, Y.Y. Lin, T.N. Jackson, S.F. Nelson, and D.G. Schlom, "Pentacene Organic Thin-Film Transistors - Molecular Ordering and Mobility," *IEEE Electron Device Letters*, **18**(3), pp.87-89 (1997).

[Haas, Haase 2004] U. Haas, A. Haase, H. Maresch, B. Stadlober, and G. Leising, "Growth process control of pentacene thin films and its application in full organic thin film transistors," *IEEE Int'l Conf. on Polymers and Adhesives*, (2004).

[Haddon, Chi 2002] R.C. Haddon, X. Chi, M.E. Itkis, J.E. Anthony, D.L. Eaton, T. Siegrist, et al., "Band Electronic Structure of One- and Two-Dimensional Pentacene Molecular Crystals," *J. Phys. Chem. B*, **106**(33), pp.8288-8292 (2002).

[Halik, Klauk 2003] M. Halik, H. Klauk, Z. Ute, S. Gunter, R. Wolfgang, P. Sergei, et al., "High-mobility organic thin-film transistors based on α,α'-didecyloligothiophenes," *Journal of Applied Physics*, **93**(5), p.2977 (2003).

[Heil 1935] O. Heil, "Improvements in or relating to electrical amplifier or other control arrangements." U.K. Patent 439,457, 1935.

[Herwig and Mullen 1999] P.T. Herwig and K. Mullen, "A Soluble Pentacene Precursor: Synthesis, Solid-State Conversion into Pentacene and Application in a Field-Effect Transistor," *Advanced Materials*, **11**, p.480 (1999).

[Hiremath, Varney 2004] R. Hiremath, S.W. Varney, and J.A. Swift, "Oriented Crystal Growth of 4-Iodo-4'-nitrobiphenyl on Polar Self-Assembled Monolayer Templates: A Case for "Chemical Epitaxy"," *Chemistry of Materials*, **16**(24), pp.4948-4954 (2004).

[Hong, Kim 2005] M. Hong, B.S. Kim, Y.U. Lee, K.K. Song, J.H. Oh, J.H. Kim, et al., "Recent Progress in Large-Sized High-Performance Organic-TFT Arrays," *SID International Symposium*, Boston, MA, (2005).

[Horowitz 1998] G. Horowitz, "Organic field-effect transistors," *Advanced Materials*, **10**, p.365 (1998).

[Kakyou 2004] Kakyou, "First look at the Sony EBR-1000 Librie eBook reader." http://www.dottocomu.com/b/archives/002571.html (April 26, 2004),

[Klauk, Gundlach 1999] H. Klauk, D.J. Gundlach, J.A. Nichols, and T.N. Jackson, "Pentacene Organic Thin Film Transistors for Circuit and Display Applications," *IEEE Transactions on Electron Devices*, p.1258 (1999).

[Klauk, Schmid 2003] H. Klauk, G. Schmid, W. Radlik, W. Weber, L. Zhou, C. D.Sheraw, et al., "Contact resistance in organic thin film transistors," *Solid-State Electronics*, **47**, pp.297-301 (2003).

[Kline, McGehee 2003] R.J. Kline, M.D. McGehee, E.N. Kadnikova, J. Liu, and J.M. Frechet, "Controlling the field-effect mobility of regioregular polythiophenes by changing the molecular weight," *Advanced Materials*, **15**, pp.1519-1522 (2003).

[Koch, Kahn 2003] N. Koch, A. Kahn, J. Ghijsen, J.-J. Pireaux, J. Schwartz, R.L. Johnson, et al., "Conjugated organic molecules on metal versus polymer electrodes: Demonstration of a key energy level alignment mechanism," *Appl. Phys. Lett.*, **82**(1), pp.70-72 (2003).

[Landau and Levich 1942] L.D. Landau and B.G. Levich, "Entrainment of fluid by the driven plate," *Acta Physiochimm, U.R.S.S.*, **17**, pp.42-54 (1942).

[Laquindanum, Katz 1998] J.G. Laquindanum, H.E. Katz, and A.J. Lovinger, "Synthesis, morphology, and field-effect mobility of anthradithiophenes," *J. Am. Chem. Soc.*, **120**, p.664 (1998).

[LeGrange and Markham 1993] J.D. LeGrange and J.L. Markham, "Effects of surface hydration on the deposition of silane monolayers on silica," *Langmuir*, **9**, pp.1,749 (1993).

[Lide 2004] D.R. Lide, *Handbook of Chemistry and Physics*, 84th ed, CRC Press, Boca Raton, FL, (2004).

[Lilienfield 1930] J.E. Lilienfield, "Method and apparatus for controlling electric currents." U.S. Patent no. 1,745,175, 1930.

[Lilienfield 1935] J.E. Lilienfield, "Device for controlling electric current." U.S. Patent no. 1,900,018, 1935.

[Lin, Gundlach 1996] Y.Y. Lin, D.J. Gundlach, and T.N. Jackson, "High-Mobility Pentacene Organic Thin Film Transistors," *54th Device Research Conference Digest*, p.80 (1996).

[Lin, Gundlach 1997] Y.Y. Lin, D.J. Gundlach, S.F. Nelson, and T.N. Jackson, "Pentacene-Based Organic Thin-film Transistors," *IEEE Transactions on Electron Devices*, **44**(8), pp.1325-1331 (1997).

[Lin, Gundlach 1997] Y.Y. Lin, D.J. Gundlach, S.F. Nelson, and T.N. Jackson, "Stacked Pentacene Layer Organic Thin Film Transistors With Improved Characteristics," *IEEE Electron Device Letters*, **18**(12), pp.606-608 (1997).

[Loo, Willett 2002] Y.-L. Loo, R.L. Willett, K.W. Baldwin, and J.A. Rogers, "Additive, nanoscale patterning of metal films with a stamp and a surface chemistry mediated transfer process: Applications in plastic electronics," *Applied Physics Letters*, **81**(3), p.562 (2002).

[Maliakal, Raghavachari 2004] A. Maliakal, K. Raghavachari, H. Katz, E. Chandross, and T. Siegrist, "Photochemical Stability of Pentacene and a Substituted Pentacene in Solution and in Thin Films," *Chem Mater.*, **16**, pp.4980-4986 (2004).

[Marcus 1993] R.A. Marcus, "Electron Transfer Reactions in Chemistry: Theory and Experiment (Nobel Lecture)," *Rev. Mod. Phys.*, **65**, p.599 (1993).

[McGovern, Kallury 1994] M.E. McGovern, K.M.R. Kallury, and M. Thompson, "Role of Solvent on the Silanization of Glass with
Octadecyltrichlorosilane," *Langmuir*, **10**, pp.3607-3614 (1994).

[Meyer, Heringdorf 2004] F.J. Meyer, Z. Heringdorf, M.C. Reuter, and R.M. Tromp, "The nucleation of pentacene thin films," *Applied Physics A*, **78**, pp.787-791 (2004).

[Necliudov, Shur 2003] P.V. Necliudov, M.S. Shur, D.J. Gundlach, and T.N. Jackson, "Contact Resistance Extraction in Pentacene Thin Film Transistors," *Solid-State Electronics*, **47**, pp.259-262 (2003).

[Nichols, Gundlach 2003] J.A. Nichols, D.J. Gundlach, and T.N. Jackson, "Potential Imaging of Pentacene Organic Thin-Film Transistors," *Appl. Phys. Lett.*, **83**, (2003).

[Ostroverkhova, Cooke 2005] O. Ostroverkhova, D.G. Cooke, S. Shcherbyna, R.F. Egerton, F.A. Hegmann, R.R. Tykwinski, et al., "Bandlike transport in pentacene

and functionalized pentacene thin films revealed by subpicosecond transient photoconductivity measurements," *Physical Review B*, **71**, p.35204 (2005).

[Parikh, Schivley 1997] A.N. Parikh, M.A. Schivley, E. Koo, K. Seshadri, D. Aurentz, K. Mueller, et al., "n-Alkylsiloxanes: From Single Monolayers to Layered Crystals. The Formation of Crystalline Polymers from the Hydrolysis of n-Octadecyltrichlorosilane," *J. Am. Chem. Soc.*, **119**, pp.3135-3143 (1997).

[Park, Kuo 2005] S.K. Park, C.-C. Kuo, M.M. Payne, J.E. Anthony, and T.N. Jackson, "High Mobility Solution-Processed OTFTs," *IEEE International Electron Devices Meeting*, Washington DC, USA, (2005).

[Paul, Wong 2003] K.E. Paul, W.S. Wong, S.E. Ready, and R.A. Street, "Additive jet printing of polymer thin-film transistors," *Appl. Phys. Lett.*, **83**, pp.2070-2072 (2003).

[Payne, Odom 2004] M.M. Payne, S.A. Odom, S.R. Parkin, and J.E. Anthony, "Stable, Crystalline Acenedithiophenes with up to Seven Linearly Fused Rings," *Organic Letters*, **6**(19), pp.3325-3328 (2004).

[Rang, Haraldsson 2001] Z. Rang, A. Haraldsson, D.M. Kim, R.J. Chesterfield, C.D. Frisbie, P.P. Ruden, et al., "Hydrostatic Pressure Dependence of the Photoconductivity of Single Crystal Pentacene and Tetracene," *Appl. Phys. Lett.*, **79**(17), p.2731 (2001).

[Ruiz, Nickel 2003] R. Ruiz, B. Nickel, N. Koch, L.C. Feldman, R.F. Haglund, A. Kahn, et al., "Pentacene ultrathin film formation on reduced and oxidized Si surfaces," *Physical Review B*, **67**, p.125406 (2003).

[Ruiz, Nickel 2003] R. Ruiz, B. Nickel, N. Koch, L.C. Feldman, R.F.H. Jr., A. Kahn, et al., "Dynamic Scaling, Island Size Distribution, and Morphology in the Aggregation Regime of Submonolayer Pentacene Films," *Physical Review Letters*, **91**(13), p.136102 (2003).

[Salleo, Chabinyc 2002] A. Salleo, M.L. Chabinyc, M.S. Yang, and R.A. Street, "Polymer thin-film transistors with chemically modified dielectric interfaces," *Appl. Phys. Lett.*, **81**, pp.4383-4385 (2002).

[Schmidt and Mennig 2000] H. Schmidt and M. Mennig, "Wet coating technologies for glass." http://www.solgel.com (Nov. 2000),

[Schon, Berg 2000] J.H. Schon, S. Berg, C. Kloc, and B. Batlogg, "Ambipolar pentacene field-effect transistors and inverters," *Science*, **287**, p.1022 (2000).

[Schroder 1998] D.K. Schroder, *Semiconductors Material and Device Characterization*, 2nd ed, p.45, Wiley, NewYork, (1998).

[Schroeder, France 2002] P.G. Schroeder, C.B. France, J.B. Park, and B.A. Parkinsona, "Energy level alignment and two-dimensional structure of pentacene on Au (111) surfaces," *J. Appl. Phys.*, **91**(5), (2002).

[Shaheen, Radspinner 2001] S.E. Shaheen, R. Radspinner, N. Peyghambarian, and G.E. Jabboura, "Fabrication of bulk heterojunction plastic solar cells by screen printing," *Appl. Phys. Lett.*, **79**(18), pp.2996-2998 (2001).

[Shankar, Sheraw 2003] K. Shankar, C.D. Sheraw, E. Bullock, J.E. Anthony, and T.N. Jackson, "High mobility solution processed organic thin film transistors," *61st Device Research Conference*, (2003).

[Sheraw 2003] C.D. Sheraw. *Pentacene-based Organic Thin Film Transistors, Circuits, and Active Matrix Displays on Polymeric Substrates*. Penn State University, University Park, 2003.

[Sheraw, Zhou 2002] C.D. Sheraw, L. Zhou, J.R. Huang, D.J. Gundlach, T.N. Jackson, M.G. Kane, et al., "Organic Thin-Film Transistor-Driven Polymer-Dispersed Liquid Crystal Displays on Flexible Polymeric Substrates," *Applied Physics Letters*, **80**(6), (2002).

[Shockley 1952] W. Shockley, "A unipolar field-effect transistor," *Proc. IRE*, **40**, pp.1365-1376 (1952).

[Shockley and Pearson 1948] W. Shockley and G.L. Pearson, "Modulation of conductance of thin film of semiconductors by surface changes," *Physical Review*, **74**, pp.232-233 (1948).

[Sihvonen, Parker 1967] Y.T. Sihvonen, S.G. Parker, and D.R. Boyd, "Printable insulated-gate field-effect transistors," *J. Electrochem. Soc.*, **114**, pp.96-102 (1967).

[Silinsh, Klimkans 1995] E.A. Silinsh, A. Klimkans, S. Larsson, and V. Èápek, "Molecular polaron states in polyacene crystals: formation and transfer processes," *Chem. Phys.*, **198**, p.311 (1995).

[Sirringhaus, Tessler 1998] H. Sirringhaus, N. Tessler, and R.H. Friend, "Integrated Optoelectronic Devices Based On Conjugated Polymers," *Science*, **280**, p.1741 (1998).

[Smith and Dolan 2003] J.J. Smith and S.P. Dolan, *Historic Firsts: Notebooks Outsell Desktops and LCD Monitors Unit Sales Surpass CRT Monitors According to The NPD Group*. *The NPD Group, Inc.*, (2003).

[Stolka and Abkowitz 1993] M. Stolka and M.A. Abkowitz, "Trap-free charge transport in polymers, with tunable mobilities," *Synthetic Metals*, **54**(1), p.417 (1993).

[Thomas, Rudich 1999] E. Thomas, Y. Rudich, S. Trakhtenberg, and R. Ussyshkin, "Water absorption by hydrophobic organic surfaces: experimental evidence and implications to the atmospheric properties of organic aerosols," *J. Geophysical Research*, **104**(D13), pp.16053-16059 (1999).

[Thorsmølle, Averitt 2004] V.K. Thorsmølle, R.D. Averitt, X. Chi, D.J. Hilton, D.L. Smith, A.P. Ramirez, et al., "Ultrafast conductivity dynamics in pentacene probed using terahertz spectroscopy," *Appl. Phys. Lett.*, **84**, p.891 (2004).

[Tsumura, Koezuka 1986] A. Tsumura, H. Koezuka, and T. Ando, "Macromolecular electronic device: Field-effect transistor with a polythiophene thin film," *Appl. Phys. Lett.*, **49**(18), pp.1210-1212 (1986).

[Ulman 1991] A. Ulman, *An Introduction to Ultrathin Organic Films From Langmuir-Blodgett to, Self-Assembly*, 1st ed, Academic Press, New York, (1991).

[Ulman 1998] A. Ulman, *Thin films: self-assembled monolayers of thiols*, 1st ed, Academic Press, San Diego, CA, (1998).

[United-Chemical-Technologies 1993] United-Chemical-Technologies, *Silicon compounds: resister and review*, 5th ed, Bristol, PA, (1993).

[Watkins, Le 2001] N.J. Watkins, Q.T. Le, S. Zorba, L. Yan, Y. Gao, S.F. Nelson, et al., "Photoemission Characterization of Interfaces between Au and Pentacene," *SPIE Proc.*, (2001).

[Watkins, Yan 2002] N.J. Watkins, L. Yan, and Y. Gao, "Symmetry of Interfaces between Pentacene and Metals," *Appl. Phys. Lett.*, **80**, p.4384 (2002).

[Weimer 1961] P.K. Weimer, "An evaporated thin-film triode," *IRE Trans. Electr. Dev.*, **8**, p.421 (1961).

[Weimer 1962] P.K. Weimer, "Evaporated circuits incorporating a thin-film transistors," *International Solid-State Circuits Conference*, Philadelphia, PA, (1962).

[Wijsa, Mattheusa 2003] G.A.d. Wijsa, C.C. Mattheusa, R.A.d. Groota, and T.T.M. Palstra, "Anisotropy of the mobility of pentacene from frustration," *Synth. Met.*, **139**, pp.109-114 (2003).

[Young 1805] T. Young, *Phil. Trans Roy. Soc.*, **95**, p.65 (1805).

[Zhang, Cote 2005] X. Zhang, A.P. Cote, and A.J. Matzger, "Synthesis and Structure of Fused r-Oligothiophenes with up to Seven Rings," *J. Am. Chem. Soc.*, **127**, pp.10502-10503 (2005).

Appendix A

Fabrication Data and Tables

Film thickness of PVA, PMMA, 1811, and ma N 440 in the lithographic processing

Because the control of resist thickness is important for estimating parameters used in lithographic processes, particularly the controlled oxygen plasma etching of the buffer PVA layer, the thickness and etching rate of this multiple layer stacking have to be precisely known. Table **A-1** is an index for different combination of resist stacks, and can be used as a reference for direct lithographic top contacts.

Table A-1: Film thicknesses of materials used in the photolithographic process for fabricating top contacts.

Materials \ Process	RIE etch	Spin 1500rpm	2000rpm	3000rpm	4000rpm	5000rpm	6000rpm
Si/PVA30 6% in H2O (MMW)	138nm/m			271nm			
Si/PVA30 6%/1811 40% dilute	52.5nm/m					130nm	
Si/PVA30 6%/PMMA 495k 4%	84-108/m					326-350nm	
PVA86 6% (ADC) in H2O (HMW)	136nm/m					410-426nm	
PVA86 (ADC) 6%			574nm, 2L: 1107nm			370nm	
PMMA 4% 495K						330nm	
PMMA 4% 500K			537nm				
PMMA 4% 100K		443nm					
1811					1130nm		
1811 3:1 dilute					713nm		~ 580nm
ma-N 400 27:15 dilute				~1500nm			
MR standard PMMA C 495K 2, 4, 6% in ClBenzene (Cauchy An= 1.491)			145nm, 370nm, 700nm	130nm, 340nm, 640nm	140nm, 330nm, 600nm		
MR standard PMMA C 495K 8, 9% in ClBenzene			1400nm, 1580nm		750nm, 1310nm		
MR standard PMMA C 950K 2, 4, 7% in ClBenzene (Cauchy 1.488, 2.898e-3, 1.579e-4)					150nm, 470nm, 980nm		
MR standard PMMA C 950K 9, 10% in ClBenzen					1700nm, 2300nm		
PVA86 5%				436-403nm		343nm	8k: 123nm
PVA13 5%				198nm			
PVA LMW 5%						141nm	8k: 123nm
PVA LMW 10%				309-339nm		367nm	

Appendix B

User's Guide of AutoData Software

B.1 **Quick Start Guide**

AutoData software is developed to provide a convenient and rapid control of the semiconductor parameter analyzer as an efficient device testing vehicle. The system's architecture includes the GPIB card, electrical measurement device (EMD, also called Analyzer), the switch box, the probes and probe card, and the probe station. It is capable of controlling Agilent 4145A/B, 4155A/B/C, and 4156A/B/C, 4141B, and Keithley switch matrix 706, 707, and 708. (Although Hewlett Packard had spun off Agilent for years, many electronics made by HP remain have the same mark. In this software, these two names are considered as equivalent. The device to be tested is denoted as "EDev".)

Figure **B-1** is the start-up screen that shows the author information and the license type of this software. Please follow the "Basic operating steps" to get start.

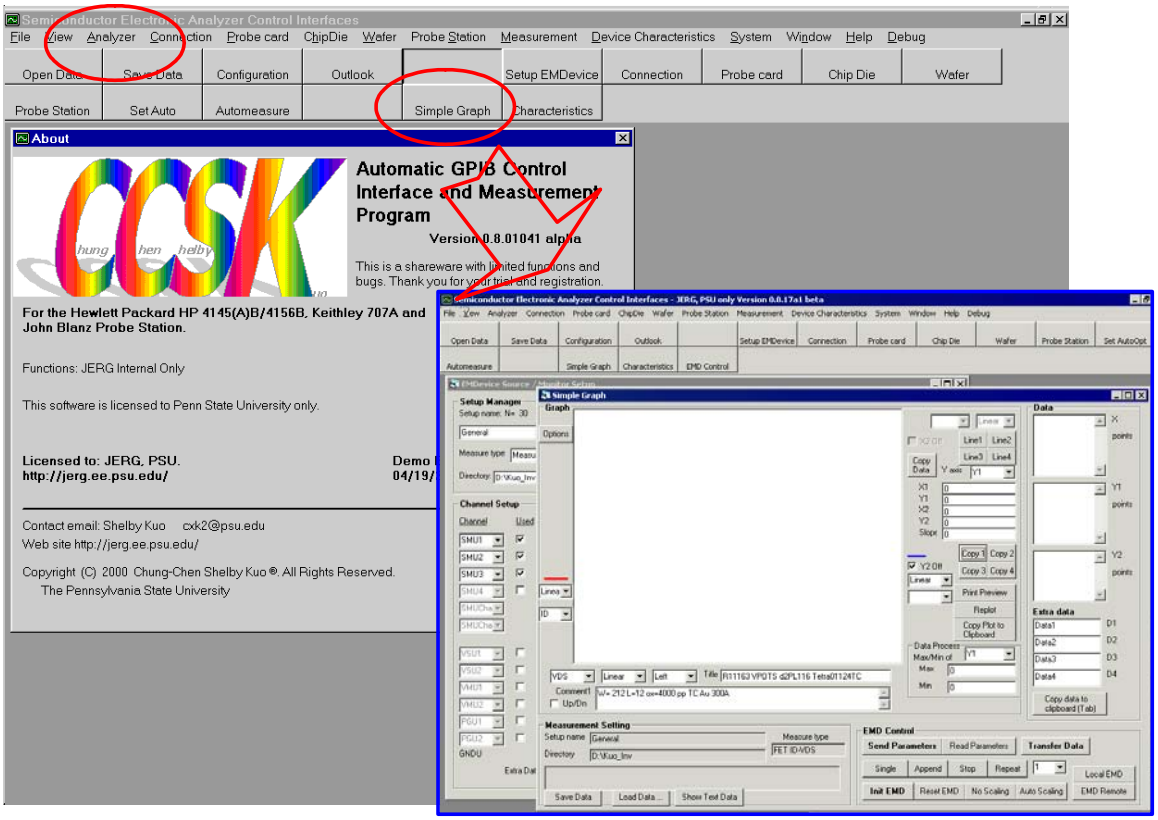

Figure B-1**: The start-up screen of AutoData.**

Basic operating steps

1. Run AutoData program
2. Use the "virtual GPIB" setting if you do not have either NI software installed or GPIB card installed: [Menu/Debug][Virtual GPIB]
3. Choose an analyzer. Any electrical measurement devices (EMDs) are denoted as “EMD” in AutoData: [Menu/Analyzer][HP 4145], HP 4156], [HP 4194], or [HP4141]. The “EMD setup” and “Simple Graph” windows pop up (Figure **B-2** and). If the “Simple Graph” widow does not, click the "Simple Graph" button on the tool bar.

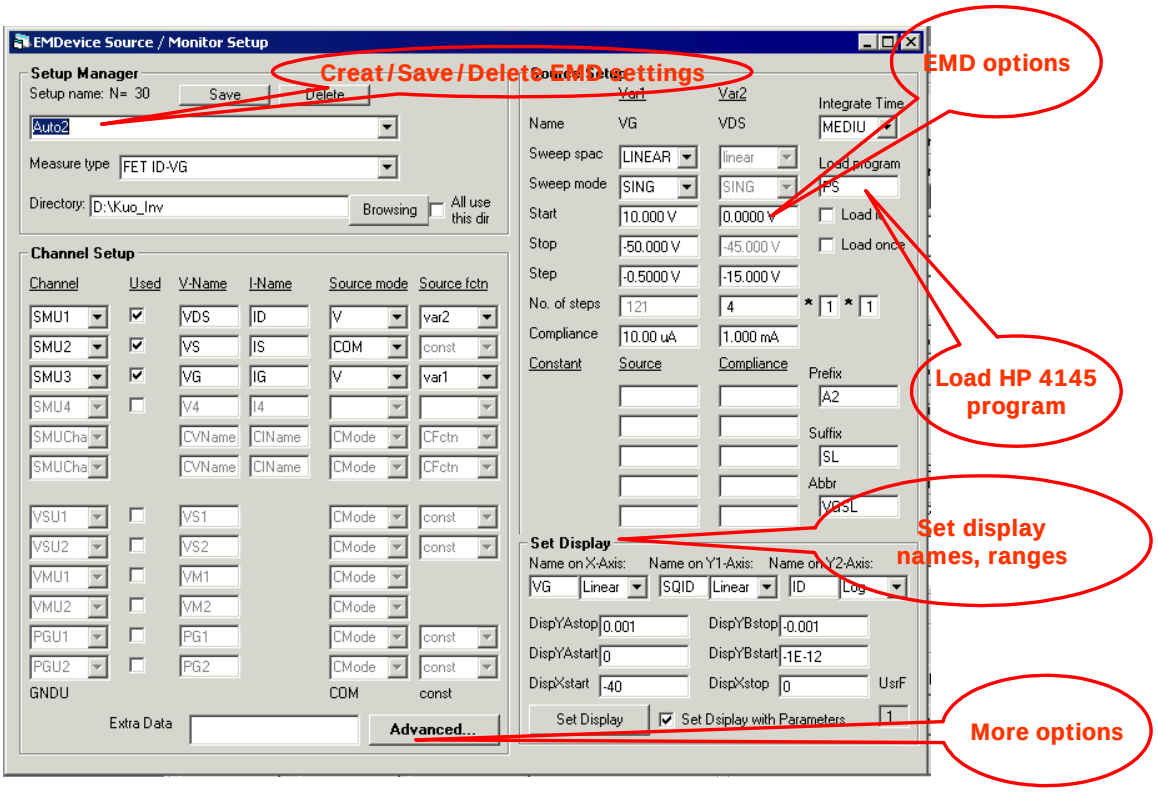

Figure B-2**: The "EMD Setup" window.**

4. Pick up the EMD setup name you want from the "EMDevice source/monitor setup" window.
5. Ex: Auto1 (Each name is associated with a set of parameters. Maximum of fifty different sets can be stored. If the number is more than that, the program often halts.)
6. The settings and parameters will be refreshed.
7. Click the "Init EMD" button in Simple Graph window as shown in Figure **B-3**.

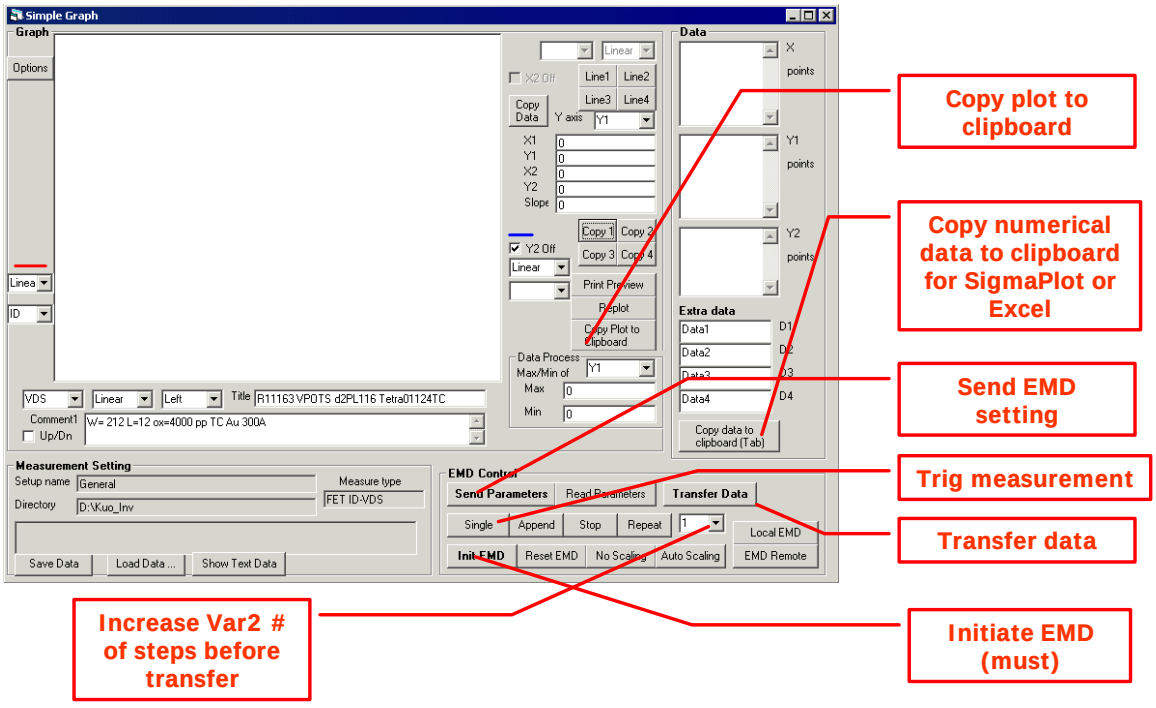

Figure B-3**: The "Simple Graphic" windows with basic EMD control buttons.**

8. The background turned red afterward.
9. Click the "Send parameters" button in the Simple Graph window.
10. Check the condition of the EMD
11. Click the "Single" button in the "EMD Control" frame to trigger a single measurement.
12. After the measurement on the EMD is done, click the "Transfer Data" in the "EMD Control" frame.
13. Wait for three seconds on Agilent 4155/4156 or twelve seconds on Agilent 4145.
14. Check the data in the lists on the right side and the figure in the plot window.
15. Click the "Save Data" in the "Measurement Setting" frame.
16. Pick up the directory and select the file name.
17. Both the numerical data and the figure are saved in plain-text and jpeg graphic formats, respectively. The plain text data has a fixed-width-column format if you want to import it. The measurement settings and parameters are storage at the end of the text data. They are not in a fixed-width-column format.

Load data

18. Click "Load Data" in the "Measurement Setting" frame of the Simple Graph window or Select [Menu/File][Open Data]

    Figure **B-4** shows the data processing and display functions.

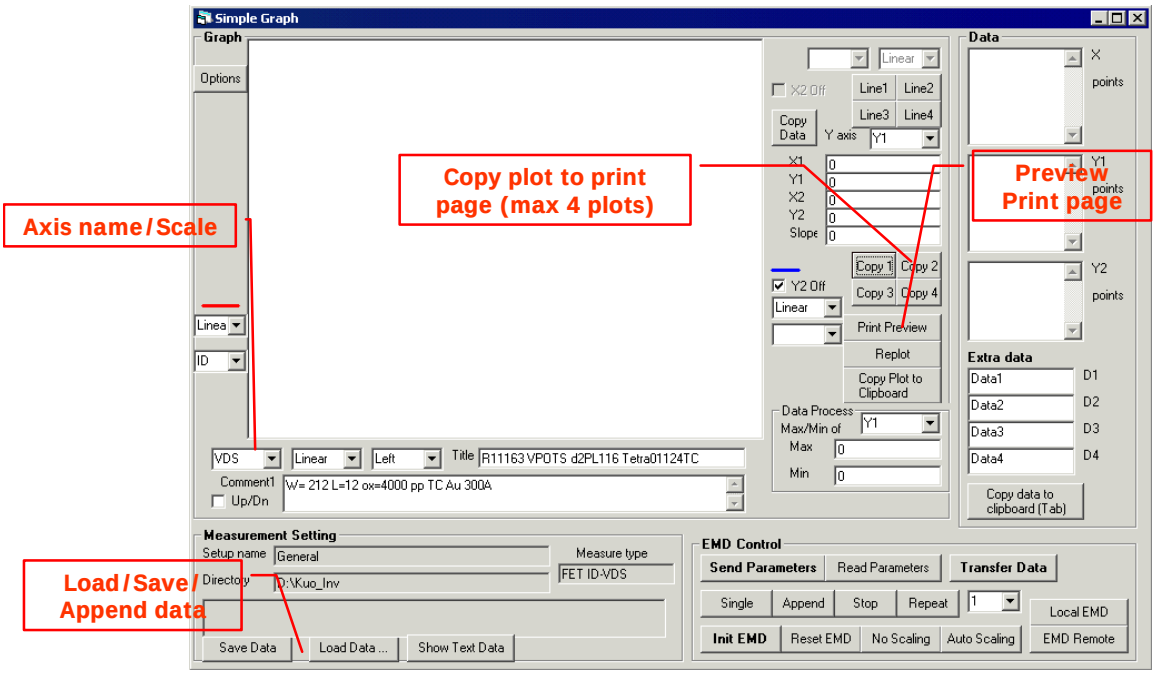

Figure B-4**: The data processing and display functions in the "Simple Graphic" window.**

Configuration of GPIB interface

1. Click "Configuration" on the tool bar to show the setup windows or Select [Menu/System][IEEE 488 Interface Configuration] as seen in Figure **B-5**.
2. Select the GPIB device to be defined. "Measurement Electronics" means EMD.
3. Choose the "Primary address" of this GPIB device.
4. Click the "Save" button.

Notice: Usually, the "Secondary address" is not used. "Operating mode" is for the control command mode (SCIP or the older HP4145 command set) Agilent-4156 only.

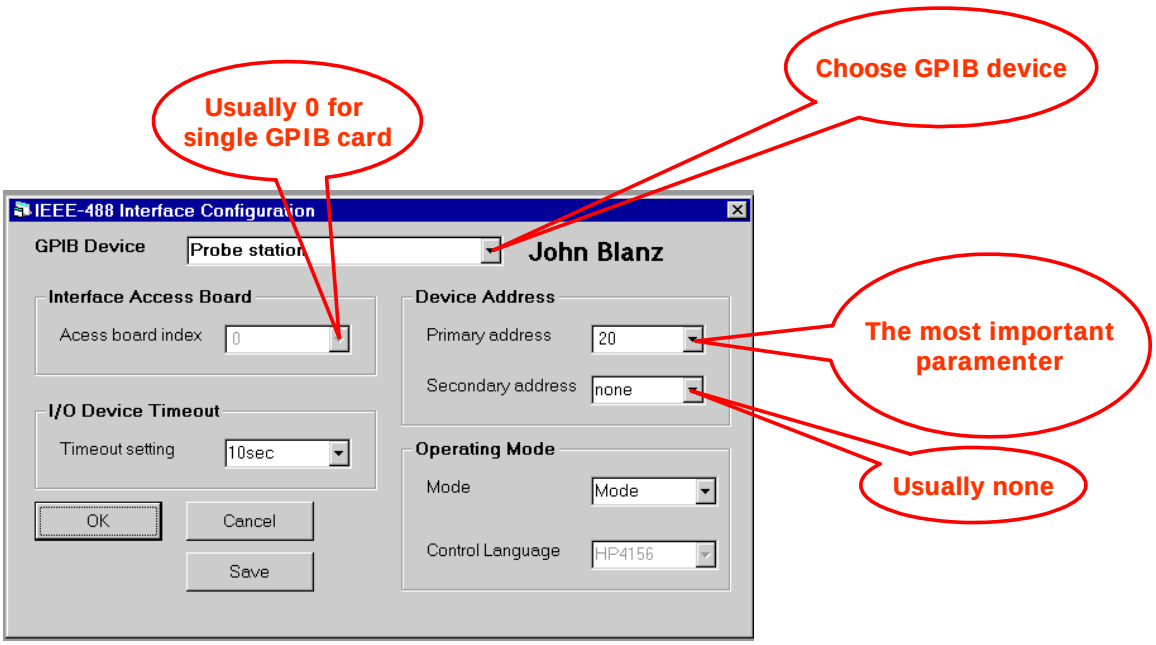

Figure B-5**: The GPIB configuration window.**

B.2 **Automatic Testing Cycles**

AutoData can automatically measure a device using a group (up to nine sets) of parameter sets for certain times. This allows the EMD cycling an device at various parameter sets. For example, let the EMD drive the device at low voltage and high voltage back and forth. This is useful for stress test and monitoring the time dependent variation, etc. Figure **B-6** shows the “Options” window of the “Auto Measurement”.

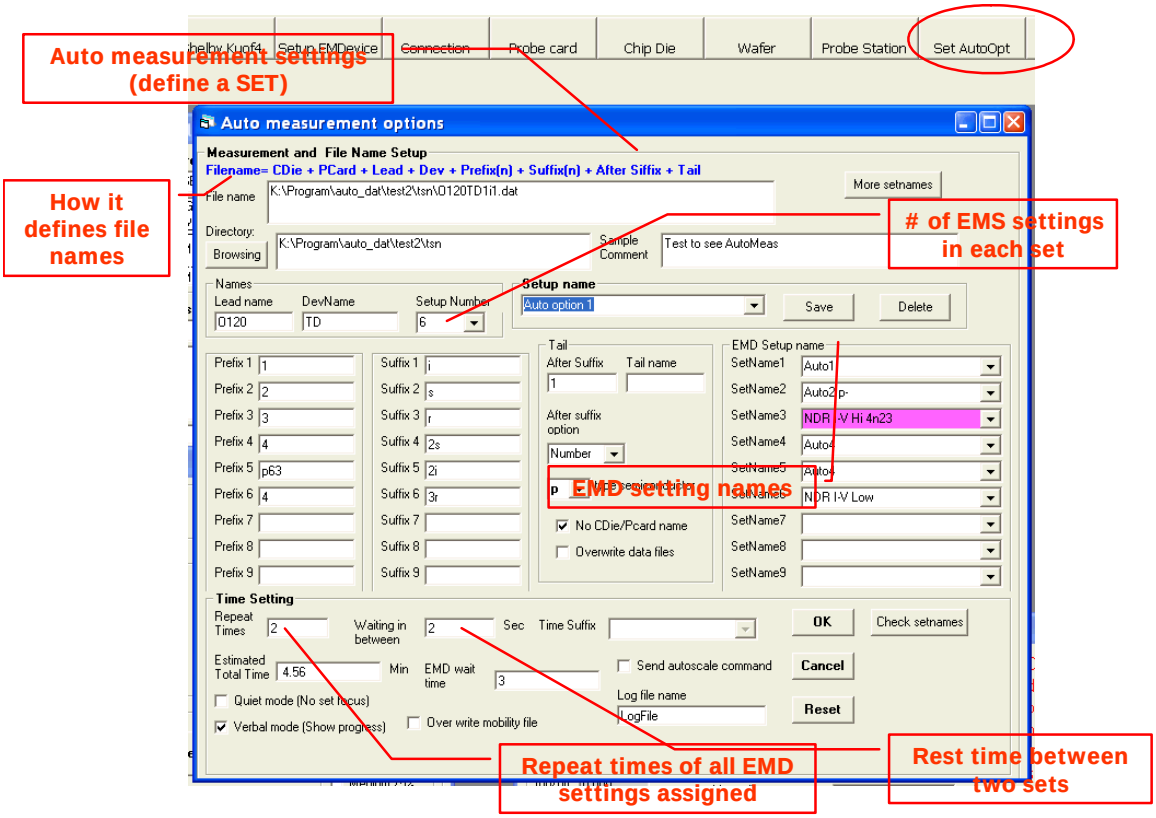

Figure B-6**: The "Options" window of the "Auto Measurement".**

Once the options are decided, the control commands in the "Auto Step" can guide you through the test as seen in Figure **B-7**. Although AutoData was design to do multiple-device testing, the feature is not done yet. Hence, the commands in the "Auto Multi EDev" frame are not working.

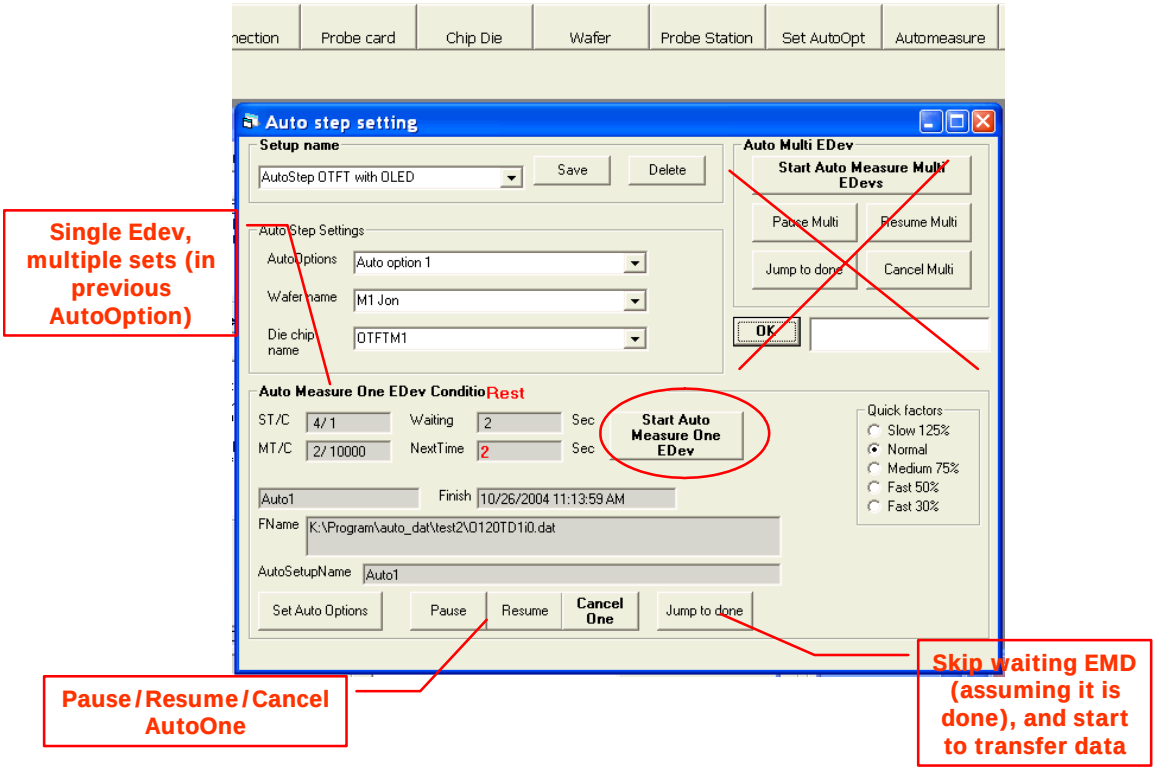

Figure B-7**: The "Auto step" window.**

Summary of AuotData Software

Thank for your support of this shareware. The graphic interface and functions remains rough because of my limited ability and time. However, many functions are easy to use for an academic research environment. The latest version was compiled in 2005 and available for download on JERG web site. The URL is http://jerg.ee.psu.edu/software/. To contact the author, please send email to shelbykuo@gmail.com.

VITA

Chung-Chen Kuo

Chung-Chen Kuo (also known as Shelby) was born on July 23rd , 1971, in Changhua, Taiwan, Republic of China. He attended Ming-Dao High School for six years, graduating in 1989. He received his bachelor of engineer degree in electrophysics from National Chiao Tung University (NCTU), Hsinchu, Taiwan, Republic of China, in 1993. Following the completion of his baccalaureate degree he served for two years in active duty at the Army Missile Defense of R.O.C. in Taipei County, during which time he received practical training in basic maintenance and legislation. In 1995, he worked as a research assistant at the Solid-State Physics Laboratory.

In 1996 Kuo enrolled in graduate school as a graduate student at the Department of Electrical Engineering at The Pennsylvania State University and began his study on organic thin film transistors (OTFTs) in Professor Thomas N. Jackson's group. In 1999 he made some progress in high-performance OTFTs, and he has continued to pursue his doctoral degree.

Kuo is completing the requirements for a doctoral degree in electrical engineering under Professor Tom Jackson with scientific contributions in the area of high performance OTFTs, small-molecule organic active layer materials, contact engineering for OTFTs with improved linear region performance, and solution processed OTFTs. He expects to graduate in December of 2005 with a grade point average of 3.65/4.0. Kuo's areas of interest include exploratory devices, microfabrication, and device characterization. His pursuit of these interests within a laboratory environment has included work on organic electronics, nanotechnology, and molecular electronic materials for electronic applications. Kuo is a member of the Institute of Electrical and Electronics Engineers and the American Physics Society, and he has authored or co-authored more than fourteen journal publications and conference presentations.

Upon completing his many years of graduate study, Kuo plans on continuing his exploration of science and technology.